# DEVELOPMENT OF MICROFABRICATED BIOHYBRID ARTIFICIAL LUNG MODULES

by

**Kristie Henchir Burgess**

B.S., University of Pittsburgh, 2000

Submitted to the Graduate Faculty of

the School of Engineering in partial fulfillment

of the requirements for the degree of

Doctor of Philosophy

University of Pittsburgh

2007

UNIVERSITY OF PITTSBURGH

SCHOOL OF ENGINEERING

This dissertation was presented

by

Kristie Henchir Burgess

It was defended on

June 4, 2007

and approved by

Harvey S. Borovetz, Ph.D.
Professor and Chair, Department of Bioengineering; Robert L. Hardesty Professor, Department of Surgery; Professor, Department of Chemical & Petroleum Engineering

Xinyan Tracy Cui, Ph.D.
Assistant Professor, Department of Bioengineering

Hsin-Hua (Sandy) Hu, Ph.D.
Research Assistant Professor, Department of Mechanical Engineering

William R. Wagner, Ph.D.
Professor, Departments of Surgery, Chemical & Petroleum Engineering and Bioengineering

Dissertation Director: William J. Federspiel, Ph.D.
William Kepler Whiteford Professor, Departments of Chemical & Petroleum Engineering, Surgery and Bioengineering

**DEVELOPMENT OF MICROFABRICATED BIOHYBRID**

**ARTIFICIAL LUNG MODULES**

Kristie Henchir Burgess, Ph.D.

University of Pittsburgh, 2007

Current artificial lungs, or membrane oxygenators, have limited gas exchange capacity due to their inability to replicate the microvascular scale of the natural lungs. Typical oxygenators have a surface area of 2 – 4 $m^2$, surface area to volume ratio of 30 $cm^{-1}$, and gas diffusion distances of 10 – 30 μm. In comparison, the natural lungs have a surface area of 100 $m^2$, surface area to volume ratio of 300 $cm^{-1}$, and diffusion distances of only 1 – 2 μm. Membrane oxygenators also suffer from biocompatibility complications, requiring systemic anticoagulation and limiting length of use. The goal of this thesis was to utilize microfabrication and tissue engineering techniques to develop biohybrid artificial lung modules to serve as the foundation of future chronic respiratory devices. Microfabrication techniques allow the creation of compact and efficient devices while culturing endothelial cells in the blood pathways provide a more biocompatible surface. Soft lithography techniques were used to create 3-D modules that contained alternating layers of blood microchannels and gas pathways in poly(dimethylsiloxane) (PDMS). The blood microchannels were fabricated with widths of 100 μm, depths of 30 μm, and inter-channel spacing of 50 μm. The diffusion distance between the blood and gas pathways was minimized and a surface area to blood volume ratio of 1000 $cm^{-1}$ was achieved. The gas permeance of the modules was examined and maximum values of $9.16 \times 10^{-6}$ and $3.55 \times 10^{-5}$ $ml/s/cm^2/cmHg$, for $O_2$ and $CO_2$ respectively, were obtained. Initial work examining thrombosis

in non-endothelialized modules demonstrated the need for endothelial cells (ECs). Several surface modifications were explored to improve EC adhesion and growth on PDMS. Finally, endothelial cells were seeded and dynamically cultured in prototype modules. Confluent and viable cell monolayers were achieved after ten days. The work described in this thesis provides a strong foundation for creating more compact and efficient biohybrid artificial lungs devices.

## TABLE OF CONTENTS

## LIST OF FIGURES

## ACKNOWLEDGMENTS

I would like to thank my advisor, William Federspiel, for his support and guidance over the years. Thank you for giving me the opportunity and the freedom to develop a new project in the lab, which allowed me to grow in creative and technical ways. I appreciate all of the knowledge I have gained from you, which enabled me to improve my research, writing, and presentation skills. I would also like to thank my co-advisor, William Wagner, for his support and expertise on the tissue engineering aspects of this project. I am grateful that you extended valuable resources and time to assist my project development. Deep gratitude goes to the rest of my committee: Harvey Borovetz, Tracy Cui, and Sandy Hu, for their invaluable time and suggestions over the years. Special thanks to Harvey Borovetz for giving me the opportunity to be his teaching assistant.

I would also like to thank Robert Kormos, Steve Winowich, and all of the members of the Artificial Heart Program. It was an honor to work with a group that not only has exceptional technical knowledge of VADs but extraordinary compassion for the patients. Working at AHP has been such a rewarding experience and is one that I will never forget.

Sincere thanks go to all of my lab-mates, past and present, in the Medical Devices Lab for your willingness to help, your friendship and for making each day enjoyable. I wish you all the best of luck. My appreciation goes to the members of the Wagner lab for their cell culture assistance and friendship. I would like to express gratitude to the Nanofabrication Facility and

the graduate students at CMU who provided so much microfabrication knowledge and assistance when I was starting this project. I would also like to thank the undergraduates that have helped me throughout the years: Amber Clausi, Qing Yang, Jean-Claude Rwigema, and Amber Loree. Special thanks go to Amber Loree, who not only built what seems like a million modules but became a good friend.

On a personal level, I have gained many wonderful friends and memories throughout my years at Pitt. I cannot possibly name all of you here, but I thank all of you for your help, support, and friendship. I would especially like to thank Mary Sullivan, Erin Driggers, and Heide Eash. I also want to thank Stephanie Kute for being a great mentor and friend. Thanks to Lauren Johnson for her friendship – I will never forget all those Sundays at AHP.

I would like to express my deepest gratitude to my family and husband. To my wonderful parents: thank you for always believing in me and for giving me the ability to believe in myself. Your love, guidance, and support gave me the courage to pursue my dreams. To my brothers and extended family: thank you for your support, love and understanding – I am so blessed to have you all in my life. Thanks go to my niece and nephew, who could bring a smile to my face even if all of my experiments failed. To my incredible husband: thank you for supporting me throughout the ups and downs of graduate school. From cleaning the house to helping me draw schematics, words cannot express my gratitude for your help. I love you dearly and look forward to our life together.

Finally, I acknowledge the sources of funding that allowed me to pursue and complete my doctorate: The Whitaker Foundation Biomedical Engineering Graduate Fellowship and the University of Pittsburgh Provost Development Fund. This work was funded in part by the Commonwealth of Pennsylvania.

# 1.0 INTRODUCTION

The natural lung has a large capacity for oxygen and carbon dioxide exchange due to a highly branched geometry and the intimate interaction between the alveoli and the pulmonary capillaries. A large surface area to blood volume ratio and small gas diffusion distances create an environment conducive to efficient gas transfer. Unfortunately, lung diseases, such as emphysema, can damage the structure of the lungs, increase the resistance for gas transfer, and decrease the overall efficiency of the lungs leading to a need for respiratory support. Current artificial lungs, or membrane oxygenators, have a limited gas exchange capacity due to their inability to replicate the microvascular scale of the natural lung. Membrane oxygenators are also plagued by biocompatibility complications, require systemic anticoagulation, and cannot be used for extended periods. The goal of this thesis is to develop biohybrid artificial lung technology using microfabrication and tissue engineering techniques to create more efficient and biocompatible devices in the future. Microfabrication technology, specifically soft lithography, is used to create small modules that contain alternating layers of blood microchannels and gas pathways in poly(dimethylsiloxane) (PDMS) as shown in Figure 1-1. The blood microchannels have diameters less than 100 microns and are packaged closely within each layer. Each gas layer consists of one large, open pathway to increase the interaction between the gas and blood pathways. The thickness of the PDMS layers is minimized to decrease the resistance for gas transfer and to reduce the overall size of the device.

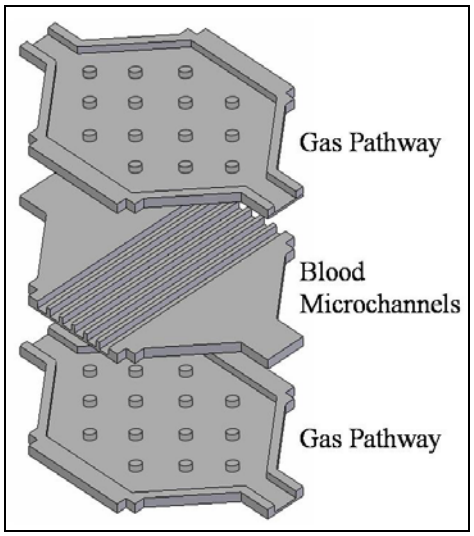


**Figure 1-1: Schematic of microfabricated artificial lung module**

The modules developed in this thesis are an improvement over current hollow fiber membrane technology due to the ability to create blood microchannels that approach the microvascular scale found in the natural lung. The surface area to blood volume ratio of the modules is two orders of magnitude greater than that found in current oxygenators enabling the creation of a more compact, efficient device. Additionally, tissue engineering techniques are used to produce confluent monolayers of endothelial cells (ECs) in the blood microchannels. The endothelial cells will maintain a non-thrombogenic/non-inflammatory phenotype and will provide a more biocompatible surface for the blood as it passes through the device. This will reduce, or even eliminate, the need for systemic anticoagulation and the biocompatibility complications associated with current oxygenators and ECMO. Future work will include the scale-up of the modules into a compact device and incorporation of autologous cells (i.e. cells from the patient) to form next generation biohybrid artificial lungs for chronic respiratory support.

The purpose of this thesis was to prove the feasibility of creating small biohybrid modules using microfabrication and tissue engineering techniques. The specific aims were to:

1. Use microfabrication techniques to fabricate small modules in gas permeable poly(dimethylsiloxane) (PDMS). Several fabrication techniques were explored to create intimate arrays of blood microchannels and gas pathways that approach the microvascular scale of the natural lung. These techniques included molding tungsten wire arrays, double molding and stacking layers, molding SU-8 pillar arrays, creating sacrificial photoresist channels, using soft lithography techniques, and utilizing photopatternable PDMS. Prototype modules were fabricated using soft lithography for gas permeance and cell culture testing.
2. Evaluate the mass transfer characteristics of the modules using gas permeance testing. The effect of the diffusion distance between gas and blood pathways on the permeance of the modules was examined.
3. Evaluate and optimize methods for growing and maintaining stable endothelial cell (EC) layers in the modules. This aim included examining thrombosis in non-endothelialized modules, exploring surface modifications to improve EC adhesion and proliferation on 2-D PDMS constructs, determining EC detachment due to shear stress, and evaluating EC growth in 3-D devices.

Chapter 2 provides an overview of the lung, diseases of the lung, and treatments options, including mechanical ventilation and extracorporeal oxygenation. Current membrane oxygenators, the principles of gas exchange, and devices under development are discussed. Chapter 2 also provides the relevant microfabrication and tissue engineering background and motivation for the work described in this thesis. Chapter 3 provides an overview of the

fabrication techniques that were explored and describes in detail the soft lithography methods that were used to create modules for gas permeance and cell culture studies. Gas permeance experiments are described in Chapter 4 and the endothelial work is detailed in Chapter 5. Complete details on all of the fabrication techniques, including molding tungsten wire arrays with PDMS, double molding and stacking PDMS layers, molding SU-8 pillar arrays with PDMS, creating sacrificial photoresist channels in PDMS, and utilizing photopatternable PDMS, are described in Appendix A.

# 2.0 BACKGROUND

## 2.1 THE NATURAL LUNG

The natural lung is capable of high levels of oxygen and carbon dioxide exchange due to the intimate interaction between the alveoli and the pulmonary capillaries. Twenty-three generations, or levels of branching, occur in the lung from the trachea to the alveoli. The upper sixteen generations of the lung make up the conducting zone, from the trachea to the terminal bronchioles. The transition into the respiratory zone occurs when the terminal bronchioles branch into respiratory bronchioles, which contain sparse alveoli, giving rise to the ability for low levels of gas exchange. Seven additional levels of branching occur to form alveolar ducts that terminate with the alveolar sacs, where the majority of gas exchange occurs [1]. The adult lung contains 250 – 350 million alveoli, each of which has a diameter of 200 – 300 microns leading to a total surface area of 100 $m^2$ for gas exchange [2]. The high surface area for exchange is packaged compactly with the surrounding capillaries, which have diameters of only 5 – 10 microns and lengths less than one millimeter giving rise to a surface area to blood volume ratio of 300 $cm^{-1}$ [3].

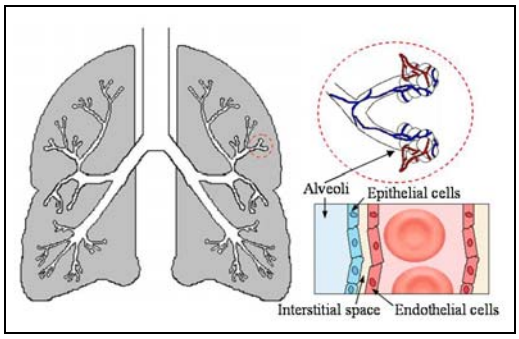


**Figure 2-1: Schematic of the natural lung**

The membrane across which oxygen and carbon dioxide transfer occurs is only 1 – 2 microns and consists of the alveolar epithelium, a thin interstitial space, and the capillary endothelium [4]. The overall $O_2$ or $CO_2$ gas exchange in the lung can be simply expressed as the product of the diffusing capacity, $D_L$, and the partial pressure difference between the alveolar gas space and the pulmonary capillaries ($\Delta P_{A\text{-}c}$) [5].

$$\dot{V} = D_L \, \Delta P_{A-c} \qquad \textbf{Equation 1}$$

The diffusing capacity of the lungs is proportional to the product of the surface area for gas exchange, A, the gas permeability, K, and the inverse of the diffusion distance, δ, across the alveolar-capillary membrane:

$$D_L \propto \frac{KA}{\delta} \qquad \textbf{Equation 2}$$

Equation 2 demonstrates how the large surface area and small diffusion distances of the natural lung are critical for achieving high levels of gas exchange. The lung can easily support gas exchange varying from resting levels of ~200 ml/min for $O_2$ and $CO_2$ to 3200 ml/min during strenuous exercise with 20% oxygen as the supply gas [6]. Unfortunately, lung disease, which is discussed below, can have a negative impact on the diffusing capacity thereby reducing the ability to exchange adequate levels of oxygen and carbon dioxide.

## 2.2 LUNG DISEASE

Lung disease is the third leading cause of death in the United States responsible for one in seven fatalities. Respiratory diseases cause 350,000 deaths a year in addition to costing the economy in excess of $150 billion in direct and indirect costs, and these numbers continue to climb [7]. Lung disease can either be acute, such as acute respiratory distress syndrome (ARDS), or chronic, such as chronic obstructive pulmonary disease (COPD). Acute respiratory distress syndrome is an inflammatory condition in which the lungs can no longer provide adequate gas exchange due to fluid accumulation in the lungs. ARDS is responsible for the rapid respiratory failure in approximately 150,000 Americans each year with a mortality rate of 30 to 40% [8]. Causes include direct injury to the lungs, as in pneumonia, smoke inhalation, shock, near-drowning, and aspiration, and indirect injury, such as sepsis and shock [8, 9]. Patients with ARDS present with dyspnea, hypoxemia, and pulmonary infiltrates evident on chest x-rays. Decreased gas exchange occurs due to the accumulation of fluid in the alveoli and interstitial spaces, damage to the epithelial and endothelial cells separating the pulmonary capillaries from the alveoli, and decreased lung compliance due to fibrosis [9, 10].

Chronic obstructive pulmonary disease (COPD), including emphysema and chronic bronchitis, affects between 11 and 24 million Americans [7]. In general, COPD is due to obstruction to airflow, which increases the work of breathing for the patient, leading to dyspnea, coughing, and the inability to perform daily activities. In emphysema, the walls of the alveoli are irreversibly destroyed, which decreases the number of alveoli and increases their size. This reduction in the surface area to blood volume ratio leads to inadequate gas exchange [1]. In addition, the lungs lose elasticity, which makes it very difficult for the patient to exhale. Emphysema is primarily caused by smoking and takes years to develop as demonstrated by the

fact that over 90% of the patients with emphysema are over 45 [11]. Chronic bronchitis is characterized by the inflammation and infection of the bronchial lining and an increased mucus production. Over time, scarring develops causing the bronchial lining to thicken and reduce airflow. Patients with COPD can be managed at home with pharmacotherapy, including supplemental nasal oxygen, bronchodilators, and glucocorticosteroids [11]. However, patients with these chronic conditions often have acute exacerbations of their disease leading to 600,000 hospitalizations a year [11].

Patients suffering from ARDS, acute exacerbations of COPD, or other chronic respiratory insufficiencies are treated with mechanical ventilation when non-invasive treatment, such as pharmacotherapy and non-invasive ventilation, fails. In mechanical ventilation, the patient is intubated with an endotracheal tube and air is forced into and out of the lungs to achieve adequate gas exchange. Ventilators are operated in either a volume mode, which introduces a specific tidal volume into the lungs during inspiration, or a pressure mode, which delivers air until the desired airway pressure is met. Other ventilator settings, such as the respiratory rate, the oxygen concentration, and the positive end expiratory pressure (PEEP) are adjusted to maximize gas exchange. Mechanical ventilation can support patients with respiratory insufficiencies for many days; however, it has been found that this treatment can further worsen lung failure due to ventilator-induced lung injury (VILI), such as volutrauma, barotrauma, atelectrauma, and biotrauma [12, 13]. Typically, large tidal volumes (~12ml/kg) are used when ventilating patients, but these volumes overdistend the lungs and can cause alveolar damage and increase the permeability of the alveolar-capillary membrane. Consequently, pulmonary edema occurs leading to an increased difficulty in maintaining adequate gas exchange. Barotrauma can occur due to the high pressures used during inspiration and can cause pneumothorax, pulmonary

interstitial emphysema, or air embolism. However, this injury is less common and may also be linked to the overstretching of the lungs and not the pressure alone. Atelectrauma can develop due to the repetitive closing and opening of the alveoli increasing the shear stress on the epithelial cells and damaging them. Higher levels of PEEP (> 5 $cmH_20$) are recommended to open and maintain large numbers of alveoli. Finally, biotrauma includes injury to the lungs from inflammation. Studies have shown increased levels of inflammatory mediators, such as neutrophils and cytokines, in the lungs with traditional mechanical ventilation therapy. To reduce the level of VILI, lung protective ventilation strategies have been employed using lower tidal volumes (6 ml/kg) and have demonstrated a decrease in patient mortality [12].

Extracorporeal membrane oxygenation (ECMO) is used when mechanical ventilation fails to maintain adequate gas exchange for the patient. In ECMO, blood is removed from the patient, perfused through a circuit containing a pump, a heat exchanger, and a membrane oxygenator, and then returned to the patient. The membrane oxygenator removes carbon dioxide from and adds oxygen to the blood independently of the lungs, allowing the lungs to rest and heal. A more detailed description of membrane oxygenators is provided in the following section (Section 2.3). The blood removal and return cannulation sites for ECMO can be venovenous, arteriovenous, or venoarterial. Venovenous is the most commonly used cannulation technique, while venoarterial is used if cardiac support is also required. ECMO can be used to support patients for up to 30 days with survival rates of 81, 49, and 38% in neonatal, pediatric, and adult patients, respectively [14]. Many complications are associated with ECMO therapy [15]. The blood exposure to the large surface area of the ECMO circuit activates the thrombotic and inflammatory pathways. The patient must be systemically anticoagulated with heparin to increase the activated clotting time to 160 – 240 seconds to prevent thrombus formation in the

oxygenator [16]. However, the higher level of anticoagulation can lead to undesired bleeding, such as in the brain or gastrointestinal tract. Several different heparin coatings, such as the Carmeda™ Bioactive Surface, Trillium™ Biopassive Surface, and Bioline Coating™, have been developed to coat the entire ECMO circuit, including the oxygenator, with heparin and reduce the need for systemic heparin [17, 18]. The heparin coatings have been shown to decrease platelet and white blood cell adhesion and activation and reduce compliment activation [18]. Even with these improvements, many other complications arise including rupturing of the circuit tubing, air in the circuit, and oxygenator failure due to plasma leakage [19]. ECMO therapy is also expensive, labor intensive, and requires the patient to be sedated in the intensive care unit.

## 2.3 MEMBRANE OXYGENATORS

### 2.3.1 Description of Membrane Oxygenators

The most commonly used artificial lungs, or membrane oxygenators, are composed of bundles of hollow fiber membranes that are wrapped into specific configurations within a plastic housing. Blood enters the device and flows along the outside of the hollow fibers, while oxygen, or a mixture of oxygen and carbon dioxide, flows through the lumens of the fibers. The device can be operated in the reverse mode but a high pressure drop develops due to the intralumenal blood flow. Membrane oxygenators also include a heat exchanger, which the blood perfuses through before exiting the device, to maintain body temperature. Oxygenators that are commonly used include the Medtronic Affinity® NT oxygenator, the Jostra Quadrox®, and the Terumo Cardiovascular Systems Capiox® SX. All of these devices are designed to reduce the priming

volume, minimize blood flow resistance, and eliminate blood stagnation regions to prevent thrombosis formation. The fibers are hydrophobic, typically made of polypropylene, and microporous, with submicron pores and porosities of 40 – 50% [20]. The inner diameter of the fibers ranges from 200 – 400 μm and wall thicknesses vary between 20 – 50 μm [21]. The fibers are wrapped to achieve bundle porosities of 40 – 60% and a total surface area for gas exchange of 2 – 4 $m^2$ [22]. The blood priming volume for an adult device is between 135 – 340 ml giving rise to a surface area to blood volume ratio of approximately 30 $cm^{-1}$, which is one order of magnitude less than that found in the natural lung. Oxygenators can achieve gas exchange levels of 200 – 400 ml/min with 100% oxygen as the supply gas [20].

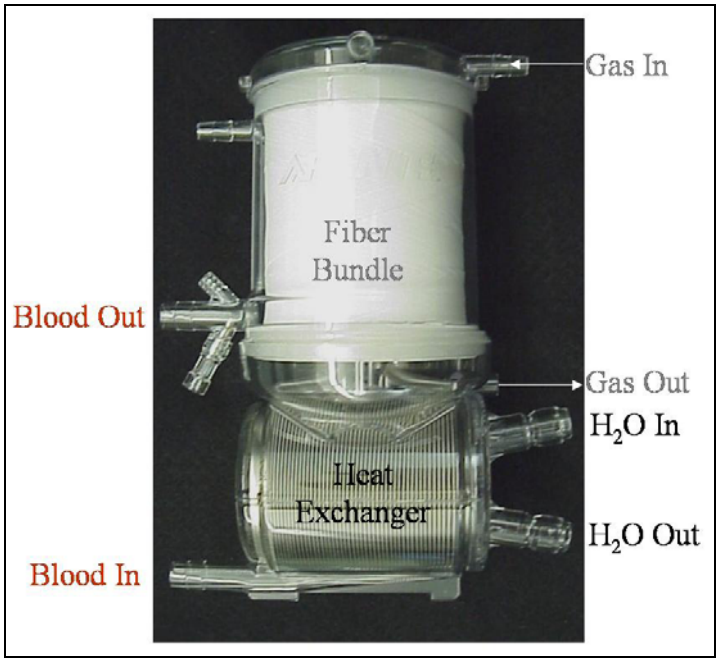


**Figure 2-2: Commercially available membrane oxygenator**

### 2.3.2 Theory of Gas Exchange in Membrane Oxygenators

Current artificial lungs must supplement oxygen and remove carbon dioxide at adequate rates to meet basal metabolic requirements, 270 and 240 ml/min, respectively [6]. Gas exchange is driven by the concentration gradients between the fibers and blood: high $pO_2$ in the fibers and low $pO_2$ in the blood and the reverse for $pCO_2$. Oxygen diffuses from the fiber lumen, across the fiber wall, and into the blood flowing past the fibers. Carbon dioxide diffuses across the fiber wall into the fiber lumens and is removed from the device. The total gas exchange rate for oxygen is equal to the product of the permeance, or mass transfer coefficient ($Ko_2$), of the device, the surface area for exchange (A), and the difference in the average concentration of the gas ($PO_{2g}$) and blood pathways ($PO_{2b}$).

$$\dot{V}O_2 = K_{O_2} A\left(PO_{2g} - PO_{2b}\right) \qquad \textbf{Equation 3}$$

Similarly, the overall rate of carbon dioxide exchange can be expressed using the mass transfer coefficient for $CO_2$ ($Kco_2$) and the difference in the $CO_2$ concentration between the blood ($PCO_{2b}$) and gas pathways ($PCO_{2g}$).

$$\dot{V}CO_2 = K_{CO_2} A\left(PCO_{2b} - PCO_{2g}\right) \qquad \textbf{Equation 4}$$

The mass transfer coefficient is inversely related to the overall resistance to gas exchange, which is the sum of the resistances due to the gas pathway, the membrane, and blood pathway, as shown in Equation 5.

$$\frac{1}{K} = \frac{1}{K_g} + \frac{1}{K_m} + \frac{1}{K_b} \qquad \textbf{Equation 5}$$

The resistance to transfer in the gas pathway ($K_g$) is negligible and can be eliminated from Equation 5. As described above, the hollow fibers used in membrane oxygenators are microporous and provide little resistance to mass transfer. Therefore, the majority of the

resistance is due to the formation of a blood boundary layer along the outside of the fibers. The boundary layer thickness can be reduced by increasing the velocity along the fiber length, by flowing blood perpendicular to the fibers, as in the Jostra Quadrox®, or by using active mixing to disrupt the boundary layers [6, 23].

### 2.3.3 Brief Overview of Devices Being Developed

The membrane oxygenators described above are passive devices that were designed primarily for short-term application, such as cardiopulmonary bypass. There is a need for improved artificial lung devices that can support patients for much longer periods (weeks to several months) and reduce the complications like those seen with ECMO. Many devices that utilize hollow fibers are under various stages of development and are discussed below. Additionally, Section 2.3.3.2 describes work from several groups that have begun using microchannels, rather than hollow fibers, as a means to create more compact and efficient devices.

#### 2.3.3.1 Devices Utilizing Hollow Fiber Membranes

Current research efforts are focused on developing membrane based devices that are either intravascular or paracorporeal. Intravascular devices are designed to be inserted into the vena cava via the femoral or jugular vein and to supplement 40 – 60% of basal gas exchange requirements for short periods [24]. Some of the advantages of intravenous respiratory support over ECMO include eliminating the removal of blood from the body, decreasing the amount of blood contact with a foreign biomaterial surface, and reducing the complexity and cost of treatment. The challenges of intravenous oxygenation include the limited surface area of the device due to the size of the vena cava and the requirement for patient immobilization. The first

device based on this technology, the IVOX, was developed by Mortensen et al. and CardioPulmonics [25-29]. The IVOX consisted of a bundle of hollow fiber membranes, which were crimped to decrease blood boundary layers thereby increasing gas exchange [25, 26]. A clinical trial performed in patients with acute respiratory distress syndrome demonstrated limited gas exchange capabilities, providing only 20 – 30% of basal requirements [27]. Due to these results, the clinical trial and development of this passive device was terminated. Two groups are currently working to improve this technology as discussed below.

The Hattler Catheter, formally known as the intravenous membrane oxygenator (IMO), was developed by Hattler, Federspiel and coworkers at the University of Pittsburgh [6, 30-38]. The Hattler Catheter (HC) improved upon the IVOX technology by incorporating a pulsating balloon within the fiber bundle. The hollow fibers are woven into a fiber mat which keeps the fibers uniformly spaced and prevents blood shunting. The balloon pulsation creates radial blood flow through the fiber bundle decreasing the blood boundary layers, which leads to increased gas exchange performance. Balloon pulsation increased gas exchange by 200 – 300% at low flow rates (1 – 2 L/min) and by 50 – 100% at the higher flow rate (4.5 L/min) compared to the IVOX in ex-vivo experiments [32]. Both acute [30, 36] and chronic [38] animal experiments were performed at the university, and the device is now being commercialized by ALung Technologies, Inc. Current research efforts at the University of Pittsburgh are focused on using rotational mechanisms, rather than balloon pulsation, to actively mix the blood and increase gas exchange efficiency while reducing the size of the device to allow for percutaneous insertion [39].

The Helmholtz Institute for Biomedical Engineering in Germany is developing a highly integrated intravascular membrane oxygenator (HIMOX) [40-42]. The HIMOX consists of disk-shaped bundles of hollow fiber membranes that can slide on a centrally located shaft. The disk-shaped bundles increase the surface area for exchange and reduce blood boundary layers due to cross flow. The bundles are elongated to reduce the diameter of the device for easier insertion. The device is then positioned in the vena cava where the bundles are compressed and twisted to form a shorter (10 vs. 40 mm) and wider device (25 vs. 10 mm) that spans the diameter of the vessel [42]. The twisting of the bundles allows for a uniform and high fiber density and reduces the shunting around the fibers. A miniature blood pump is incorporated into the device upstream of the bundles to overcome the pressure drop across the device, and a sheath surrounds the device to protect the vena cava from the high pressure environment. A maximum oxygen exchange efficiency of 480 ml/min/$m^2$ has been demonstrated in in-vitro blood tests, and current work is focused on evaluating in-vivo performance of the device in an animal model [41].

Several paracorporeal devices are currently under development that either incorporate a pump within the device or use fiber rotation to induce pumping. The HEXMO is being developed at the Helmholtz Institute for Biomedical Engineering in Germany [40]. This device consists of a bundle of hollow fiber membranes surrounding a small rotary blood pump. Both the blood inlet and outlet ports are on the top of the device to allow for easy attachment to a dual lumen catheter. This configuration reduces the priming volume and the amount of blood contact with a foreign surface. The heat generated by the pump is used to maintain body temperature. The HEXMO is in the preliminary testing phase.

A paracorporeal respiratory assist lung (PRAL) was developed at the University of Pittsburgh to supplement respiratory support while allowing the natural lungs to rest and heal

[43]. The PRAL consists of a rotating hollow fiber bundle surrounding a center core that distributes the blood as it enters the device. The rotation of the bundle not only increases the gas exchange efficiency of the device but provides pumping capabilities, which allows for venovenous cannulation. The device is able to achieve 101 ml/min of carbon dioxide exchange, half of the basal requirements, at a low flow rate of 0.75 L/min [44]. The PRAL is now being commercialized as the Hemolung™ by ALung Technologies, Inc.

Another device that utilizes fiber bundle rotation is being developed by Wu et al. to provide long-term (>21 days), total respiratory support in ambulatory patients [45]. The ambulatory pump-lung (APL) contains a four inch disk of hollow fiber membranes that is connected to a dual-lumen shaft used to supply the oxygen gas source and rotate the disk. The surface area of the device is 0.5 $m^2$ and the priming volume is 100 ml. Gas exchange levels of 200 ml/min for both oxygen and carbon dioxide were achieved during in-vitro experiments using bovine blood perfused at 5 L/min. Hemolysis levels throughout six hour in-vitro tests were comparable to levels seen in clinically accepted oxygenators and ventricular assist devices. The APL was also evaluated in acute and chronic (5 days) experiments in calves and achieved oxygen exchange levels of 175 and 110 ml/min respectively. The decreased level of exchange with the chronic device was due to utilizing silicone-coated hollow fibers, which have a decreased permeability compared to uncoated fibers. Future work is focused on improving the fiber coating and the commercialization of the device by Ension, Inc.

#### 2.3.3.2 Devices Utilizing Microchannels

Several groups have begun exploring the use of microchannels to achieve higher surface area to blood volume ratios leading to more efficient devices. Mockros et al. are developing arrays of microchannels with diameters of only 10 – 25 μm in gas permeable polymers [46].

Initial work consisted of creating an array of commercially available glass fibers (12 μm diameters) and molding the array with a polymer mixture of methylmethacrylate, dimethylitaconate, and ethylenglycodimethacrylate. The fibers were then dissolved and the array was machined into a wafer with the desired dimensions. Wafers with a thickness of 0.6 mm were fabricated to contain 5000 microchannels per $mm^2$. Calculations demonstrated that 100 million channels would be needed to oxygenate blood flowing at 4 L/m using room air. Further work explored a variety of techniques to fabricate microchannel arrays, including the wafers with circular channels described above, silicon membranes with support posts, and rectangular channels that were sealed on one side with a flat silicone layer. Preliminary blood experiments using the rectangular channels demonstrated the ability to increase hemoglobin saturation from 65 to 96% [47].

Another group from the Utrecht Micro Engineering Competence Center in the Netherlands is developing a micro-oxygenator, also known as the UMMOX [48-50]. Originally, the micro-oxygenator consisted of layers of rectangular microchannels that were etched into metal plates. The microchannels had widths, heights, and interchannel spacing of 100 μm and the metal sheet had a total thickness of 200 μm. A gas permeable membrane sheet (~35 μm thick) was sandwiched between two metal plates to form a subunit of the device. Each subunit consisted of one gas layer and one blood layer with the gas and blood channels perpendicular to one another to allow for manifolding. The subunits were stacked to form an oxygenator for mice that was 40 x 40 x 25 cm and had a surface area of 0.009 $m^2$ and a priming volume of 3 ml. Several improvements were made to the original design to create the UMMOX. The use of metal plates to create a device was very costly. To overcome this, nickel molds were fabricated using UV-LIGA. Hot embossing was then utilized to create the microchannels in plastic sheets, such as

polycarbonate, polypropylene, and polymethylmethacrylate. Also, the surface area for gas exchange in the original design was only a small amount of the total surface area of the device (~25%) due to the perpendicular relationship between the blood and gas channels. The channel geometry was modified to increase the surface area for exchange using widths of 200 μm, heights of 50 μm, and interchannel spacing of 50 μm. The device was further improved to incorporate heat exchangers in the blood inlet and outlet plates. Finally, three different sized modules were fabricated to accommodate patients with 4, 10, or 30 kg bodies. Any combination of the modules can be used to create a device specific to the size of each patient.

Finally, Gilbert et al. are developing an artificial lung that uses a photolytic process to convert water to dissolved oxygen, therefore eliminating the need for a gas pathway and oxygen source [51-54]. The prototype photolytic cell is fabricated on a glass slide, which is first coated with titanium metal, the conducting layer, and then titanium dioxide ($TiO_2$) and $MnO_2$, the photoactive surface. The backside of the cell is exposed to UV light forming activated oxygen and then dissolved oxygen at the photoactive surface. Experiments have been performed using a synthetic serum and bovine blood, which showed an increase in oxyhemoglobin from 83 to 92%. The calculated oxygen transfer based on the photolytic reactions was 1.08 ml/min/$m^2$. Future work will focus on increasing the yield of the photolytic process and fabricating cells using microfluidic circuits like those described by Vollmer et al [52].

## 2.4 MICROFABRICATION

### 2.4.1 General Overview

Microfabrication techniques are derived from integrated circuit processing and MicroElectroMechanical Systems (MEMS), which combine mechanical elements, electronics, sensors and actuators. These techniques are widely used in automotive, aerospace, and military applications. Examples of microfabricated devices include inkjet print heads, airbag crash sensors, and pressure and inertial sensors. Microfabrication has become more widely used in biological and biomedical applications to form invasive and noninvasive biomedical sensors, biochemical analytical instruments, pacemakers, catheters, and drug delivery devices [55]. Microfabrication techniques are also being utilized in tissue engineering to examine protein and cell patterning [56-58], cell motility [59], cell – cell interaction [60], and cell – biomaterial interaction [61-64]. Many studies in this area provide the basis for the work in this thesis and will be summarized below.

### 2.4.2 Replicating Microvascular Structures

Microfabrication techniques have been widely used to produce channels with in-vivo capillary dimensions in silicon and Pyrex wafers to study microvascular blood flow [65-72]. Channels of different geometries including rectangular, triangular, and semicircular have been etched in these substrates with diameters ranging from 4 – 100 μm. Brody et al. examined red blood cell deformation in rectangular channels (widths from 2.5 – 4 μm and depth of 4 μm) etched in a silicon wafer [71]. Cokelet et al. etched glass slides and coverslips to produce semi-circular

channels of 20-micron diameter [68]. Two slides were then bonded using electrofusion to create circular channels that could be perfused with blood. Kikuchi et al. etched v-shaped grooves in silicone wafers based on anisotropic wet etching [65]. A parallel array of 2600 channels with equivalent diameters of 6 microns and length of 14.4 microns was used to study flow behavior of red blood cells. Kikuchi et al. also used similar arrays of channels with lengths of 10, 20, and 100 microns to study the effects of platelets and leukocytes on blood flow [66]. Sutton et al. explored erythrocyte volume and velocity in rectangular channels with widths between 3 – 4 microns, depth of 4 microns, and length of 100 microns [67].

### 2.4.3 Soft Lithography Using Poly(dimethylsiloxane)

Silicon wafers, however, are not the optimal material to use for a biohybrid lung, as well as other tissue engineering applications, due to their rigid and opaque nature, resistance to gas transfer and high cost. For these reasons many researchers have shifted to soft lithography, which replicates the micron-size features in polymers, specifically poly(dimethylsiloxane) (PDMS) [58, 73, 74]. Many characteristics of PDMS make it an excellent material for the biohybrid lung and other tissue engineering applications [74]. 1) Micron-size features can be reproduced with high fidelity by replica molding. 2) The transparent properties are important for visualizing flow and cell growth in the channels. 3) PDMS is biocompatible and non-toxic to cells. 4) PDMS is highly permeable to oxygen and carbon dioxide ($60 \times 10^{-9}$ and $325 \times 10^{-9}$ ml (STP) cm/s/cm$^2$/cmHg respectively). 5) Two-part curing systems consisting of a prepolymer and curing agent are commercially available and are inexpensive. The two parts can be easily mixed in a 10:1 ratio (prepolymer:curing agent) by weight and cured at room temperature or at an elevated temperature to decrease the curing time. Two of the more commonly used siloxanes are Sylgard

184 from Dow Corning and RTV 615 from General Electric. 7) A variety of techniques, which are described in the following section, can be used to irreversibly bond individual layers of PDMS.

In soft lithography, a silicon wafer is etched, or patterned, using typical photolithography techniques. The liquid PDMS mixture is then poured onto the etched silicon wafer and cured to reproduce the desired structures in PDMS. The silicon master mold can be reused many times without structural loss thus decreasing the overall cost of production. After curing, the individual PDMS layers can be peeled off the mold, stacked, and bonded to create 3-dimensional devices.

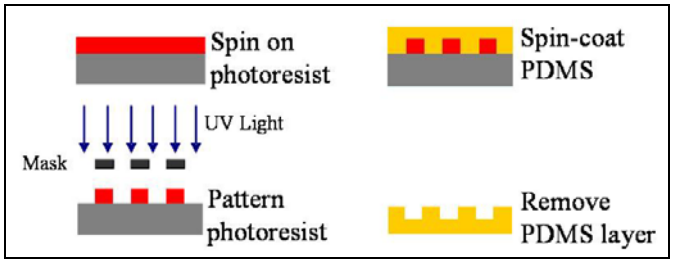


**Figure 2-3: Schematic of soft lithography process**

### 2.4.4 Creating Three-dimensional Devices

Several different techniques have been utilized to create 3-dimensional microfluidic devices and are described in this section. Most techniques focus on stacking and bonding layers by modifying the surfaces with oxygen plasma, changing the PDMS curing ratio between layers, and using liquid PDMS as "glue" between layers. Only one technique avoids the need to bond layers by embedding sacrificial photoresist channels in PDMS.

Jo et al. demonstrated that thin, patterned layers of PDMS could be stacked and bonded using oxygen plasma to form a 3-dimensional microchannel circuit [73]. SU-8 photoresist was

patterned on a silicon wafer and molded with PDMS. A “sandwich” molding technique was developed using weights or specific clamping pressures to minimize the PDMS thickness. A 75-μm thick layer could be created using ½ lbs. weights. The individual PDMS layers were then stacked and irreversibly bonded by treating both surfaces with oxygen plasma. Exposure to the oxygen plasma forms silanol groups (Si-OH) on each surface, which condense to form tight covalent bonds capable of withstanding pressures of 30 – 50 psi [74]. After plasma treatment, a thin layer of methanol was placed between the PDMS layers to facilitate alignment. The layered structure was heated to 85°C for 80 minutes to evaporate the methanol and complete the bonding. The authors were able to stack 5 layers (each 120 μm thick) to create a 3-D microchannel device. Anderson et al. also created three-dimensional microchannels in PDMS using similar techniques [75]. A thin PDMS layer was fabricated by molding PDMS between two wafers that had been patterned with SU-8. The PDMS layer was then bonded to two flat pieces of PDMS using oxygen plasma. Up to five PDMS layers were bonded to create complex 3-D microchannels.

Another method used to bond layers of PDMS consists of altering the composition of the adjacent layers as developed by Quake et al [76]. As described above, the PDMS mixture consists of a prepolymer base and a curing agent supplied by General Electric (Silicone RTV 615). The prepolymer base contains vinyl-terminated PDMS and a platinum catalyst while the curing agent contains oligomers that have silicon-hydride groups. Normally, the PDMS is mixed in a 10:1 ratio of prepolymer:curing agent. Quake et al. mixed the PDMS using a 30:1 ratio for one layer (more vinyl groups) and a 3:1 ratio for the adjacent layer (more silicon hydride groups). Each layer was cast onto a mold of channels and cured for 1.5 hours at 80°C. The layers were then stacked and cured for an additional 1.5 hours at 80°C. During this time cross-linking

occurred between the excess groups on the surface of each layer thus bonding the layers. Devices with up to seven layers were fabricated using this technique. The channels were able to withstand pressures up to 20 psi, thus demonstrating the strength of the bond.

Several groups have developed techniques that use liquid PDMS as a glue between stacked layers [77, 78]. A “stamp-and-stick” technique was used to bond a fully cured, patterned PDMS layer to a glass slide [77]. Liquid PDMS was spun onto a slide at very high speeds (8000 rpm) to create a 1 – 1.5 μm thick layer of PDMS. After 15 minutes, the patterned PDMS layer was “stamped” onto the liquid PDMS layer, transferring 50% of the liquid onto the patterned layer. This structure was then placed onto a clean glass slide and bonded for 15 minutes at 90°C. Devices were built with various sizes and geometry (channels vs. squares) and were tested to determine the burst pressure. Channels with widths of 20 – 100 μm burst at 200 kPa (~29 psi) while squares of 1 – 2.5 mm could withstand pressures up to 400 kPa. No correlation was found between the burst pressure and channel size. Important findings were that the channel height and width must be greater than 20 μm and a wait period of 15 minutes was required to prevent the channels from filling in with the liquid PDMS layer when stamping. Another group at Stanford University used liquid PDMS as glue between two PDMS layers to form microchannels with a similar technique [78]. The authors diluted the liquid PDMS with toluene to achieve thinner layers (less than 1 μm) when spinning since the amount of liquid PDMS transferred when stamping must be less than 0.5 μm to prevent features from filling in. Channels with aspect ratios down to 1:7 (height:width) were fabricated using this technique. One difference from the “stamp-and-stick” technique described above is that the patterned PDMS layer was only partially cured for 20 min at 70°C versus being fully cured. The authors found that if the patterned PDMS layer was cured for more than 30 minutes bonding would not occur.

Bucaro et al. developed a different method to create a 3-D array of rectangular microchannels in PDMS [79]. Photolithography was used to create sacrificial line widths (channels) of photoresist in PDMS. A glass slide was coated with a thick layer (1 mm) of PDMS and cured. A 50-μm thick layer of photoresist was applied to the slide in four spin-coats, each at 4000 rpm for 20 seconds. The resist was soft baked on a hotplate at 90°C for 5 minutes after each spin-coat. After the final spin-coat, the photoresist was further baked for 30 minutes at 90°C. Next, the photoresist was exposed to UV light and developed to reveal line widths on the PDMS. Another layer of PDMS was cast onto the slide to cover the resist line widths. Finally, the resist was removed using a developer to open the channels in the PDMS. Channel widths of ten to several hundred microns were fabricated. This technique needs to be further evaluated for creating devices with multiple channel layers.

## 2.5 TISSUE ENGINEERING

### 2.5.1 Need for Endothelial Cells

Endothelial cells (ECs) line all of the blood vessels in the body and play a critical role in maintaining vascular homeostasis. Some of the important functions of endothelial cells include regulating vascular tone and blood pressure, controlling fluid permeability and solute flux across the vessel, orchestrating the adhesion and transmigration of leukocytes, directing angiogenesis, and maintaining the balance between coagulation (thrombosis formation) and fibrinolysis (thrombosis breakdown) [80, 81]. In a non-activated state, endothelial cells synthesize and secrete anticoagulant factors and exhibit anti-thrombogenic groups on their surface. Nitric oxide

(NO) and prostacyclin ($PGI_2$) are synthesized and secreted by ECs to induce vasodilation and to inhibit platelet activation, adhesion and aggregation. Tissue factor pathway inhibitor (TFPI) is also produced by ECs to prevent the activation of the extrinsic pathway of the coagulation cascade. Endothelial cells also release inhibitors of smooth muscle cell proliferation, which prevents intimal hyperplasia formation. The glycocalyx surface of endothelial cells prevents the adhesion of platelets. The surface also contains ectonucleotidases that metabolize adenosine diphosphate (ADP) to prevent platelet recruitment. Endothelial cells express thrombomodulin, a transmembrane protein that binds thrombin and coverts it to an anti-thrombotic form due to a change in confirmation. Anti-thrombin, when bound to glycosaminoglycans on the surface of ECs, can also bind thrombin to form an inactive complex. Lastly, endothelial cells can increase the level of fibrinolysis, the breakdown of fibrin, by secreting tissue plasminogen activator (tPA) [81, 82].

Under certain conditions, endothelial cells can become activated and shift the coagulation / fibronolysis balance towards a pro-coagulant state. ECs produce and store von Willebrand Factor (vWF), which is a protein that binds to Factor VIII, an important component of the intrinsic pathway, and stabilizes it to prevent breakdown. vWF is secreted at both a constitutive level and at a larger, more rapid level due to the release of amounts stored in the Weibel-Palade bodies of endothelial cells. When activated, ECs can express tissue factor and trigger the extrinsic pathway of coagulation. Also, plasminogen activator inhibitor-1 (PAI-1) is secreted from activated ECs to decrease fibrinolysis. Thus, it is important to confirm that endothelial cells are expressing an anticoagulant phenotype when utilizing the cells in tissue engineering applications.

Due to their inherent anticoagulant properties, researchers have been working towards seeding small diameter vascular grafts with endothelial cells to improve their patency. Synthetic grafts are inherently thrombogenic and are currently limited to larger vessel applications (> 6 mm diameter) and high flow regions. Reasons for small diameter graft failure include compliance mismatch between the graft and native vessel, poor surgical technique, graft occlusion due to thrombosis formation, and intimal hyperplasia at the anastomoses [83]. Thrombosis formation in small diameter grafts is attributed to the lack of an endothelial cell lining on the luminal surface. This problem will most likely be exacerbated in the microchannels of the artificial lung modules and provides the motivation for seeding ECs in our device.

Various seeding techniques, cell sources, and surface modifications have been explored to increase the success of culturing ECs in synthetic grafts. Cell seeding can be one-stage, in which the cells are harvested and introduced into the graft at implantation, or two-stage, in which the cells are seeded into the graft and cultured for a specific length of time to achieve complete graft coverage. Human endothelial cells can be harvested from nonessential vessels, such as the saphenous vein, or from microvascular sources, including the omentum and subcutaneous fat [82, 84]. Liposuction has the advantages of being less invasive than harvesting veins or arteries while providing large numbers of cells, over one million ECs per gram of fat [83]. Unfortunately, clinical trials using microvascular ECs from fat were not as successful as trials with venous ECs. This has been attributed to contamination of the EC population with other cell types and work has been done to improve EC purity to over 90% [85]. The graft lumens have been modified with adhesive proteins, such as collagen, fibronectin, and laminin, to improve EC adhesion. Other culturing techniques such as increasing the cell incubation time and culturing the cells under shear (shear conditioning) have also been shown to improve cell adhesion [86]. Similar seeding

and culturing procedures can be used to incorporate endothelial cells into the microchannels of the artificial lung modules. Several groups have already begun to evaluate EC growth in microchannels for tissue engineering purposes as described below.

### 2.5.2 Endothelial Cell Culture in Microchannels

The group led by Borenstein and Vacanti have pioneered the use of endothelial cells in 3-D microchannels [87-91]. Initial work by Borenstein et al. utilized soft lithography techniques in PDMS to create vascular networks that could be used to provide oxygen and nutrients to tissue engineered organs [89]. A fluid dynamics model was used to design a microvascular network that was fabricated on silicon wafers using photolithography. The wafers contained convex channels that were molded with PDMS. The semi-circular channels in PDMS were sealed with a flat PDMS sheet using oxygen plasma, sterilized in an autoclave, and surface modified with poly-L-lysine, gelatin, fibronectin, or collagen. The capillary network was connected to a recirculation flow loop consisting of a pump, oxygenator, reservoir, and bubble trap. Endothelial cells were dynamically seeded into the network using a peristaltic or positive displacement pump at flow rates of ~100 μl/min. Confluent cell monolayers were seen after 4 weeks of culture in semi-circular channels down to 30 microns in diameter. Vascular networks have also been constructed in biodegradable polymers, including poly(lactic-co-glycolic acid) and poly(glycerol sebacate), and similar endothelial growth and coverage was found [90].

Shin et al. expanded on this work by using immortalized human microvascular endothelial cells (HMEC-1) rather than primary ECs [91]. Immortalized cells have rapid expansion and can be passaged up to 50 times, a 5-fold increase compared to primary cells [80, 91]. The PDMS vascular networks were modified with collagen and incorporated into a single-

pass perfusion loop consisting of a syringe pump, oxygenator, air trap, and waste container. A concentration of 20 million cells/ml was injected into the network and left static for six hours to allow cell attachment. The network was then perfused with media at 0.5 ml/hr for up to 14 days of culture. The immortalized cells became confluent after only one week in culture, four times as fast as primary ECs, and remained confluent throughout the 14 days. A disadvantage of using immortalized cells is that they could possibly lose their endothelial characteristics leading to a loss of anti-thrombotic properties or tumor formation. Therefore, the use of immortalized cells is not currently accepted for clinical applications.

Another group led by Wang et al. are also exploring the use of microfabrication techniques to create artificial capillaries for tissue engineering [92-94]. Branching networks of channels with dimensions of 60 x 20 x 800 microns (w x h x l) were fabricated in polycarbonate, poly(dimethylsiloxane), poly(lactic-co-glycolic acid), and poly(methylmethacrylate). Bovine endothelial cells were seeded into the networks, perfused using a recirculation loop, and maintained in culture for up to 48 hours. Current work in focused on improving the culture system and examining longer culture periods.

In conclusion, endothelial cells possess anticoagulant properties that can potentially eliminate thrombosis in the microchannels of our artificial lung modules. The studies detailed above provide motivation that the formation of a confluent EC layer is feasible in PDMS microchannels. Chapter 5 discusses the experiments performed towards achieving this goal.

# 3.0 FABRICATION OF MODULES

## 3.1 INTRODUCTION

The goal of this thesis was to create three-dimensional modules in poly(dimethylsiloxane) (PDMS) consisting of layers of blood microchannels and gas pathways. The design requirements included fabricating blood channels with diameters of 100 μm or less, minimizing the inter-channel spacing, and minimizing the PDMS thickness between the blood and gas pathways (i.e. diffusion distance). Several fabrication techniques were evaluated based on the design requirements, as well as the cost and ease of fabrication. The techniques explored were molding tungsten wire arrays, molding SU-8 pillar arrays, creating sacrificial photoresist channels, utilizing photopatternable PDMS, and using soft lithography techniques. All of the fabrication techniques will be briefly described here and more detailed information is given in Appendix A.

The first technique consisted of creating 3-dimensional arrays of tungsten wires that could be molded with poly(dimethylsiloxane). The advantages of this technique included the ability to fabricate circular channels, low cost, and eliminating the need to handle thin PDMS layers. Tungsten wire was obtained in diameters from 15 - 100 microns (Alfa Aesar, Ward Hill, MA). A parallel array (10 x 10) of wires (Figure 3-1) was fabricated by using a metal screen to control the inter-channel spacing. The array was molded with PDMS and the wires were removed to create the 3-D microchannel prototype.

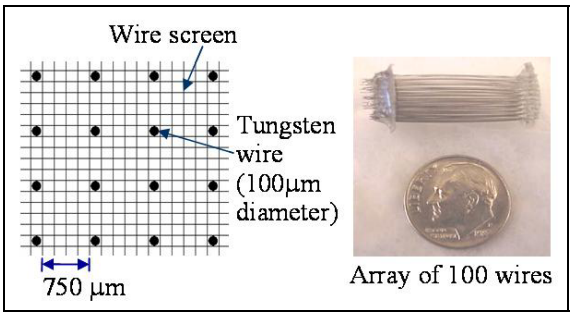


Figure 3-1: Parallel array of 100 tungsten wires

The array shown in Figure 3-1 contains 100 μm diameter wires with inter-channel spacing of 750 μm. This technique suffered from several limitations. The fabrication of arrays with smaller diameter wires was difficult due to the wires easily bending or kinking. The screen allowed inter-channel spacing down to 70 μm; however, fabrication became more difficult as the spacing decreased. Also, maintaining enough tension in the wires to keep them taut was challenging. Finally, only arrays of parallel wires could be fabricated, which makes manifolding the gas and blood pathways difficult.

A weaving loom and base were fabricated by our machinist, Brian Frankowski, in order to create perpendicular wire arrays and to eliminate the limitations described above. The weaving loom contained 25 small pins on each side to control the wire spacing. The loom could be screwed onto the base, which was fabricated to fit onto the vacuum chuck of a spin-coater. First a base layer of PDMS was spun onto the loom. Next, wire of any diameter was wrapped in one direction on the loom. PDMS was then spun onto the loom to cover the wires. The thickness of the PDMS could be controlled by the spin speed. Then, wire was wrapped onto the loom perpendicular to the previous layer, spin-coated with PDMS and cured. The process was repeated until the desired numbers of layers was achieved and then the wire was removed.

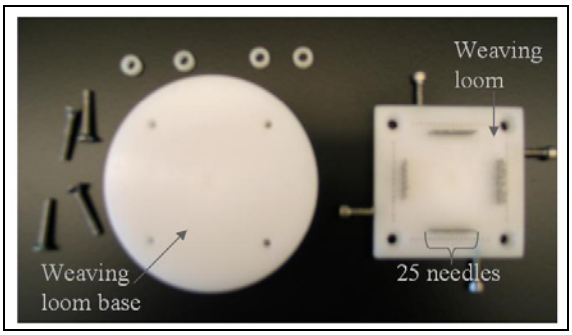


**Figure 3-2: Weaving loom used to create perpendicular gas and blood channels from wires**

This technique allowed for perpendicular gas and blood pathways, however, several disadvantages prevented further use. Wrapping the wires tightly by hand was difficult and time consuming. The minimum inter-channel spacing was limited to 300 μm, which was an order of magnitude greater than the achievable spacing with microfabrication techniques. The diffusion distance also became difficult to control after the fabrication of a few layers due to the formation of a meniscus between the pins.

The second fabrication technique utilized photolithography processing with a thick, epoxy based negative photoresist, SU-8, to produce an array of high aspect ratio pillars, which could be molded with PDMS (Figure 3-3). The SU-8 pillar technique produced circular channels with smaller and more controlled spacing than the tungsten wire methods. First, SU-8 (MicroChem Corp., Newton, MA) was spun onto a silicon wafer and baked to create a layer thickness (channel length) of 150 microns. Next, the SU-8 was exposed to UV light through a mask that contained circles with the desired channel diameter (21 – 70 μm) and spacing (21 – 49 μm). Cross-linking of the negative resist occurred in the areas that were exposed (the circles). A post-exposure bake was performed and then the resist was developed to remove the unexposed SU-8.

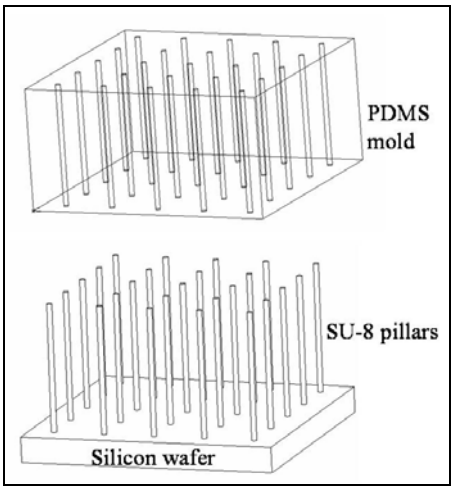


**Figure 3-3: Schematic of SU-8 pillar array and corresponding PDMS mold**

The length of the channels was a limitation of this processing. SU-8 can be used to create features that are several hundred microns thick; however, the processing becomes more challenging as the thickness increases. The channels for the biohybrid lung need to be several millimeters long. Layers of PDMS that were molded on the pillars could be stacked to elongate the channels, but the high degree of alignment necessary would be quite challenging. Also, some pillars would likely be pulled off when peeling the PDMS off the wafer, thus ruining the silicon wafer molds [95]. Another disadvantage of this technique was that only parallel arrays of channels could be fabricated thereby increasing the complexity of manifolding the gas and blood pathways.

The next fabrication technique consisted of creating sacrificial photoresist channels in PDMS [79]. This technique (Figure 3-4) eliminated the handling and stacking of thin PDMS layers making it easier to minimize the diffusion distance between the gas and blood pathways. Also, perpendicular blood and gas pathways could easily be fabricated by rotating the mask or using different masks for each pathway. First, a thin layer of PDMS was spun onto a plain silicon wafer. Next, positive photoresist was spun on top of the PDMS and soft baked to create a

thickness equal to the desired channel height. The photoresist was exposed to UV light through a mask that contained the channel patterns. The exposed areas of the positive resist were broken down; the opposite of negative resist, which was cross-linked due to exposure. Developing away the exposed resist rendered photoresist lines (channels) with the desired channel widths and spacing. Rectangular channels were typically constructed using photolithography; however, semi-circular channels could be fabricated by reflowing the resist after development. Next, another thin layer of PDMS was spun on top of the patterned resist and was cured. This process could be repeated until the desired number of layers was achieved. Finally, the sacrificial photoresist was removed.

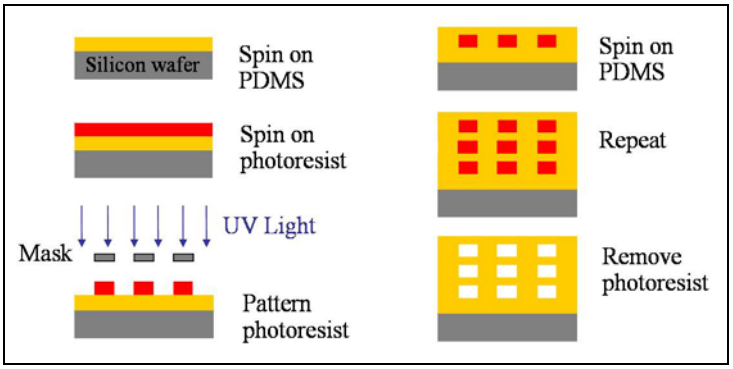


**Figure 3-4: Fabrication of sacrificial photoresist channels in PDMS**

One of the challenges with fabricating sacrificial photoresist channels is poor adhesion of the resist on the hydrophobic PDMS surface. Oxygen plasma was used to increase the hydrophobicity of PDMS and increase resist adhesion; however, delamination of smaller features still occurred. Another challenge with this technique is completely removing the photoresist from the module. As more layers are stacked, the bottom layers of resist are baked for longer periods of time, thus increasing the difficulty in removing the resist.

The use of photopatternable PDMS was also explored to create 3-dimensional modules using photolithography. Photopatternable PDMS acts as a negative resist, so layers can be exposed and patterned using UV light. The advantage of this processing (Figure 3-5) was the elimination of handling and stacking thin layers of PDMS, thus making it easier to minimize the diffusion distance for gas exchange. This technique is an improvement to the sacrificial photoresist technique described above because the adhesion problems between resist and PDMS have been eliminated. First, a thin layer of PDMS was spun onto a silicon wafer and cured. Next, photopatternable PDMS was spun onto the wafer with a thickness equal to the desired channel height. The photopatternable PDMS was exposed to UV light through a mask, and the exposed areas were cross-linked. Another thin layer of PDMS was spun onto the wafer to cover the exposed layer. This process can be repeated until the desired number of layers is achieved. Lastly, the unexposed PDMS is removed to open the channels.

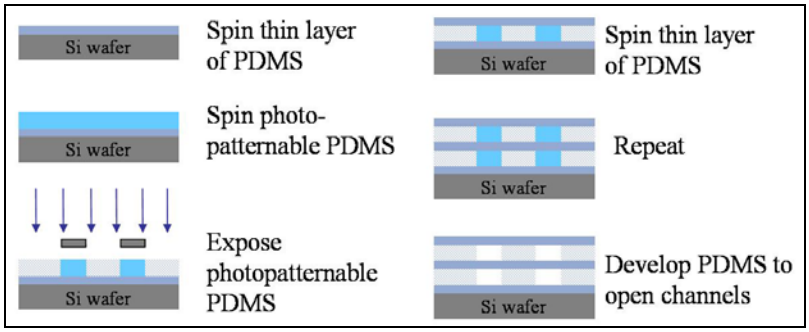


**Figure 3-5: Schematic of fabrication process for Photopatternable PDMS**

The photopatternable PDMS was difficult to work with due to tackiness of the material even after soft baking. The material itself is quite expensive in addition to the cost of performing lithography for each layer. The biggest challenge with this technique, however, is performing lithography for multiple layers. The unexposed PDMS of the lower channel could potentially be

cross-linked when the upper layer is exposed due to light reflection, thus rendering the lower channels unable to be developed. Also, the bottom (unexposed) channels are soft baked for longer periods of time as the number of layers increase, which increases the difficulty to develop the PDMS.

Lastly, soft lithography was explored and found to be the best technique for fabricating prototype modules. Initially, the soft lithography technique consisted of double molding and stacking PDMS layers (Figure 3-6). Semi-circular channels were etched into a silicon wafer using xenon difluoride plasma. Next, a negative cast of the channels was fabricated by molding the wafer with PDMS. The negative cast was then coated with parylene to provide a non-stick surface. PDMS was molded on the negative cast using weights to control the thickness of the layers. Finally, the layers could be stacked and bonded to form a module. The advantages of this technique included the ability to create semi-circular channels and to accurately control channel width, height, and spacing.

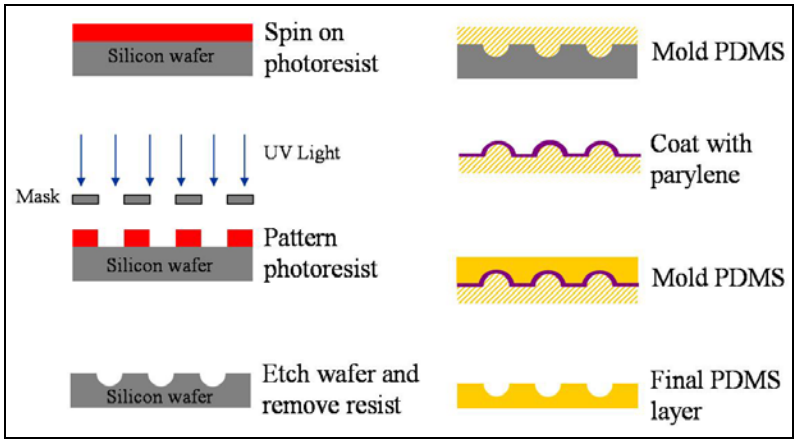


**Figure 3-6: Schematic of double molding process to create PDMS layers**

This process was further improved to eliminate the need for double molding. Positive photoresist was patterned to create the inverse of the channels on silicon wafer masters. The silicon wafers were then spin-coated with PDMS, which allowed more control over the thickness of the layers than the weighted molding technique. This soft lithography process was used to fabricate first and second generation modules as described in the following sections.

## 3.2 FIRST GENERATION MODULES

The first generation modules were designed to consist of alternating layers of perpendicular blood and gas microchannels. Photolithography techniques were used to create silicon wafer masters that contained rectangular, positive photoresist ridges with the desired channel width (30, 50, or 100 μm), height (20 μm), and spacing (100 μm). PDMS is typically mixed 10:1 (pre-polymer:curing agent) by weight and can either be cured at room temperature or at an elevated temperature to accelerate curing. For the first generation modules, two solutions of poly(dimethylsiloxane) were mixed using ratios of 20:1 (more pre-polymer) and 10:2 (more curing agent). The solutions were each spun onto two silicon masters and partially cured. The individual PDMS layers were stacked by alternating the 20:1 and 10:2 layers. The module was cured overnight to bond the layers, and then polycarbonate manifolds were attached to create blood and gas inlet and outlet ports. A flow chart of the entire fabrication process is shown in Figure 3-7. The steps in red, designing and fabricating the mask, are described in Section 3.2.1. Fabrication of the silicon wafer masters (blue) is detailed in Section 3.2.2. Finally, the molding, stacking and bonding of the PDMS layers is discussed in Section 3.2.3.

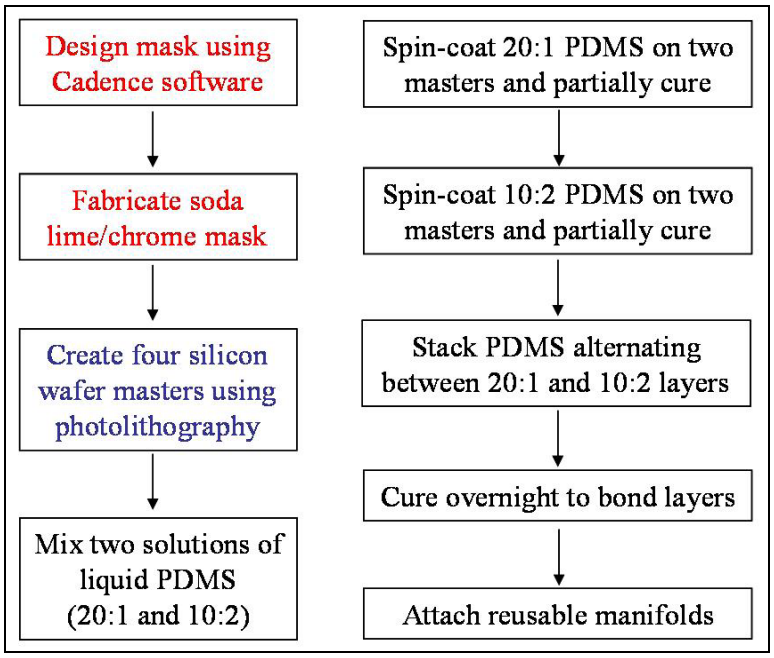


**Figure 3-7: Flow chart of fabrication process for first generation modules**

### 3.2.1 Mask Design and Fabrication

The mask was designed using the Virtuoso Layout Editor in Cadence software (Cadence, San Jose, CA). The mask layout was a 3.5 inch square and contained 12 patterns that were each 1.5 cm long and 1 cm wide (Figure 3-8). The patterns consisted of lines (i.e. channels) that were either 30, 50, or 100 microns wide with 77, 67, or 50 lines per pattern, respectively. Spacing between the lines was maintained at 100 microns for all of the patterns. Four patterns of each line width were drawn on the layout and are shown in the figure below.

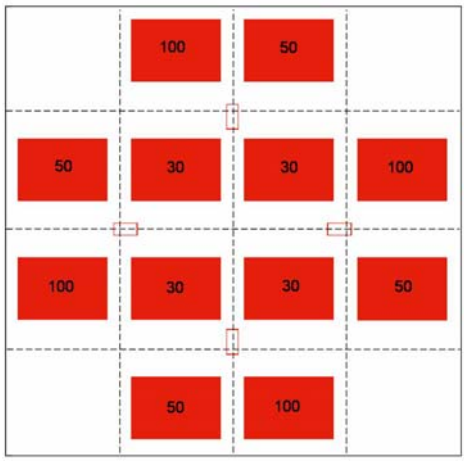


**Figure 3-8: Mask design for first generation modules**

The design was then exported from Cadence as a .gds file. The mask fabrication was done at Carnegie Mellon University in the MEMS Chemistry Lab using a direct write laser (DWL) lithography system (Heidelberg DW66, Heidelberg, Germany). A five-inch square soda lime/chrome mask containing a layer of AZ1518 photoresist (Nanofilm, West Lake Village, CA) was placed onto a stage in the DWL machine. The .gds file was loaded onto the DWL computer, converted to .lic format and then transferred to the DWL machine. The direct write system works by scanning a laser onto the mask as the stage moves back and forth in the y-direction while stepping forward in small increments in the x-direction. The photoresist on the mask is positive, so exposure to the laser breaks down the resist allowing it to be removed (developed). The mask was written overnight (approximately 10 hours) using 25% energy and a 10mm lens, which corresponds to a 1.7 μm spot size. The exposed photoresist on the mask was then developed using AZ400K developer (Clariant Corporation, Somerville, NJ) diluted with DI water in a 1:3 ratio. The exposed chrome was etched away using chromium mask etchant for 2 minutes. The remaining (unexposed) photoresist was removed using acetone leaving just the chrome pattern on the mask.

### 3.2.2 Photolithography

The photolithography processing was performed in the Nanofabrication Facility at Carnegie Mellon University. Silicon wafers were purchased from Montco Silicon Technologies, Inc. (100mm <100> single side polished, test grade silicon wafers, Spring City, PA). First, the wafer was cleaned with acetone and propanol and dried with a nitrogen gun. The wafer was then dehydrated in a 200°C oven for 15 minutes. Hexamethyldisilazane (HMDS) was spun onto the wafer using a Solitec Photoresist Spinner (Solitec Wafer Processing, Inc., Milpitas, CA) in order to promote photoresist adhesion. The HMDS spin recipe included a six-second spread at 500 rpm and a thirty-second spin at 3000 rpm. Next, positive photoresist (AZ4620, Clariant Corporation, Somerville, NJ) was spun onto the wafer using a six-second spread at 500 rpm to coat the wafer with resist and then a thirty-second spin at 3000 rpm to create a thickness of 9-10 microns. A five-minute rest period was used to eliminate any non-uniformity in the resist coating. The wafer was then soft baked for 30 minutes in a 90°C oven. The soft bake partially removes solvents in the resist and improves uniformity of the resist coating, adhesion to the wafer, and line-width control. A second layer of photoresist was applied using the same spin recipe, rest period, and soft bake as described above to produce a total thickness of approximately 20 microns. Another rest period of one-hour was used to allow rehydration of the photoresist. During this time, the photoresist edge bead was removed in order to promote uniform contact between the mask and the wafer. The wafer and mask were placed into a Karl Suss MA56 Mask Aligner (SUSS MicroTec, Inc., Waterbury Center, VT) and exposed for 60 seconds using a power density of 14 $mW/cm^2$. The wafer was developed 30 minutes after exposure using AZ400K developer diluted with DI water in a 1:3 ratio.

### 3.2.3 Molding, Stacking, and Bonding PDMS Layers

Four silicon wafer masters were placed into a vacuum dessicator (Fisher Scientific, Pittsburgh, PA) along with a small beaker containing 30 - 50 microliters of tridecafluoro-1,1,2,2-tetrahydrooctyl-1-trichlorosilane (United Chemical Technologies, Inc., Bristol, PA) for at least two hours. The silanating treatment improved the release of the PDMS from the silicon master. For our bonding technique, two solutions of PDMS were mixed: solution A contained a higher ratio of prepolymer (20:1) and solution B contained a higher ratio of curing agent (10:2). Each PDMS solution was mixed in a glass beaker with a metal spatula. The beakers were then placed in a vacuum oven (Fisher Isotemp Model 281, Fisher Scientific, Pittsburgh, PA) at room temperature, and vacuum was applied until the solutions were completely de-aired. Next, a wafer was spin-coated (WS 400A-6NPP/LITE, Laurel Technologies, North Wales, PA) with approximately five grams of solution A using the following spin recipe: twenty-second spread at 200rpm (86 rpm/s acceleration) and a one-minute spin at 200rpm (86 rpm/second acceleration). A five-minute rest period was used to eliminate any non-uniformity in the PDMS coating. The wafer was then partially cured for 5 minutes at 100°C in the Isotemp oven. This process was repeated for a second wafer using solution A and for two additional wafers using solution B. The only difference in processing with solution B was that the partial curing time was reduced from 5 minutes down to 2 minutes, since this solution contained more curing agent and, therefore, cured faster. The curing times were established by finding the minimum time needed for the layers to be firm enough to handle with tweezers. After curing, the PDMS was cut around the patterns as shown in Figure 3-8. A plain square slab of PDMS from a solution B wafer was removed and placed on a glass slide to be used as the base of the module. Next, a patterned PDMS square from solution A was removed from the wafer and the two ends were cut in order to open the

channels. This could not be done while the PDMS was still on the wafer because it would damage the photoresist. Both the plain slab of PDMS and the patterned square were cleaned with ethanol to eliminate any dust that could prevent bonding. The patterned PDMS square was placed, using tweezers, with the channels facing down on top of the plain slab thereby sealing the channels. Avoiding dust and air entrapment between the layers was critical for bonding. A small amount of ethanol between the layers allowed the top layer to easily be aligned with the bottom. Next, a patterned square with the same channel width was removed from a wafer with solution B. The patterned square was cut and rinsed with ethanol and placed on top of the module with the channels facing down and perpendicular to the channels below it. This process was repeated alternating the layers from solutions A and B until 14 layers of channels were stacked. After each layer was added, the module was examined under a microscope to ensure that no air or dust was trapped between the layers. The module was then completely cured at 100°C overnight to bond the layers. The corners of the modules were cut as shown in Figure 3-9 to allow the ends of the module to fit into manifolds discussed below. The final size of the module was 1.3 x 1.3 x 0.45 cm (l x w x h) and contained seven layers of blood channels and seven layers of gas channels. Modules were fabricated with channel diameters of 30, 50, or 100 μm and contained 1078, 938, or 700 channels, respectively. Images of the cross-section of two modules with channels widths of 100 and 50 μm are shown below.

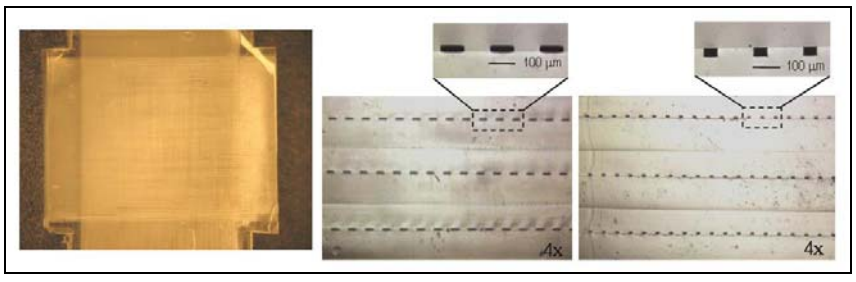


**Figure 3-9: Top view and cross-section of modules with 100 and 50 μm wide channels**

Manifolds were fabricated to create gas and blood inlet and outlet ports for the module. Four manifolds were fabricated in polycarbonate and each contained a female luer that could easily be connected to a perfusion loop. Each side of the module was inserted into a recessed area on the end of a manifold and was attached using silicone. A module with blood and gas manifolds is shown in Figure 3-10. There were several key features of these manifolds. They were transparent, which was important both for the cell culture work and for examining the module for leaks. The manifolds were also reusable, easy to sterilize, and had a very small priming volume.

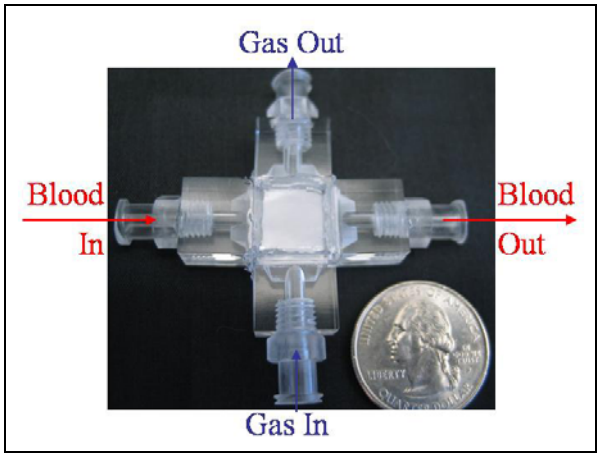


**Figure 3-10: Picture of module with four manifolds for blood and gas pathways**

### 3.2.4 Limitations of First Generation Modules

Modules containing 14 layers of blood and gas pathways were successfully fabricated; however, several limitations needed to be addressed. The most challenging part of fabricating the modules was handling the PDMS layers with tweezers. The layers were spun at 200 rpm, corresponding to a PDMS thickness over 300 μm. This thickness allowed easy handling of the layers but would

cause a large resistance to gas transfer. Layers that were spin-coated at 1000 rpm to produce a thickness less than 100 μm were too thin to handle with the tweezers. Another limitation of the fabrication process was the variability in the partial curing times for the two different solutions of PDMS. A curing time of 5 minutes was used for the mixture with more pre-polymer. This time was minimized to allow enough reactive groups on the surface to still be available for cross-linking with the adjacent layers. However, these layers were very tacky, which made it difficult to peel them off of the wafer. Also, if the layers were too tacky, channels in the subjacent layers could become filled in with PDMS ruining the module. There was also day-to-day variability in the degree of tackiness after curing for 5 minutes. Often the layers had to be cured for an additional 30 seconds to one minute in order to be able to peel and stack the layers. The design of the blood and gas pathways as perpendicular channels of the same size was another limitation of the modules. In this arrangement, the interaction between the pathways was restricted to where the channels crossed. This interaction could be improved by creating parallel gas and blood channels; however, this increases the complexity of creating inlet and outlet manifolding. Finally, improvements were needed in manifolding the module. The polycarbonate manifolds were very difficult to seal to the module and leaking frequently occurred.

## 3.3 SECOND GENERATION MODULES

The design and fabrication of the second generation modules were modified to address the limitations described above. First, two masks were designed: one for the blood microchannels and one for the gas pathways. The gas design was changed from an array of microchannels to one large, open pathway with pillar supports (Figure 1-1). This maximized the interaction

between the gas and blood layers. Next, improvements were made to the stacking and bonding methods for second generation modules to allow the use of thinner PDMS layers. Double-sided heat release tape (Revalpha 90°C, Nitto Denko America, Fremont, CA) was found to be the best method to handle the thin PDMS layers. The tape eliminated the need to use tweezers and allowed the layers to be easily peeled off the wafer and rolled down onto the module. The modules were fabricated by bonding one layer at a time rather than stacking all the layers and then bonding. Changing the curing ratio did not work to bond layers in this manner, so a method was developed to bond layers by partial curing. Finally, a manifolding technique was developed that eliminated the polycarbonate fixtures and prevented leaks. The following section (3.3.1) describes the mask design and fabrication. The photolithography processing is detailed in Section 3.3.2. Finally, the improved stacking, bonding, and manifolding techniques are discussed in Section 3.3.3.

### 3.3.1 Mask Design and Fabrication

New blood and gas masks were designed using Cadence software and fabricated using the direct write lithography machine as described in Section 3.2.1. The blood mask design was 4 x 4 inches and consisted of four patterns as shown in Figure 3-11. Each pattern contained an inlet region, an array of 56 channels, and an outlet region. The channels were 100 μm wide and 1.8 cm long with an inter-channel spacing of 50 μm. The inlet and outlet regions were created to allow for easier manifolding of the channels. These regions were open pathways with 100 μm diameter pillars used to prevent the region from collapsing. The pillars were spaced 400 μm apart in the y-direction and 200 μm apart in the x-direction.

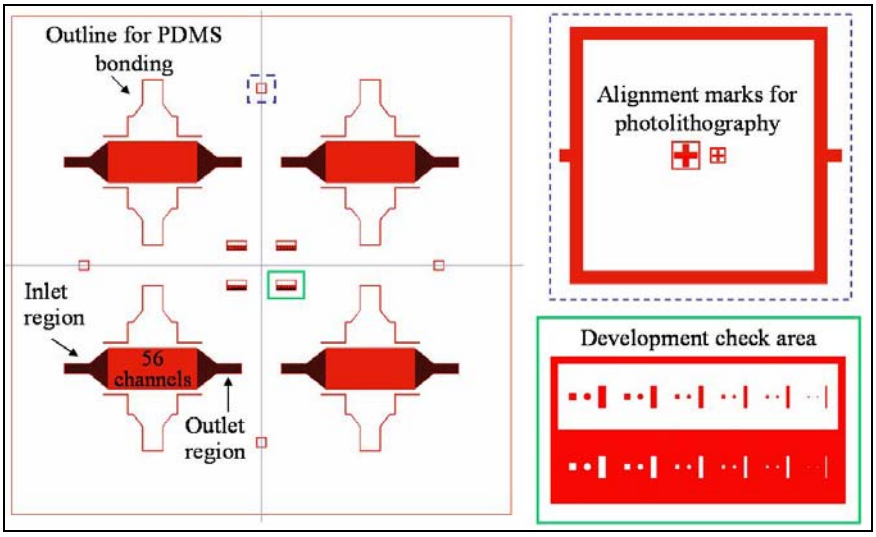


**Figure 3-11: Blood mask design (left) for second generation modules including alignment marks (top) and development areas (bottom)**

The red outlines above and below the microchannels are used to align the blood and gas layers when stacking. The mask also contained 4 small patterns in the center that were used to examine the exposure and development protocol. Each pattern was 4000 x 2000 μm and contained a light field and a dark field area, which would create posts or holes in positive photoresist, respectively. There were six groups of differently sized structures, each group containing a square, a circle, and a rectangle. The size of the structures varied from 20 μm to 100 μm. The mask also contained four alignment marks towards the edges of the mask that contained features consisting of a cross in a square. These alignment marks were not used to stack the individual PDMS layers as described below. However, the alignment marks were included in the mask design since they were important for several of the other fabrication techniques described in Appendix A.

The gas pathway mask (Figure 3-12) consisted of four patterns in a 3 x 3 inch square. Each pattern consisted of a large, open gas pathway containing pillar supports. The pillars were

100 μm in diameter and spaced 200 μm apart in both the x and y-directions. The mask also contained exposure and development check areas, as described for the blood mask, and corresponding alignment marks. The lines surrounding the patterns were used to help align the gas and blood pathways when stacking the individual PDMS layers described below in Section 3.3.3.2.

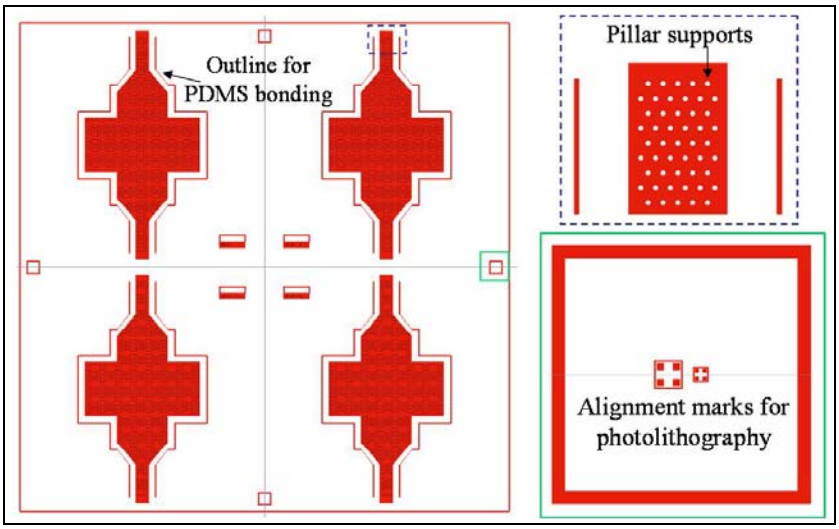


**Figure 3-12: Gas mask design (left) for second generation modules including pillar supports (top) and alignment marks (bottom)**

### 3.3.2 Photolithography

The photolithography processing for the second generation modules was performed in the John A. Swanson Micro and Nanosystem (JASMiN) Laboratory at the University of Pittsburgh. The processing was slightly different from the first generation modules due to the use of hotplates instead of ovens. Hotplates bake the resist from the bottom up due to conduction and require less time than when baking in an oven, which bakes from the top down. The silicon wafer was

dehydrated on a 200°C hotplate for 30 minutes. Hexamethyldisilazane (HMDS) was spun onto the wafer using a Karl Suss RC8 Spinner (SUSS MicroTec, Inc., Waterbury Center, VT) in order to promote photoresist adhesion. The HMDS spin recipe included a ten-second spread at 100 rpm (300 rpm/s acceleration) and a thirty-second spin at 3000 rpm (1000 rpm/s acceleration). The wafer was then placed on a 95°C hotplate for three minutes. Next, AZ4620 photoresist was spin-coated onto the wafer using a three-step recipe. First, the resist was dynamically dispensed onto the wafer via a dropper while the wafer was spinning at 100 rpm (500 rpm/s) for 45 seconds. Second, the resist was spread on the wafer using a spin speed of 500 rpm (1500 rpm/s) for ten seconds. Finally, the lid on the spin-coater was closed and the wafer was spun at 2000 rpm (1500 rpm/s) for thirty seconds. A five-minute rest period was used to eliminate any non-uniformity in the resist coating. The wafer was then soft baked for seven minutes on a 95°C hotplate. A second layer of photoresist was applied using the same spin recipe and rest period to produce a total thickness of approximately 30 microns. The second layer of resist was baked for ten minutes on the 95°C hotplate. Another rest period of one-hour was used to allow rehydration of the photoresist. The wafer and mask (either blood or gas mask) were placed into a Karl Suss MA 6 Double-Side Mask Aligner (SUSS MicroTec, Inc., Waterbury Center, VT) and exposed for 50 seconds. The wafer was developed using AZ400K developer diluted with DI water in a 1:3 ratio. The last step of the photolithography process was to hard bake the wafer on a hotplate at 125°C for 15 minutes. Hard bakes were used to drive out any remaining solvent in the resist and increase the adhesion between the resist and the wafer. The hard bake also caused the photoresist to reflow slightly thus rounding the top of the resist. The wafers in Figure 3-13 are the result of the photolithography processing and are ready to be molded with PDMS.

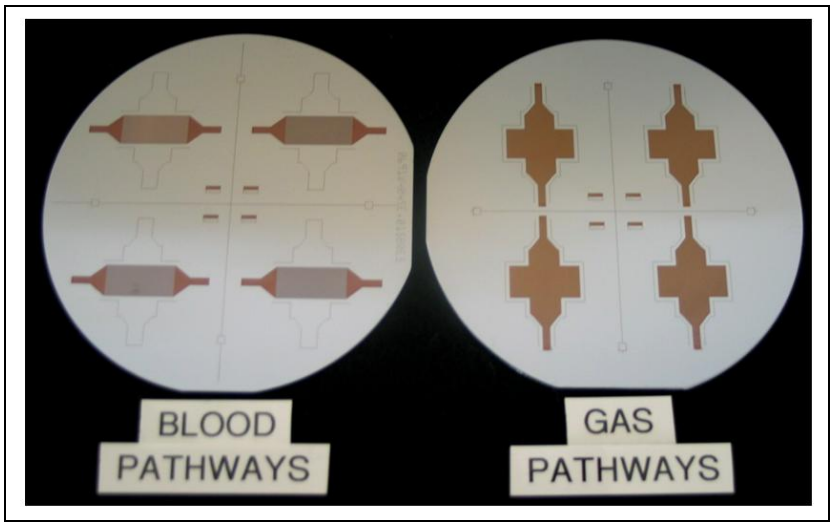


**Figure 3-13: Picture of silicon wafers with blood and gas pathways**

### 3.3.3 Molding, Stacking, and Bonding PDMS Layers

All modules were fabricated in the Medical Devices Laboratory at the University of Pittsburgh using the following protocol. Detailed methods to fabricate both cell culture and gas permeance modules are described below.

#### 3.3.3.1 Cell Culture Modules

1. The silicon wafer masters that were patterned with the blood pathways described in Section 3.3.1 were diced into four chips, each chip containing one pattern. To dice a wafer, a glass cutter was used to scratch a 2 – 3 mm line on the edge of the wafer. A small needle was placed directly under the scratch on the wafer. Tweezers were then used to put pressure on the wafer on each side of the needle until the wafer broke in half. This process was repeated to break the wafer into four chips.

2. Two patterned chips and three plain silicon wafers were placed into a vacuum dessicator along with a small beaker containing 30 - 50 microliters of tridecafluoro-1,1,2,2-tetrahydrooctyl-1-trichlorosilane for at least one hour.

3. The Fisher Isotemp vacuum oven was pre-heated to 65°C.

4. PDMS (Sylgard 184) was mixed in a 10:1 ratio (pre-polymer:curing agent) by weight. In detail, ten grams of pre-polymer and one gram of curing agent were added to a glass beaker. The two parts were mixed using a metal spatula for one minute, allowed to rest for one minute, and then mixed again for another minute. Two eppendorf tubes were each filled with 1.5 ml of PDMS and centrifuged (Galaxy 7, VWR, West Chester, PA) for two minutes to remove the air bubbles that were introduced during mixing. The remaining PDMS was placed in a 15 ml conical tube and also centrifuged for two minutes (Centrific Model 228, Fisher Scientific, Pittsburgh, PA). The PDMS was not used until 30 minutes after mixing according to the manufacturer's recommendation.

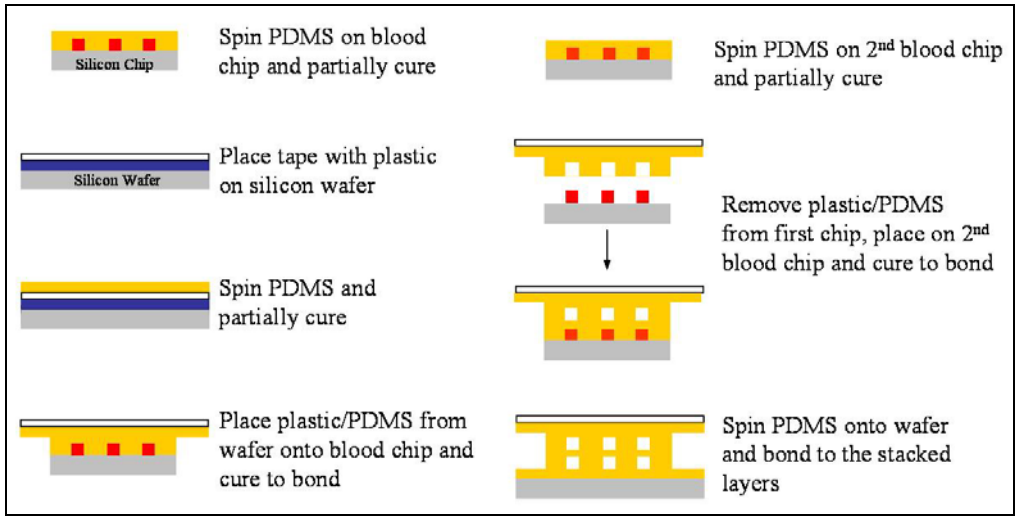


**Figure 3-14: Schematic of fabrication process for cell culture modules**

The following fabrication steps are shown in Figure 3-14.

5. PDMS from one eppendorf tube (1.5 ml) was carefully poured onto a patterned chip to completely cover the photoresist. The chip was then positioned on a thick acrylic plate, which was placed into the vacuum oven. A vacuum of -28 inHg was applied for 1 minute in order to remove any air bubbles that were introduced during pouring or trapped within the photoresist structures. If air bubbles still existed, the vacuum could be released and re-applied to completely eliminate the bubbles. Applying the vacuum was especially important for the inlet and outlet regions, which contained holes in the photoresist that would fill with PDMS to become pillars.

6. After applying the vacuum, the chip was removed from the oven and spin-coated using a twenty-second spread at 500 rpm and a one-minute spin at 1000 rpm. A five-minute rest period was used to eliminate any non-uniformity in the PDMS layer. The chip was then placed onto a thin acrylic plate and partially cured in the oven for 20 minutes at 65˚C. The acrylic plates were used to easily move the chips into and out of the oven without touching the chips.

7. Meanwhile, a handling layer was fabricated using double-sided heat release tape. The tape was supplied as 6 x 6 inch squares and each adhesive side was protected by a clear piece of plastic, one side thicker than the other. The tape was cut into a 3 x 3 inch square and the thicker side of plastic was removed. The adhesive side of the tape was then placed onto a silanated wafer. Approximately four grams of PDMS from the conical tube was spin-coated onto this wafer using the same spin recipe, rest period, and partial curing time as the chip in Step 6.

8. After the wafer was partially cured, the piece of plastic, which now had a layer of PDMS on it, was removed from the wafer and placed PDMS-side down onto the partially cured chip. The PDMS was inspected to ensure that no air or dust was trapped between the layers during this step. This structure was placed in the oven (65˚C) for twenty minutes in order for the two layers of PDMS to bond.
9. Meanwhile, a second chip was spin-coated, as described in Steps 5 and 6, and partially cured for twenty minutes.
10. Next, more PDMS was mixed 10:1 as described in Step 4, placed into a 15 ml conical tube, and centrifuged.
11. After the second chip (from Step 9) was cured, the structure on the first chip was peeled off of the mold parallel to the channels, placed down on the second chip, and bonded for forty minutes at 65˚C. Using shorter bonding times resulted in the two patterned layers of PDMS pulling apart when trying to peel the module from the second chip. The layers were aligned using the photoresist outlines above and below the channels, as shown in Figure 3-11. The structure must be slowly rolled down onto the second chip using a smooth motion starting from the outline below the channels, moving across the channels, towards the top outline. Touching any areas of the inlet region, channels or outlet region can cause the PDMS to fill in those areas and thus must be avoided.
12. Concurrently, a plain silicon wafer was spin-coated with the newly mixed PDMS (from Step 10) using a twenty-second spread at 500 rpm and a one-minute spin at 1000 rpm. A five-minute wait period was used and then the wafer was partially cured for twenty minutes at 65˚C.

13. Next, the PDMS structure was peeled from the second chip, carefully rolled down onto the wafer sealing the bottom layer of channels, and bonded for twenty minutes at 65˚C.

14. Simultaneously, more PDMS was mixed 10:1 as described in Step 4, placed into a 15 ml conical tube and centrifuged.

15. Next, the module was cut into the shape shown in Figure 3-15 (top left) and the layer of plastic was removed from the top of the module exposing the PDMS. Small rings, which were 2 mm slices of a 3 ml plastic syringe, were placed on the ends of the inlet and outlet regions. The rings were filled with PDMS and cured for 40 minutes at 65˚C to create a thick enough area for tubing to be inserted.

16. Holes were punched in the center of the rings through the entire module thickness using 3 mm diameter biopsy punches (Premiere Uni-Punch, Fisher Scientific, Pittsburgh, PA).

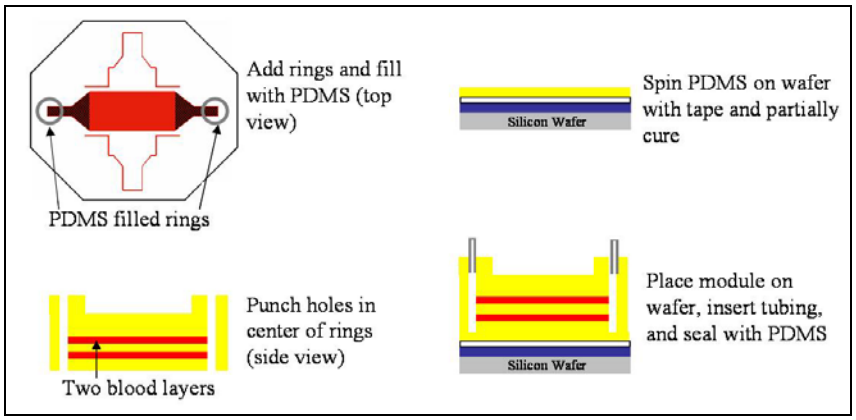


**Figure 3-15: Schematic depicting manifolding technique for second generation modules**

17. Meanwhile, double-sided tape was placed on the third silicon wafer and was spin-coated with most recently mixed PDMS (Step 14) using a twenty-second spread at 500 rpm and a thirty-second spin at 500 rpm. After a five-minute rest period, the wafer was partially cured for fifteen minutes at 65˚C.

18. The module was peeled off the wafer and placed onto the third wafer.

19. Silicone tubing (1/16” diameter, 1” long) was inserted into the holes to the bottom of the rings. Liquid PDMS was placed around the tubing and the edges of the module to prevent leaks [96].

20. Finally, the module was baked overnight at 80°C to completely cure the PDMS and create strong bonds between the layers.

A cell culture module with two layers of channels is shown in Figure 3-16. The scanning electron micrographs in Figure 3-17 demonstrate that the PDMS mold accurately replicates the resist on the silicon chip and that the channels exhibit a rounded shape. Very few flaws were seen in the PDMS mold and were most likely due to pulling the PDMS off of the chip.

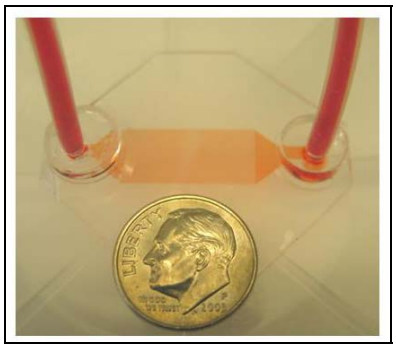

**Figure 3-16: Picture of cell culture module perfused with red dye**

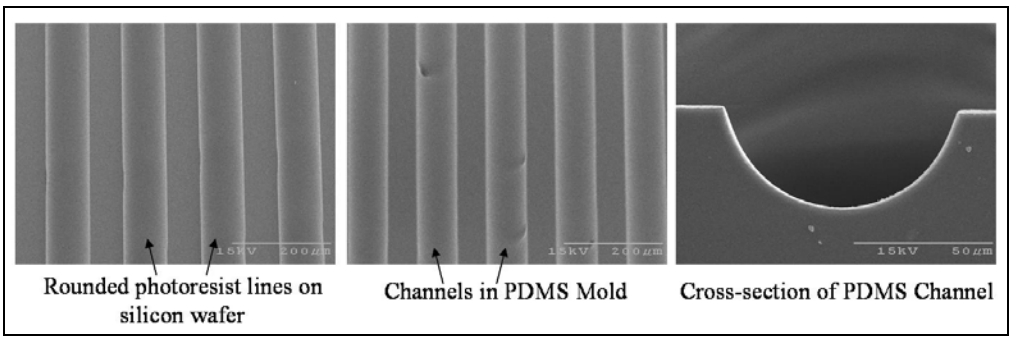


**Figure 3-17: SEMs of silicon blood chip and PDMS mold containing microchannels**

### 3.3.3.2 Gas Permeance Modules

The gas permeance modules were fabricated similarly to the cell culture modules. Two modules, each consisting of two gas layers and one blood layer, were fabricated simultaneously using the process shown in Figure 3-18. These two modules were then bonded together to form a gas permeance module with a total of six layers, which was the minimum number of layers required in order to be able to perform gas permeance testing (Chapter 4). Layers were spun at either 500 or 1000 rpm to examine the effects of thickness on permeance. This section describes the processing steps in detail.

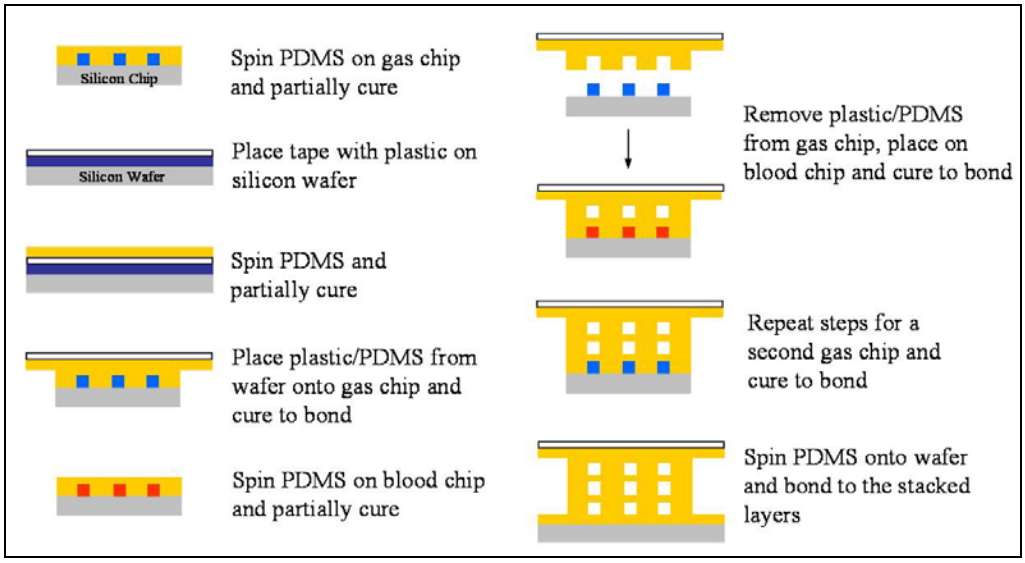


**Figure 3-18: Schematic of fabrication process for gas permeance modules**

1. The silicon wafer masters that were patterned with the blood and gas pathways were diced into four chips, each chip containing one pattern (see Step 1 of cell culture modules for details on dicing wafers).
2. Four gas chips, two blood chips, and five plain silicon wafers were silanated to improve PDMS release.

3. Meanwhile, the Fisher Isotemp vacuum oven was pre-heated to 65°C.
4. PDMS (Sylgard 184) was mixed, as described for the cell culture modules, using twenty grams of pre-polymer and two grams of curing agent. Four eppendorf tubes were each filled with 1.5 ml of PDMS, and the remaining PDMS was evenly distributed into two 15 ml conical tubes. The PDMS was centrifuged for 2 minutes to remove air bubbles.
5. After thirty minutes, PDMS from two eppendorf tubes (1.5 ml) was carefully poured onto two gas chips to completely cover the photoresist. The chips were placed in the oven and vacuum of -28 inHg was applied for one minutes to remove any air bubbles that were introduced during pouring or trapped within the photoresist structures.
6. Next, both chips were spin-coated using a twenty-second spread at 500 rpm and a one-minute spin at either 500 or 1000 rpm. A five-minute rest period was used to eliminate any non-uniformity in the PDMS layer. The chips were then placed onto a thin acrylic plate and partially cured in the oven for 20 minutes at 65˚C.
7. Meanwhile, the double-sided heat release tape was placed onto two silanated wafers. Approximately four grams of PDMS from the conical tubes was spin-coated onto each wafer using the same spin recipe, rest period, and partial curing time as the chip (Step 6).
8. After the chips and wafers were partially cured, the handling layers (plastic with PDMS) were removed from the wafers, placed onto the gas chips, and bonded in the oven for twenty minutes at 65˚C.
9. Meanwhile, two blood chips were spin-coated, as described in Steps 5 and 6, and partially cured for twenty minutes at 65˚C.
10. Next, PDMS was mixed using 15 grams of pre-polymer and 1.5 grams of curing agent, placed into two eppendorf tubes and a conical tube, and centrifuged for two minutes.

11. After the blood chips were cured, the PDMS was peeled off of the gas chips, placed down onto the partially cured blood chips, and bonded for forty minutes at 65˚C. The layers were aligned using the photoresist outlines shown on the masks (Figure 3-11 and 3-12). The structure must be slowly rolled down onto the blood chip using a smooth motion starting from the end of the gas pathway and moving to the other end. Touching any areas of the gas pathway can cause the PDMS to fill in those areas and thus must be avoided.
12. Concurrently, two more gas chips were spin-coated with the fresh PDMS (Step 10) using the same spin recipe as in Step 6 and were partially cured for twenty minutes at 65˚C.
13. Next, the PDMS structures were peeled from the blood chips (parallel to channels), placed onto the new gas chips, and bonded for forty minutes at 65˚C.
14. Meanwhile, two plain silicon wafers were spin-coated with the newly mixed PDMS (Step 10) using the same spin recipe and were partially cured for twenty minutes at 65˚C.
15. Next, the PDMS structures were peeled from the gas chips, carefully rolled down onto the wafers, and bonded for twenty minutes at 65˚C to form two three-layer modules.
16. Simultaneously, more PDMS was mixed 15:1.5, placed into a 15 ml conical tube, and centrifuged for two minutes.
17. The plastic was removed from the one of the modules and PDMS was spun onto this module using the same spin recipe. This liquid PDMS was used as the glue between the two modules and was not partially cured. The other module was removed from its wafer and carefully rolled down onto the first module without trapping air in between them. The two modules were then aligned by sliding the top module into place using the liquid PDMS as a lubricant between the modules. The liquid PDMS was then cured for 20 minutes at 65˚C thus bonding the two modules.

Scanning electron micrographs of the silicon chips (Figure 3-19, left images) and PDMS mold (right images) demonstrate high fidelity in the molding process. No pillars were lost or torn when peeling the PDMS off of the silicon chips.

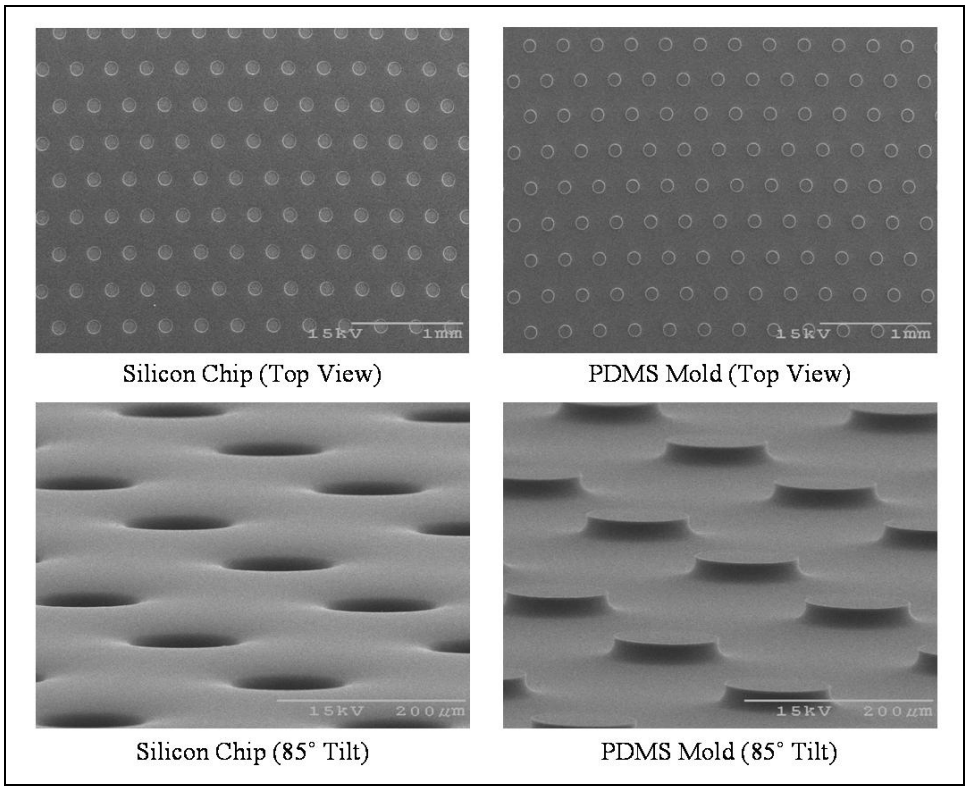


**Figure 3-19: SEMs of silicon gas chips (left) and PDMS molds (right)**

18. Next, the module with six layers was manifolded using the same techniques as stated for the cell culture modules. The module was cut into shape and the plastic was removed from the top of the module. Small rings were placed on the inlet and outlet regions of both the blood and gas pathways. The rings were filled with PDMS and cured for 40 minutes at 65˚C to create a thick enough area for tubing to be inserted.
19. Meanwhile, double-sided tape was placed on a silicon wafer and was spin-coated with most recently mixed PDMS (Step 16) using a twenty-second spread at 500 rpm and a

thirty-second spin at 500 rpm. After a five-minute rest period, the wafer was partially cured for fifteen minutes at 65˚C.

20. Holes were punched in the center of the four rings through the entire module thickness using 3 mm diameter biopsy punches.
21. The module was peeled off the wafer and placed onto the newly coated wafer.
22. Silicone tubing (1/16” diameter, 1” long) was inserted into the holes to the bottom of the rings. Liquid PDMS was placed around the tubing and the edges of the module to prevent leaks.
23. Finally, the module was baked overnight at 80°C.

The module illustrated in Figure 3-20 is perfused with red dye in the blood microchannels and blue dye in the gas pathways.

**Figure 3-20: Picture of gas permeance module with gas (blue) and blood (red) pathways**

### 3.3.4 Pressure Testing

Each module was leak tested prior to use to ensure adequate bonding between the layers. Stopcocks were placed on both the inlet and outlet of the pathways. The blood pathway inlet was

connected to a Harvard PHD 2000 syringe pump (Harvard Apparatus, Holliston, MA) and to the positive side of the Validyne pressure transducer (CD379, Validyne Engineering, Northridge, CA). The blood outlet was capped off, as well as the gas pathway in the gas permeance modules. The module was placed in a water bath (Fisher Isotemp Water Bath 202S, Fisher Scientific, Pittsburgh, PA) so leaks could easily be visualized. Air was injected into the module using the syringe pump at a rate of 0.5 ml/min until the pressure in the module reached 260 mmHg (approximately 5 psi). This was also repeated for the gas pathway. The module was successfully fabricated if it was able to reach this pressure without rupturing or bulging between the layers. Thirty-four cell culture modules were fabricated using the techniques described above. Twenty-eight modules passed the pressure test demonstrating an 82% success rate of the fabrication process.

## 3.4 DISCUSSION

Several different fabrication methods were explored to create artificial lung modules in poly(dimethylsiloxane). Processing using soft lithography was chosen to create prototype modules for tissue engineering and gas permeance testing. First generation modules were fabricated that contained 7 layers of gas microchannels and 7 layers of blood microchannels. These modules suffered from several limitations, including large diffusion distances (>300 μm), low interaction between the blood and gas pathways due to the perpendicular microchannel design, and difficulty in manifolding. Improvements were made to the techniques to successfully fabricate second generation modules with either two blood layers for cell culture testing or 6 layers (4 gas, 2 blood) for gas permeance evaluation. The gas pathway was changed from

microchannels to one large open pathway to maximize gas-blood interaction. The use of double sided heat release tape enabled the stacking of thin PDMS layers (<100 μm). Strong bonding was achieved by partially curing the PDMS layers, stacking them, and further curing. Finally, an improved manifolding process was developed that allowed easily connection to tubing and prevented leaks.

There are limitations in the work described in this chapter that need to be addressed before creating an artificial lung from the modules. First, fabrication variability was not explored for this thesis. Variability in fabricating the patterned silicon wafers can introduce differences in the channel dimensions between modules. The variability in channel height and width within one pattern, within one wafer (4 patterns) and between wafers should be carefully examined using a surface profilometer. The variability in the PDMS mold and the surface roughness, which may be important for cell culture, should also be evaluated. Another limitation is that the fabrication of the modules will be labor intensive and time consuming when stacking hundreds of layers for a device. The development of an automated process should be explored in order to scale up the modules. Also, the diffusion distance for gas exchange is still larger than desired and ways to reduce the PDMS layer thickness need to be evaluated. Techniques such as 3-D printing or stereolithography could address both the scale up and diffusion distance limitations. Three-dimensional printing based on inkjet printers has been used to deposit material and cells in specific configurations with the end goal of building an organ [97-99]. For these modules, 3-D printing could be used to automatically build the entire device layer by layer using two types of polymer. One polymer would be the material of the module (for example, PDMS). The other polymer would be a sacrificial material that would be printed with the desired channel width, height, and spacing (similarly to the sacrificial photoresist channel technique). First, a base layer

of PDMS (or polymer of choice) would be printed. Next, the lines of the sacrificial material would be printed as the channels. Then, PDMS with the same height as the channels would be printed all around the sacrificial material. Next, a PDMS layer would be printed on the entire surface to cover the channels. The thickness of this layer would be the diffusion distance for gas exchange. This process could be repeated until the desired number of layers is achieved, and then the sacrificial material would be dissolved. When this work began, stereolithography techniques were limited by the polymers that could be used and the size of features that could be created. However, improvements over the past few years merit a re-evaluation of this technology. Finally, more sophisticated manifolding techniques will need to be designed to integrate many modules and create an entire artificial lung device. One possible idea is to create parallel plate manifolds (Figure 3-21) that could attach many modules in parallel. The modules can also be redesigned to incorporate branching rather than parallel channels as described by Borenstein et al [89].

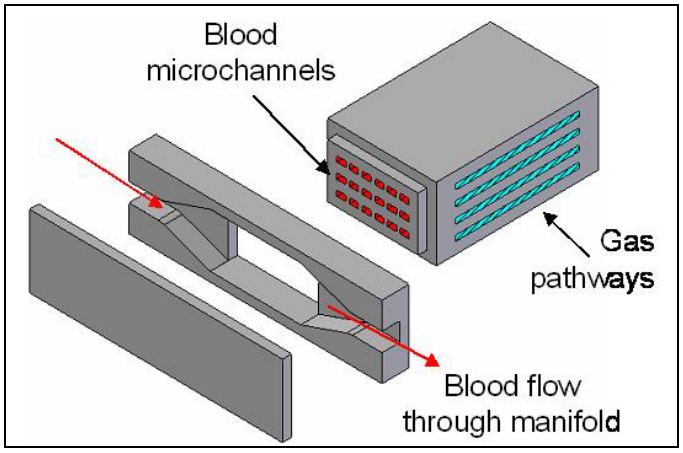


**Figure 3-21: Schematic of parallel plate manifolding concept**

# 4.0 GAS PERMEANCE EVALUATION

## 4.1 INTRODUCTION

The overall gas exchange capacity of an artificial lung is based on the mass transfer coefficient (K) of the device, as described in Section 2.3.2. The mass transfer coefficient is inversely proportional to the resistance to transfer, which is the sum of the resistances due to the membrane and the blood boundary layers that form along the lengths of the fibers. In current membrane oxygenators, the fibers are microporous and provide negligible resistance to transfer. Therefore, the mass transfer coefficient of membrane oxygenators depends solely on the blood boundary layer. The biohybrid artificial lung modules described in this thesis are fabricated in a nonporous polymer, poly(dimethylsiloxane), and the resistance to transfer due to the membrane cannot be neglected. The overall mass transfer coefficient (K) is shown in Equation 6. The permeance of the membrane ($K_m$) is based on the bulk permeability of PDMS and the thickness of the PDMS separating the blood channels and gas pathway (i.e. the diffusion distance for gas exchange).

$$\frac{1}{K} = \frac{1}{K_m} + \frac{1}{K_b} \qquad \textbf{Equation 6}$$

The focus of this chapter was to determine the oxygen and carbon dioxide membrane permeance of the modules ($K_m$) and to examine the effect of the layer thickness on permeance. Modules were fabricated with six layers (4 gas layers and 2 blood layers) using the techniques

described in Section 3.3.3.2. Spin speeds of either 500 or 1000 rpm were used to create the individual PDMS layers, and two modules were fabricated at each of the speeds to examine the effects of fabrication variability on gas permeance evaluation. To calculate the permeance of the modules, the surface area for gas exchange must be calculated. This chapter also discusses the method used to calculate the surface area of the rounded channels.

## 4.2 METHODS

The blood microchannels in the modules are rounded, but not semi-circular, so knowing the height and width of the channels was not enough to calculate the surface area. The profiles of the photoresist on the silicon wafers were evaluated using a DEKTAK3 ST surface profile measurement system (Veeco Instruments, Inc., Woodbury, NY) to more accurately calculate the gas exchange surface area (and volume) of the channels. A profile scan was performed using medium speed and resolution to capture the photoresist height along a 500 μm cross-section of several channels. The data points collected (1000 samples, 0.5 μm per sample) were imported into a MATLAB®7.0 (The MathWorks, Inc., Natick. MA) program, which can be found in Appendix C.

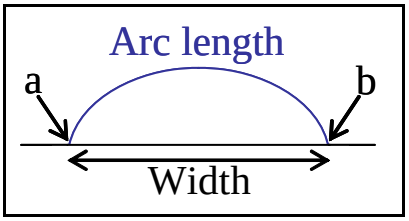


**Figure 4-1: Schematic of arc length and width between points a and b**

First, the derivative of the curve (slope) was calculated to determine the points (a and b) where the channels began and ended (slope $> |0.05|$). Next, the arc length of the curve between those points was calculated using Equation 7.

$$arc\ length = \int_a^b \sqrt{1 + \left(dy/dx\right)^2}\ dx \qquad \textbf{Equation 7}$$

The sum of the arc length and the width at the bottom of the channels was the wetted perimeter of the channel. The surface area for exchange was found by multiplying the wetted perimeter by the length (L) of the channel. Next, the cross-sectional area of the channel was found by integrating the area under the curve between points a and b. The volume of the channel was the product of the cross-sectional area and the length of the channel. Two scans were performed on the same pattern with each scan containing two channels. The surface area used to calculate the permeance was the average surface area of the four channels.

To determine the permeance, the modules were placed in a water bath (Fisher Isotemp Water Bath 202S, Fisher Scientific, Pittsburgh, PA) at room temperature. Room temperature and atmospheric pressure were recorded. Either oxygen or carbon dioxide gas was connected to the inlet of the blood pathway and the outlet was either open to atmosphere or closed off using a stopcock. The gas pathway inlet was capped off while the outlet was connected to a 0.5 ml bubble flow meter (Supelco, Bellefonte, PA). A Validyne pressure transducer was connected to the blood inlet and the gas outlet to measure the transmembrane pressure difference.

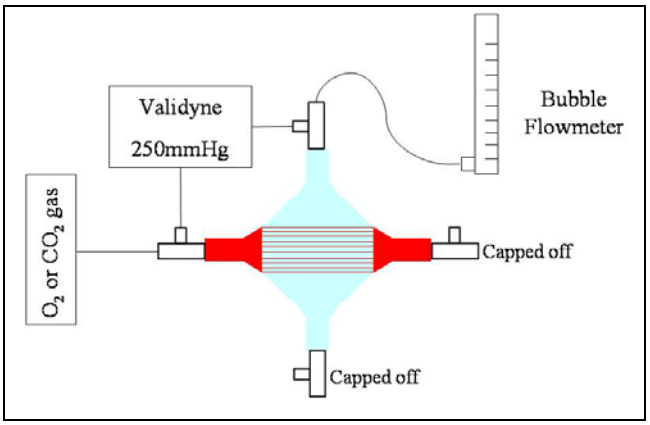


**Figure 4-2: Schematic of gas permeance experiment**

The test gas was first perfused through the blood pathway for fifteen minutes and then the outlet of the blood pathway was closed off. The transmembrane pressure drop was increased to 250 mmHg. After five minutes, three samples were taken using the bubble flow meter and a stop watch to measure the amount of time it took a bubble to move 0.5 ml. The stopcock on the blood outlet was then opened to atmosphere so the pathway could again be flushed with gas for five minutes. Next, the blood pathway was closed off, the pressure was raised to 250 mmHg, and three more samples were taken. Gas flow rates ($Q_1$) out of the module were calculated by dividing the volume of the bubble flow meter by the time. These flow rates were then converted into STP flow rates ($Q_2$) using Equation 8, where $P_1$ and $T_1$ are the test conditions and $P_2$ and $T_2$ are standard temperature and pressure.

$$Q_2 = \left(\frac{P_1}{P_2}\right)\left(\frac{T_2}{T_1}\right)Q_1 \qquad \textbf{Equation 8}$$

Permeance ($K$) was calculated by dividing the flow rate ($Q_2$) by the surface area of the module ($SA$) and transmembrane pressure ($\Delta P$) as shown in Equation 9.

$$K = \frac{Q_2}{SA \cdot \Delta P} \qquad \textbf{Equation 9}$$

The average oxygen and carbon dioxide permeance and standard deviation were calculated for each module. The error propagation associated with the permeance calculation can be found in Appendix D.

## 4.3 RESULTS AND DISCUSSION

The profile of the photoresist of one pattern is shown in Figure 4-3. The channels are very rounded with a height of approximately 33 microns. The average channel width and arc length were 104.25 ± 1.26 μm and 129.85 ± 1.56 μm, respectively. The average surface area for gas exchange for one channel was 0.042 ± 0.0005 $cm^2$ leading to a total module surface area (112 channels) of 4.72 ± 0.06 $cm^2$. The average total volume of the channels was 4.56 ± 0.12 μl giving rise to a surface area to blood volume ratio just over 1000 $cm^{-1}$. The high surface area to blood volume ratio is two orders of magnitude greater than the ratio found in current oxygenators (30 $cm^{-1}$) and is even higher than that found in the natural lung (300 $cm^{-1}$).

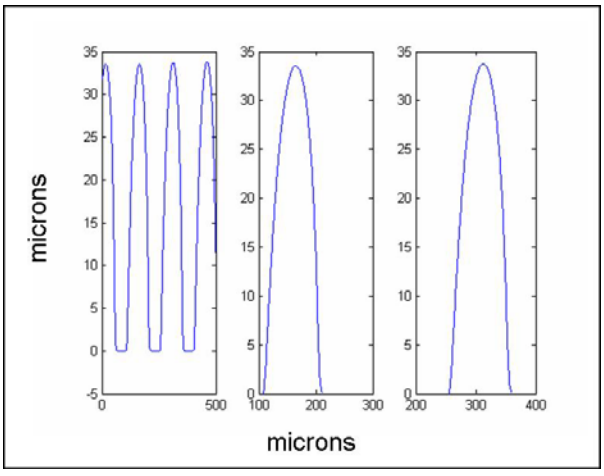


**Figure 4-3: Graph of profile data of two channels**

The average oxygen and carbon dioxide permeance for the four modules are shown in Figure 4-4. As expected, the $O_2$ and $CO_2$ permeance increase with increasing spin speed (i.e. decreasing thickness of the PDMS layers). The maximum oxygen and carbon dioxide permeance achieved were 9.16 x $10^{-6}$ and 3.55 x $10^{-5}$ ml/s/cm$^2$/cmHg, respectively. The selectivity ($Kco_2/Ko_2$) of the modules were 3.41 and 2.94 for the modules fabricated at 500 rpm and 3.82 and 4.06 for the modules fabricated at 1000 rpm.

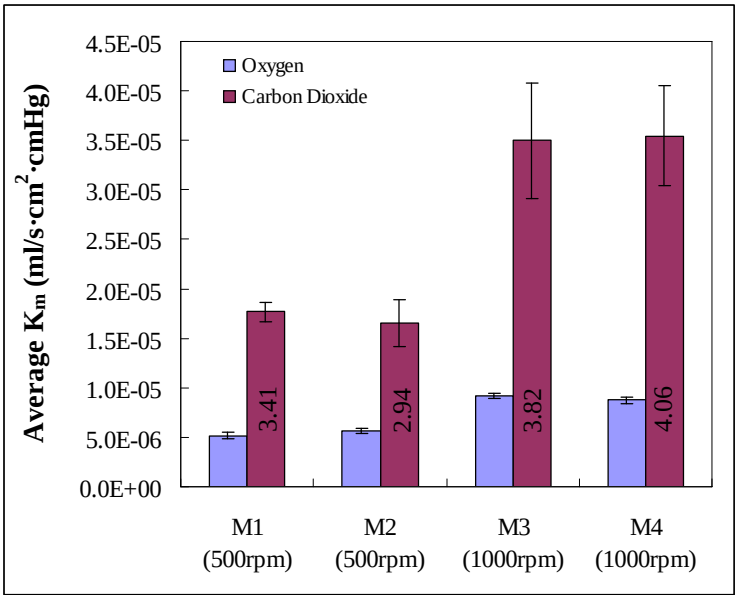


**Figure 4-4: Gas permeance results of 4 modules**

The oxygen and carbon dioxide permeance of currently used microporous hollow fibers are on the order of $10^{-2}$ to $10^{-4}$ ml/s/cm$^2$/cmHg. Siloxane coated fibers, such as Senko and AMT, have slightly decreased permeance due to the coating; however, the permeance values still range from $10^{-3}$ to $10^{-4}$ ml/s/cm$^2$/cmHg [31]. The decreased permeance values of the modules reflect the much larger thickness of the PDMS layer separating the gas and blood pathways. The thickness of the PDMS layers was measured using a WYKO NT1100 Optical Profiling System

(Veeco Instruments, Inc., Woodbury, NY) and was found to be 146 ± 1.4 μm and 63.7 ± 5.6 μm for spin speeds of 500 and 1000 rpm, respectively. The bulk permeability of PDMS is 60 x $10^{-9}$ ml·cm/(s·$cm^2$·cmHg) for oxygen and 325 x $10^{-9}$ ml·cm/(s·$cm^2$·cmHg) for carbon dioxide. The permeance for a layer of PDMS can be calculated by dividing the bulk permeability by the thickness of the layer. Thus, a 100μm-thick layer of PDMS should have an $O_2$ permeance of 6 x $10^{-6}$ ml/s/$cm^2$/cmHg, a $CO_2$ permeance of 3.25 x $10^{-5}$ ml/s/$cm^2$/cmHg, and a selectivity of 5.42. The experimental permeance results for the four modules are comparable to the theoretical values, but the selectivity results are lower than expected.

The experimental permeance values can be used to estimate the total number of channels required to achieve gas exchange levels of 270 ml $O_2$/min and 240 ml $CO_2$/min using the following equations:

$$\dot{V}O_2 = K_{O_2} A\left(PO_{2g} - PO_{2b}\right) \qquad \textbf{Equation 10}$$

$$\dot{V}CO_2 = K_{CO_2} A\left(PCO_{2b} - PCO_{2g}\right) \qquad \textbf{Equation 11}$$

The $pO_2$ and $pCO_2$ of the gas were assumed to be 760 mmHg and 0 mmHg. The values used for venous $pO_2$ and $pCO_2$ were 40 mmHg and 45 mmHg, respectively. Modules fabricated at 500 rpm would require over one million channels leading to a total surface area of 5.02 $m^2$ and a total volume of 50 ml (channels only). Modules fabricated at 1000 rpm would need approximately 162,000 channels for oxygen and 595,000 for carbon dioxide giving rise to a total surface area of 2.5 $m^2$ and volume of 24 ml (channels only). Assuming the same channel geometry (56 channels per layer), over 10,000 layers would be required in the device leading to a device height of over 0.5 meters. However, the width of the device can be easily increased with the fabrication techniques, thereby increasing the number of channels in each layer and reducing the height of the device to a more reasonable size.

This estimated number of channels, however, only takes into account the mass transfer resistance due to the PDMS wall. The overall mass transfer coefficient of the device will be lower than the values listed above due to the liquid boundary layer resistance. Therefore, more channels will be required to achieve the desired gas exchange. The permeance of the boundary layer ($K_l$) can be described by Equation 12, where $\alpha_l$ is the solubility of the gas in the liquid, $D_l$ is the diffusion coefficient, and $\delta_l$ is the average boundary layer thickness.

$$K_l = \frac{\alpha_l D_l}{\delta_l} \qquad \textbf{Equation 12}$$

The overall resistance to transfer is the sum of the PDMS (membrane) and boundary layer resistances. The inverse of the overall resistance gives the overall mass transfer coefficient. Future experiments will be performed to determine the overall mass transfer coefficient by testing the modules in a gas-liquid environment.

Several improvements can be made to the modules to increase the membrane permeance of the device. First, the PDMS layer thickness can be further decreased by increasing the spin speed used in the fabrication process. Experiments need to be executed that will determine the minimum PDMS thickness that can be spun and still be compatible with the stacking and bonding techniques used in this thesis. Different fabrication techniques, such as direct-write or 3-D printing technology, can be explored to reduce the membrane thickness. The gas pathways can be changed to a microporous polymer film, described in Appendix B, to reduce the diffusion distance for gas exchange. Finally, the modules can be constructed out of a microporous polymer. Vogelaar et al. developed a technique called Phase Separation Micro Molding (PSμM) to create porous films from pattered silicon wafers. Microchannels with widths of 100 μm were fabricated in microporous poly(methylmethacrylate) (PMMA) and acrylonitile-butadiene-styrene (ABS) copolymer. Several layers of channels were stacked and bonded to create a 3-D

microfluidic device [100]. This technique can be applied to other polymers and the porosity and pore size can be controlled. The use of a microporous polymer would increase the permeance of the module and allow easier fabrication due to thicker layers than those required in PDMS modules.

# 5.0 ENDOTHELIAL CELL CULTURE

## 5.1 INTRODUCTION

Small diameter vascular grafts (<6 mm diameter) show poor long-term patency due to the lack of endothelial cells, which can lead to thrombosis formation within the grafts. Such thrombotic complications will likely be exacerbated in the micron-scale blood channels of our biohybrid artificial lung modules preventing clinical use. Endothelial cells (ECs) in-vivo play a critical role in maintaining the balance between coagulation and fibrinolysis by secreting and exhibiting anticoagulant factors on their surface, which is described in more detail in Section 2.5.1. Lining the blood microchannels of the artificial lung modules with endothelial cells will provide the required blood biocompatibility and allow blood perfusion with minimal or no systemic anticoagulation.

This chapter describes the work performed towards establishing stable, viable monolayers of ECs in the blood microchannels. Preliminary studies were executed to determine the degree of thrombosis formation in non-endothelialized modules and to confirm the need for ECs, since a large portion of this thesis was focused on endothelial cell seeding. While poly(dimethylsiloxane) (PDMS) is biocompatible, it does not promote adequate endothelial cell adhesion and growth due to its hydrophobic surface. Therefore, several different surface modifications, such as the addition of amine groups using radio frequency glow discharge and

adsorption of fibronectin, were explored to improve growth and establish EC monolayers on flat PDMS surfaces and in open microchannels. Endothelial cell resistance to shear stress was assessed once confluence on PDMS surfaces was achieved. Finally, endothelial cell seeding and growth was examined in prototype artificial lung modules.

## 5.2 THROMBOSIS STUDIES IN NON-ENDOTHELIALIZED MODULES

### 5.2.1 Methods

Modules were fabricated using the tungsten wire array method, described in Appendix A.1.1, to create 100 circular microchannels with diameters of 100 μm and lengths of approximately 2 cm. The ends of the modules were inserted into ½ - ¼ luer connectors (Part no. 27224, Qosina, Edgewood, NY) to create inlet and outlet blood manifolds. The inlet manifold was connected to short piece of ¼ inch Tygon® tubing, a stopcock and the blood bag. The outlet manifold was connected to 1/16 inch tubing and a Harvard PHD 2000 syringe pump (Figure 5-1).

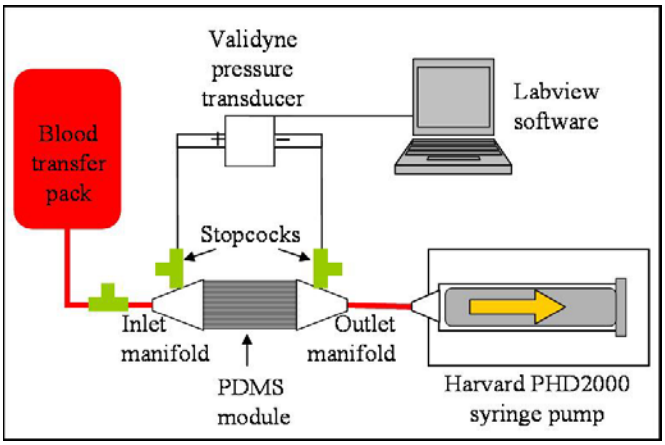


**Figure 5-1: Schematic of blood perfusion loop to evaluate thrombosis in PDMS modules**

A Validyne CD379 pressure transducer was connected to stopcocks on the inlet and outlet manifolds to continuously monitor the pressure drop across the module, and the data was recorded using Labview® data acquisition software. The blood channels were primed with ethanol to allow easier de-airing of the microchannels, rinsed with deionized water, and then primed with saline.

Bovine blood was collected and prepared by another graduate student, Trevor Snyder. Blood was withdrawn from the jugular vein of adult female Holsteins using an 18 gauge needle and mixed with 10% acid citrate dextrose (ACD) in a transfer pack. The blood was then re-calcified with 1M $CaCl^{2+}$ to achieve concentrations of 2 – 3 mM calcium and pH was adjusted to 7.4 using 1M NaOH. The blood was heparinized using 0.5 – 2 U/ml and the activated clotting time was measured. The blood bag was connected to the loop and perfused using the syringe pump in refill mode at 1 ml/min for up to 90 minutes. Immediately after blood perfusion, the modules were rinsed with heparinized saline (50 U/ml), fixed with 2.5% glutaraldehyde for one hour, rinsed with PBS three times, and stored in PBS at 4°C. The modules were cut into cross-sections, sliced parallel to the channels and were examined using scanning electron microscopy (SEM) at the Center for Biological Imaging.

### 5.2.2 Results and Discussion

Three experiments were performed using different blood samples. The activated clotting time (ACT) for each experiment was over 400 seconds, which is significantly higher than ACTs associated with extracorporeal membrane oxygenation (160-240 sec), and represents very aggressive systemic anticoagulation that could create bleeding complications in a patient. The first experiment was terminated prematurely due to problems with the pressure transducer.

Thrombosis and large increases in the pressure drop were observed in the other experiments. Several SEMs from one experiment are shown in Figure 5-2 and demonstrate that many channels were either partially or totally occluded due to thrombus formation. The pressure drop across this module increased significantly, from 25 to 73 mmHg, over the 1.5 hour perfusion and pressure-flow calculations using the Hagen-Poiseuille law suggested that more than half the channels may have been completely blocked by thrombus formation.

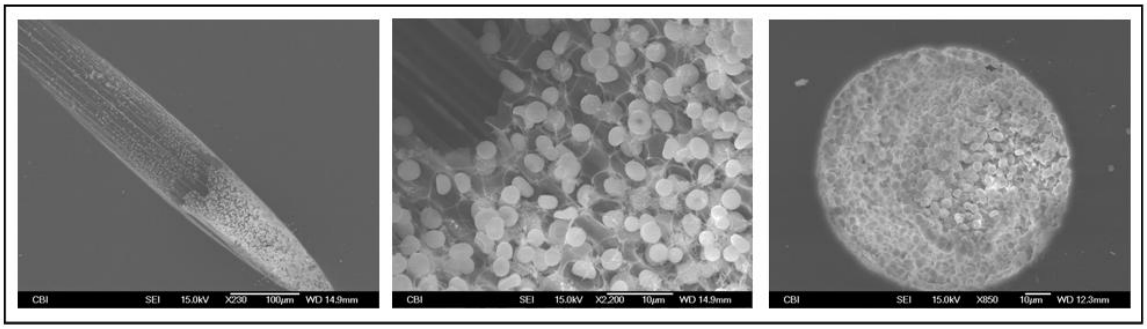


**Figure 5-2: SEMs of thrombosis formation in non-endothelialized PDMS modules**

This preliminary data suggests that thrombosis occurs even with high levels of systemic anticoagulation when perfusing blood through unmodified microchannels of the artificial lung modules. The need for endothelial cells was confirmed through these experiments so the focus shifted to EC growth on PDMS surfaces. Future work will compare the biocompatibility and thrombus resistance of blood microchannels in the biohybrid modules to non-endothelialized and heparin-coated microchannels.

## 5.3 CELL ADHESION AND GROWTH ON SURFACE MODIFIED PDMS

Poly(dimethylsiloxane) is a suitable material for 3-dimensional endothelial cell culture applications because of the high gas permeability, transparency, and biocompatibility of the polymer. Anderson et al. verified that protein adsorption and macrophage activation of PDMS is similar to that found on polystyrene and low density polyethylene [101]. Bordenave et al. demonstrated that PDMS had no toxic effect on human umbilical vein endothelial cells [102]. However, cell adhesion and proliferation on PDMS surfaces is minimal due to its hydrophobicity and low surface energy [103]. This section describes the use of surface modification techniques, specifically fibronectin (Fn) adsorption and the addition of amine groups using radio frequency glow discharge (RFGD), to promote the formation of a stable, confluent monolayer of endothelial cells on PDMS surfaces.

### 5.3.1 Methods

Cell adhesion and growth were evaluated in 24-well plates on either flat PDMS surfaces or in open PDMS microchannels. The PDMS prepolymer and curing agent (Sylgard 184 Silicone Elastomer Kit, Dow Corning, Midland, MI) were mixed in a 10:1 ratio by weight. The mixture was either centrifuged at 3300 rpm for 2 minutes or placed in a vacuum oven (25 inHg vacuum) at room temperature for 20 minutes to remove any bubbles introduced during mixing. Half of the wells in a plate were randomly coated with PDMS and cured for at least 48 hours at room temperature. For experiments with microchannels, thin layers of PDMS containing semi-circular channels (widths of 50 – 250 μm) were fabricated by double molding of a silicon master as described in Appendix A.5. The patterned layers were cut to fit into the wells using a biopsy

punch. The wells were coated and cured as described above and then the patterned layers were adhered in the wells by using a small amount of liquid PDMS. The plates were sterilized overnight under UV light in a laminar flow hood.

The PDMS surfaces were modified with radio frequency glow discharge (RFGD) to introduce amine functionality, fibronectin adsorption or both. Amine groups were introduced onto PDMS surfaces using a RFGD reactor (Plasmod, March Instruments, Concord, CA) evacuated to 300 mTorr under an ammonia atmosphere and operated at 13.6 MHz and 100W for one minute. Bovine fibronectin (F1141, Sigma-Aldrich, St. Louis, MO) was adsorbed from buffer solution (5 μg/ml) for 45 minutes at 37°C. Tissue culture polystyrene (TCPS) wells are used as positive controls and unmodified PDMS wells as the negative controls

Human umbilical vein endothelial cells (HUVECs) were obtained from BioWhittaker (CC-2519, Walkersville, MD) and cultured with endothelial basal medium + additives, including 5% fetal bovine serum, hEGF, hydrocortisone, gentamicin, VEGF, $R^3$-IGF-1, ascorbic acid, and hFGF-B (EGM2-MV, BioWhittaker). The HUVECs were used between the second and seventh passage and seeded onto surfaces with a cell density of approximately 30,000 cells/ml. EC viability was evaluated non-destructively on days 1, 4 and 7 with Alamar Blue (Biosource International, Camarillo, CA), a colorimetric indicator for cell metabolic activity. Alamar Blue was added to each well at a volume equal to 10% of the culture volume and incubated for three hours. The absorbance was quantified spectrophotometrically (Genesys 5 UV-Vis spectrophotometer, Thermo Electronics, Lanham, MD) at wavelengths of 570 and 600 nm. The percentage of Alamar Blue reduction was calculated and cell number was estimated by comparing the percent reduced to the calibration curve that was performed at the beginning of each experiment. The estimated cell number was then normalized to the target initial cell seeding

density and results are expressed as ± standard deviation. Three experiments were performed on flat PDMS surfaces and four were performed on microchannel surfaces. The different surface modifications were compared using two-way ANOVA with repeated measures (same surface repeated over time) and post-hoc Newman Kuels method (GB Stat software, Dynamic Microsystems, Inc., Silver Spring, MD). Comparisons were significant if the p-value $< 0.05$.

The wells with microchannels were stained with Giemsa (Sigma Aldrich, St. Louis, MO) on day 7 immediately after the Alamar Blue assay. The media was removed and the wells were gently washed with PBS. Gluteraldehyde (2.5%) was added to each well for 20 minutes to fix the cells and then the cells were again rinsed with PBS. Giemsa stock solution (0.5 grams Geimsa powder dissolved in 33 ml of glycerol and 33 ml of methanol) was added to each well for 20 minutes. The PDMS was carefully removed from the wells and dipped three times in fresh PBS to rinse away excess Giemsa. The cells were visualized to determine the degree of confluence using an inverted microscope (Axiovert 35, Zeiss, Thornwood, NY) and a CCD camera (CCD-1300-Y, Princeton Instruments, Monmouth Junction, NJ).

### 5.3.2 Results and Discussion

Cell proliferation was observed on all flat PDMS surfaces using the three surface modification techniques as shown in Figure 5-3. Cell densities (normalized to initial seeding densities) on all three modified PDMS surfaces were significantly higher than the density on unmodified PDMS on all days, and very little proliferation was seen on unmodified PDMS. Both Fn and RFGD-Fn modification was significantly higher than RFGD on days 1 and 4. By day seven, Fn was significantly higher than RFGD and RFGD-Fn. No difference was seen between Fn and the positive control, TCPS, on all days of culture.

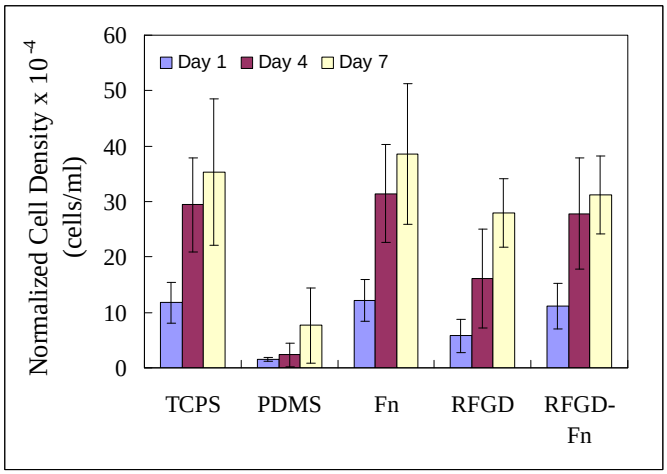


**Figure 5-3: Cell proliferation in surface modified PDMS wells over 7 days**

Similar results were found on open PDMS microchannels as shown in Figure 5-4. Again, the cell density with all surface modifications on all days was significantly higher than unmodified PDMS, except for RFGD on day 1. Cell density on day 7 for both Fn and RFGD-Fn was significantly higher than RFGD alone. All three surface modifications promoted cell growth that was comparable to the positive control, tissue culture polystyrene, by day 7. Fibronectin modification was significantly higher than the positive control on days 4 and 7.

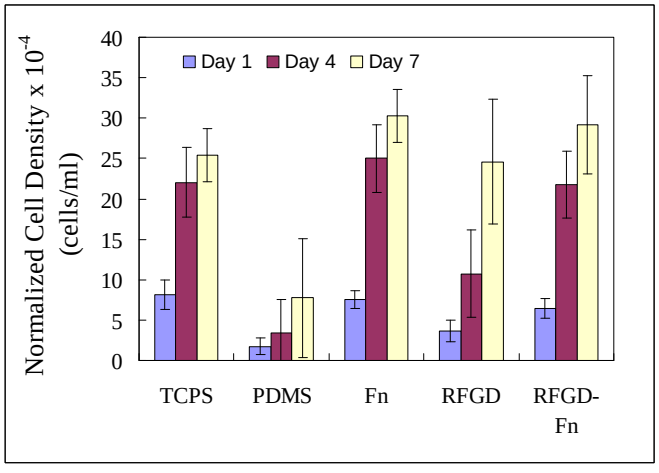


**Figure 5-4: Cell proliferation on surface modified PDMS microchannels over 7 days**

Figure 5-5 demonstrates Giemsa staining on unmodified (left), Fn modified (middle), and RFGD modified (right) surfaces after 7 days of culture. Confluent monolayers of ECs were only seen in fibronectin modified microchannels. Treatment with RFGD improved cell growth between the channels but seemed to prevent cell growth in the channels. This was true on both RFGD and RFGD-Fn surfaces. This phenomenon was observed with various channel diameters and inter-channel spacing. Modifying the operating parameters (time, power, and pressure) of the RFGD chamber could potentially improve the cell growth in the microchannels. Another improvement would be to modify the PDMS surfaces and then immediately use them for cell culture or store them in PBS to prevent changes in the surface. The PDMS in these experiments were modified with RFGD a day prior to cell seeding. Such improvements to the RFGD modification were not explored since fibronectin promoted adequate EC proliferation and confluent monolayers were formed after a week of culture. Fibronectin modification can also be easily applied to 3-dimensional devices, whereas modifying devices with RFGD might present challenges if the modification must be done after the modules are built.

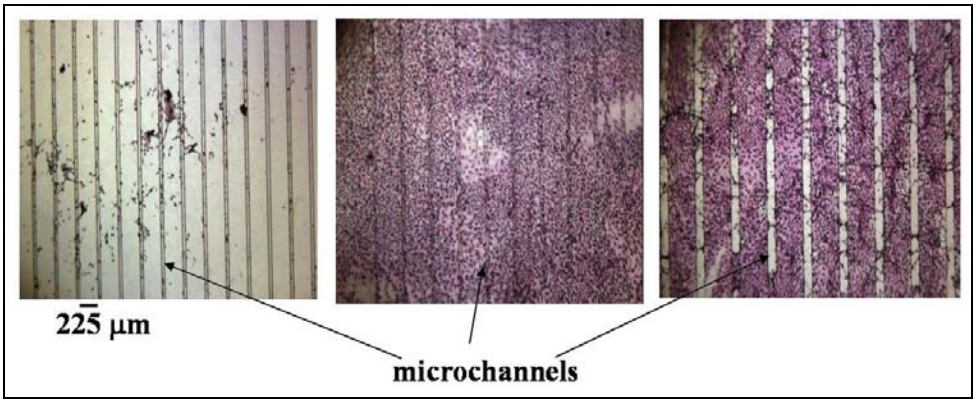


**Figure 5-5: Giemsa staining of ECs on unmodified (L), Fn (M), and RFGD (R) PDMS**

## 5.4 SHEAR STUDIES TO EXPLORE CELL DETACHMENT

One of the factors limiting the success of endothelialized small diameter vascular grafts in-vivo is low cell retention when exposed to flow [104]. Cell retention is affected by several different factors including the graft material, the cell type, the surface modification used to increase adhesion, the seeding technique, and the degree of confluence prior to implantation [105]. Clinical studies found that 30% of the cells detached after the first hour of being exposed to flow when utilizing single-stage seeding, in which the cells are harvested and seeded into the graft just prior to implantation. [83]. Experiments in the previous section demonstrated that Fn, RFGD, and Fn-RFGD modifications can improve EC proliferation on flat PDMS surfaces in static culture. The experiments described in this section evaluated endothelial cell detachment on flat, surface modified PDMS that was exposed to flow.

### 5.4.1 Methods

Glass coverslips (25mm x 75mm) were coated with PDMS by spin-coating Sylgard 184 (mixed 10:1, as described in Section 5.3.1) at 3000 rpm for 30 seconds using a Laurel Spin-Coater to produce a 25 μm thick layer. The PDMS was cured at room temperature for 48 hours. The coverslips were sterilized using low-temperature ethylene oxide and then surface modified using fibronectin (Fn) and radio frequency glow discharge (RFGD) as described above. The slides were placed into 2-compartment petri dishes and the slides were seeded with HUVECs at cell densities of approximately $2.25 \times 10^5$ cells/ml. The slides were incubated for 45 minutes to allow cell attachment and then 5 ml of media was added to each compartment to completely cover the slides. The cells were cultured until confluence and viability was measured using the Alamar

blue assay on days 1, 3, and 7 as described above. The results were normalized to the target initial cell seeding density and were expressed as ± standard deviation. The different surface modifications were compared using two-way ANOVA with repeated measures (same surface repeated over time) and post-hoc Newman Kuels method. Comparisons were significance if the p-value was less than 0.05.

After 8 days of culture, the nuclei of the cells were labeled using Hoechst 33342 DNA stain (10μg/ml) prior to perfusion. A coverslip was placed into a groove in a polymethylmethacrylate (PMMA) parallel perfusion chamber (Figure 5-6) to form the bottom of a 3.5cm x 0.75cm x 200 μm (length x width x height) flow path.

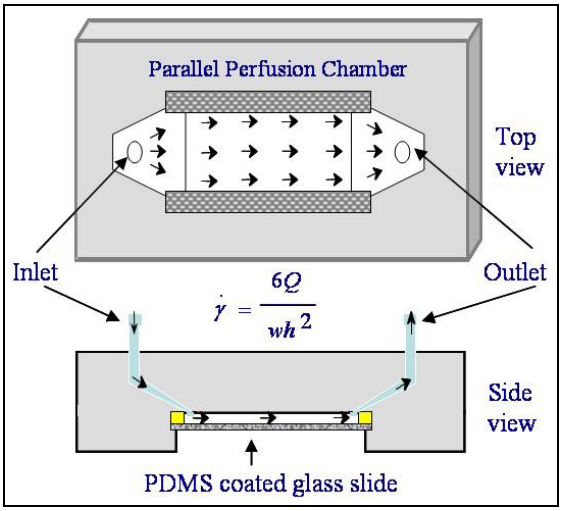


**Figure 5-6: Schematic of parallel perfusion chamber used to evaluate EC resistance to shear stress**

The chamber was sealed using a gasket and a vacuum pump. Inlet and outlet ports in the PMMA chamber were connected to Tygon® tubing, and media was perfused using a syringe pump (PHD2000, Harvard Apparatus, Holliston, MA) in refill mode. The cells were exposed to various shear rates (500, 1000 and 1500 $s^{-1}$) for 10 minutes. The cells were visualized on an inverted

epifluorescent microscope (Axiovert 35, Zeiss, Thornwood, NY) and 20 random pictures were taken both before and after the perfusion using a CCD camera (CCD-1300-Y, Princeton Instruments, Monmouth Junction, NJ). The number of cells was counted in each picture using IPLab imaging software (Scanalytics Inc., Fairfax, VA). Cell detachment was calculated from the mean number of cells before and after perfusion for each experiment.

### 5.4.2 Results and Discussion

The Alamar Blue results from PDMS-coated slides (Figure 5-7) are similar to the results found on flat PDMS and microchannels. All three surface modifications significantly improved cell density over the seven day culture period compared to unmodified PDMS. Both Fn and RFGD-Fn were significantly higher than RFGD and days 3 and 7.

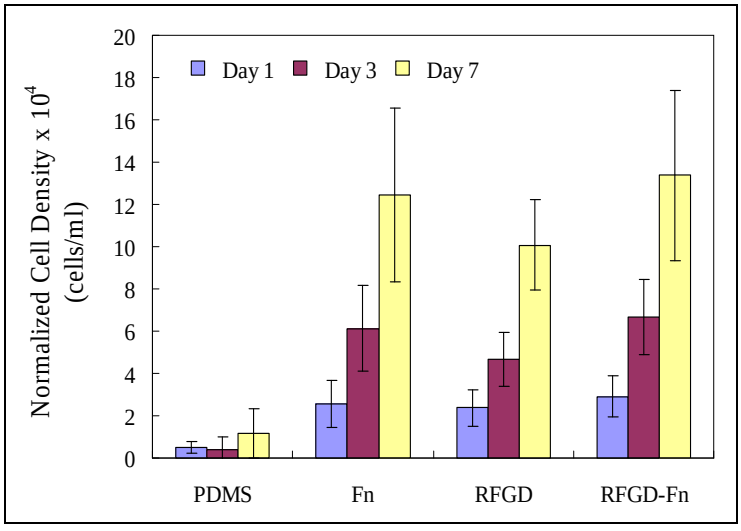


**Figure 5-7: Cell proliferation on surface modified PDMS slides over 7 days**

Fibronectin (n=2), RFGD (n=3) and RFGD-Fn (n=3) modified slides were perfused after 8 days of static culture. The results suggest that cell detachment is lower on Fn and RFGD-Fn surfaces compared to RFGD at all shear rates (Figure 5-8). The higher detachment and lower proliferation on RFGD modified PDMS demonstrate that RFGD treatment alone should not be used in the biohybrid lung application. Acceptable cell detachment, 6, 8, and 12%, was seen on fibronectin modified surfaces at the shear rates of 500, 1000, and 1500 $s^{-1}$, respectively. This level of detachment may be improved by culturing ECs under shear until confluence is achieved [105]. Future work will re-examine the effect of shear stress on cell detachment in the 3-D modules, since the channel geometry may have an impact on EC shear stress resistance. The modules will be seeded with cells and cultured under basal levels of shear (< 100 $s^{-1}$) until confluent and then exposed to various shear rates. The effect of shear conditioning will also be explored.

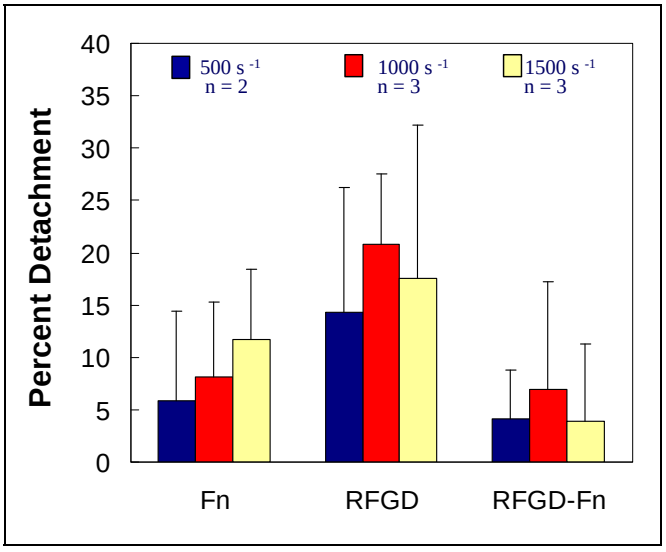


**Figure 5-8: Percent of cell detachment after exposure to flow on surface modified PDMS**

## 5.5 CELL CULTURE IN 3-DIMENSIONAL MODULES

We have established that endothelial cells can be cultured into confluent, stable monolayers on PDMS surfaces using fibronectin modification. This section describes the work performed towards achieving confluent monolayers in 3-dimensional prototypes.

### 5.5.1 Tungsten Wire and First Generation Microfabricated Modules

#### 5.5.1.1 Methods

Three-dimensional modules of microchannels were created by molding tungsten wire arrays, as described in Appendix A.1.1, or by using soft lithography techniques as described in Section 3.2. The tungsten wire technique provided a low-cost and quick alternative to microfabrication techniques for creating modules to begin preliminary cell seeding in 3-D constructs. The modules created from the tungsten wire array contained 100 circular channels with diameters of 100 μm. The first generation, microfabricated modules were simplified to contain 12 layers of blood channels and no gas pathways to allow easier manifolding. The microfabricated modules contained 600 rectangular channels (50 channels per layers) that were 100 μm wide and 20 μm high.

The modules were incorporated into a perfusion system containing a proximal flow loop, distal flow loop, roller pump, media reservoir, and sample ports (Figure 5-9). The entire cell culture system was sterilized with low temperature ethylene oxide gas prior to use. The modules were surface modified by circulating fibronectin solution (5 μg/ml) for 45 minutes in the incubator at 37°. The loops were primed with endothelial medium, and then HUVECs were seeded either statically or dynamically. For static seeding, the module was closed off from both

the proximal and distal loops and was connected to a syringe filled with 2ml of HUVEC suspension (1.6 million cells total) on the inlet seeding port and an empty syringe on the outlet seeding port. The cell suspension was slowly pulled into the inlet manifold and through the module using the empty syringe on the outlet manifold. The suspension was pulled back through the module into the inlet manifold syringe. The cell suspension could not be injected into the modules because the high pressure could rupture the microfabricated modules. This action was repeated five times to slowly oscillate the cells across the microchannels in the module and to promote an even distribution of the concentrated cell suspension. The entire perfusion system was placed in the incubator for 4 hours to let the cells settle by gravity. At the end of the second hour, the module was rotated 180° to promote even cell attachment. For dynamic seeding, cells were injected into the module in the same manner and the system was placed in the incubator. The cell suspension was perfused using a roller pump for 4 hours at 0.25 ml/min through the proximal loop. Again the module was rotated by 180° after 2 hours to promote uniform cell attachment. After 4 hours of incubation, statically and dynamically seeded modules were connected to individual reservoirs via the distal loop. The media reservoir was accessible to incubator atmosphere (5% $CO_2$) through a sterile filter. The media was circulated at 0.25 ml/min via the distal loop with the roller pump for up to ten days of culture. The shear rate was calculated using the Hagen-Poiseuille Law and was found to be 425 $s^{-1}$ and 1900 $s^{-1}$ in the wire and microfabricated modules, respectively.

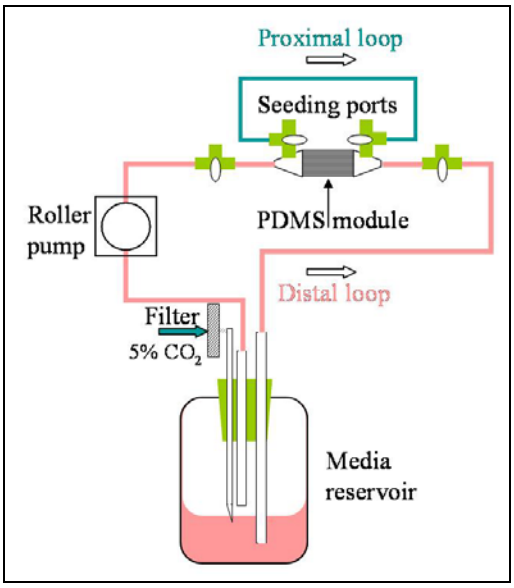


**Figure 5-9: Cell culture perfusion system**

Cell viability in the modules was assessed on days 1, 4, 7, and 10 using the Alamar blue assay. For this assay, the module was closed off from the distal loop and opened to the proximal loop. Alamar blue solution was injected into the inlet seeding port and perfused through the module for 12 hours. Samples were taken from the inlet and outlet manifolds and cell densities were estimated as described in Section 5.3.1. The module was flushed with fresh media and reconnected to the distal loop to continue perfusion for up to 10 days.

#### 5.5.1.2 Results and Discussion

Three experiments were performed in the tungsten wire modules, one using static seeding and two using dynamic seeding. Only one dynamic seeding experiment was performed in the microfabricated modules due to problems with the module leaking around the manifolds. The preliminary results suggested that both static and dynamic seeding methods could be used to introduce cells into the microchannels and that static seeding was more efficient than dynamic in

the tungsten wire modules (Figure 5-10). Cells were also introduced into the microfabricated modules using dynamic seeding as shown in Figure 5-11. However, cell density decreased over time in both module types and with both seeding techniques.

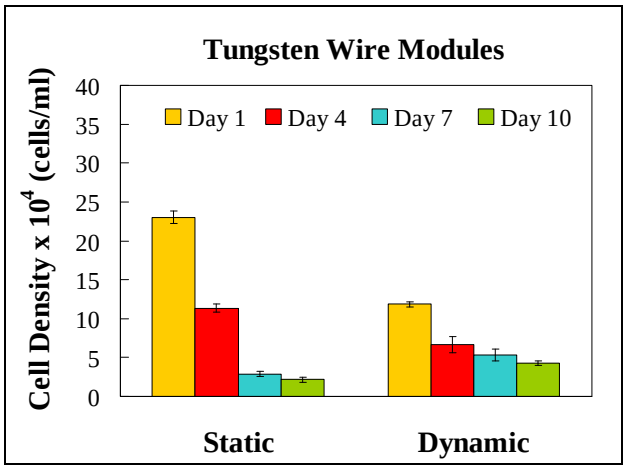


**Figure 5-10: Cell density in tungsten wire modules using static and dynamic seeding**

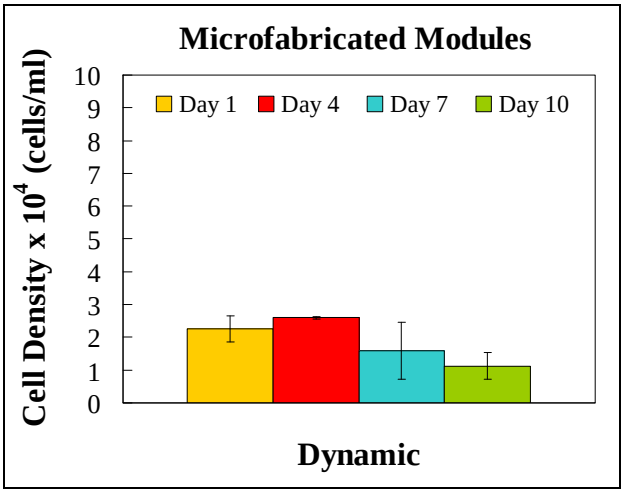


**Figure 5-11: Cell density in a microfabricated module using dynamic seeding**

Several improvements in the perfusion system were required to promote cell proliferation and the overall success of the experiments. The decrease in cell density over time was possibly due to an inadequate supply of oxygen and carbon dioxide for the cells. Tygon® tubing, which

has a very low permeability to oxygen and carbon dioxide, was used in these experiments along with a reservoir that contained a very small port open to the incubator atmosphere. Several groups that culture ECs in microchannels incorporate an oxygenator, or a long piece of silicone tubing, into the perfusion loop [88, 91]. Also, the media was not exchanged during the culture period, so nutrients may have been exhausted and waste may have accumulated over time. Improvements were also needed to improve the manifolding of the microfabricated modules. This is described in more detail in Chapter 3 and was addressed in the fabrication of the second generation microfabricated modules. Lastly, Alamar Blue is not a suitable proliferation assay for 3-dimensional culture because it is dependent on the diffusion of the metabolite into and out of the channels to where the sample is taken. One study by Ng et al. found that proliferation of rat dermal fibroblasts in 3-D culture decreased when assessed using alamar blue but increased with PicoGreen, a double-stranded DNA-specific fluorophore [106]. Thus, the cell density in our modules may not have decreased due to cell death but due to artifact in the assay. The cell density found with Alamar Blue also includes any cells that are attached in the manifolds and tubing of the perfusion system and is not a true reflection of cell attachment in the microchannels.

### 5.5.2 Second Generation Microfabricated Modules

Several improvements were made to the cell culture perfusion system for the second generation modules. The media reservoir was changed from a glass bottle to a bag with ports that allowed for easier media replacement. The tubing prior to the module was changed to silicone and the length was extended to three feet to act as an oxygenator for the system. A syringe pump was used to achieve low flow rates, which modified the system from a continuous loop to a single-

pass circuit. The cells were introduced into the modules by injecting ECs into a vertical seeding tube and infusing them through the module with the pump. Finally, cell proliferation was examined by using the Giemsa stain and cell viability was evaluated with the Live/Dead assay.

#### 5.5.2.1 Methods

Second generation modules were fabricated using the techniques described in Section 3.3. The modules consisted of two layers of channels with 56 channels per layer. The channels were semi-circular with heights of 33 μm, widths of 100 μm, and lengths of either 1 or 1.8 cm. The module and all components of the perfusion loop were sterilized by autoclaving. Low-temperature ethylene oxide was no longer used because Leclerc et al. found that it damaged the bonding between PDMS layers causing leaks in the system [107]. Borenstein et al. autoclaved PDMS circuits and found that it does not cause pattern distortion [88]. The module was first incorporated into a loop (Figure 5-12) that was used to de-air the module and modify the channels with fibronectin. The loop was assembled in the laminar flow hood using aseptic techniques to maintain sterility. A carbon dioxide gas source was connected to the stopcock prior to the module and $CO_2$ was flushed though the module for two minutes to promote easier de-airing [108]. Next, phosphate buffered saline (PBS) was perfused through the module using a syringe pump with an infusion rate of 0.1 ml/min until the module was completely de-aired. Fibronectin solution (25 μg/ml) was placed into a sterile syringe and 1.5 ml was perfused through module at 0.1 ml/min. The module was then incubated for 45 minutes at 37°C.

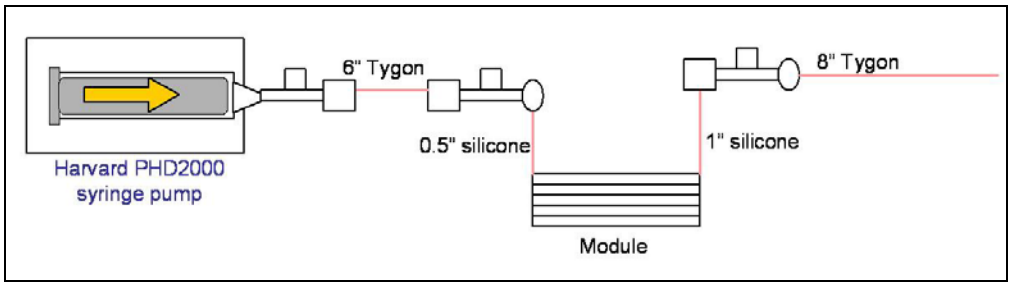


**Figure 5-12: Perfusion Loop for de-airing and modifying modules with fibronectin**

After fibronectin modification, the module and attached stopcocks were incorporated into the perfusion loop, shown in Figure 5-13, using sterile techniques. The media reservoir, a 32 ml bag with two ports (American Fluoroseal Corporation, Gaithersburg, MD), was connected to the module using three feet of silicone tubing (1/16 inch diameter) that acted as an oxygenator. Also proximal to the module was a seeding tube, which consisted of 1/8 inch diameter tubing, a small reservoir (1ml), a syringe filter, and stopcocks. The seeding tube was maintained vertical to the module by connecting two stopcocks though a hole in the incubator shelf above the module. The seeding tube was open to the incubator atmosphere via the sterile filter. The distal end of the module was connected to six feet of Tygon tubing (1/16 inch diameter) that exited the incubator and connected to a Harvard PHD 2000 syringe pump. The seeding tube and tubing distal to the module were de-aired with endothelial growth medium (described in Section 5.3.1) that had been supplemented with penicillin (200 U/ml) and streptomycin (200 μg/ml) to prevent contamination. Media was perfused from the seeding tube through the module using the syringe pump (refill mode) at 0.02 ml/min to remove the fibronectin solution from the module and examine the loop for leaks.

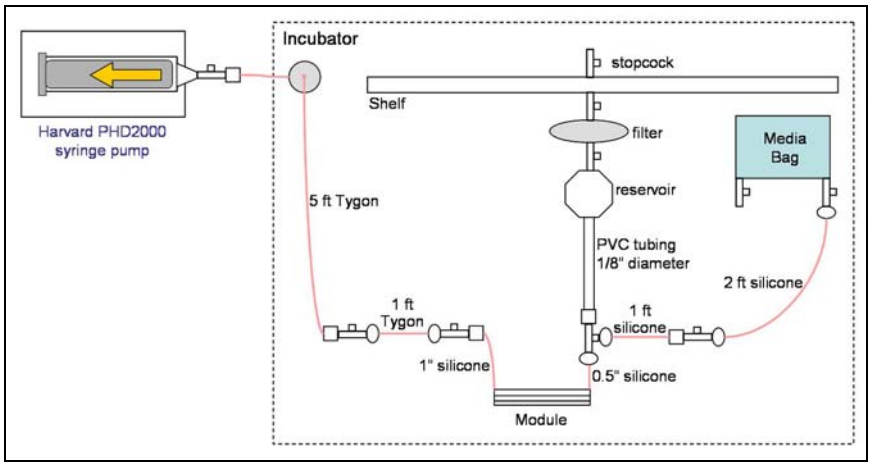


**Figure 5-13: Perfusion loop for culturing cells in second generation modules**

Next, the silicone tubing was removed from the stopcock proximal to the module, the remaining media in the seeding tube was removed, and a suspension (1 - 1.5 ml) of human umbilical vein endothelial cells (HUVECs) was added. The silicone tubing was reconnected to the stopcock and the module and loop were placed in the incubator. The cells were initially perfused at a higher rate (0.02 ml/min) until 0.2 ml had perfused in order to get the cells through the stopcock to the beginning of the module. The rate was reduced to 0.002 ml/min and the remaining suspension was perfused. The cells were then left static overnight (~12 hours) to promote attachment in the channels. On the following morning, the module and loop was disconnected from the 5 ft piece of Tygon tubing and placed in the laminar flow hood. The media bag was filled with medium + pen-strep (EGM2-MV + 200 U/ml pen and 200 μg/ml strep) and pulled through the silicone tubing into the seeding tube using sterile, disposable syringes. The loop and module were placed back into the incubator and perfusion continued at 0.002 ml/min, which corresponded to a shear rate of approximately 50 $s^{-1}$. Every other day, fresh media was added to the bag using sterile syringes and the loop was inspected for leaks or other complications.

Various seeding and culture parameters were explored, such as cell number, percent of serum in the media, double seeding, high seeding flow rate, and culture time. Two modules were seeded for each experiment. The cells were stained with Giemsa to evaluate cell coverage in the channels. To stain the cells, a volume of 0.2 ml of paraformaldehyde (1%) was perfused through the module and then rinsed with 0.2 ml of PBS. Giemsa stain was diluted with PBS (2 ml Giemsa:4 ml PBS) and filtered. The Giemsa solution was perfused (0.15 ml) through the module and then rinsed with 0.2 ml PBS. The flow rate used for all the staining was kept the same as the culture flow rate. Finally, the PBS was removed from the module and cell coverage was examined and imaged using a digital camera.

Once cells were nearly confluent in the modules, cell viability was evaluated using the Molecular Probes™ Live/Dead® Assay (Invitrogen, Carlsbad, CA). The modules were flushed with PBS for 0.2 ml. Then, the Live/Dead solution (2 μl Eth D and 0.5 μl calcein AM in 1 ml PBS) was injected into the seeding tube and 0.2 ml was perfused through the module using the syringe pump. Again the flow rate was kept constant with the culture flow rate. Cells were imaged using a fluorescent microscope.

#### 5.5.2.2 Results and Discussion

Initial experiments examined EC coverage in the modules after only one day of perfusion. The inlet and outlet regions contained many cells; however, no cells were seen in the channels. To improve EC adhesion, the level of serum in the media was increased from 5 to 20%. Serum contains high levels of growth factors necessary for proliferation and is commonly added up to 20% of the culture volume [109]. To examine this, a module was seeded with approximately 6.5 million cells and cultured at 0.002 ml/min. Figure 5-14 demonstrates EC growth in the module using 20% serum after five days of culture. The cells were confluent in the

inlet and outlet regions, which have pillar supports, and were beginning to proliferate into the channels. This could have been due to the increase in serum or the increase in culture time.

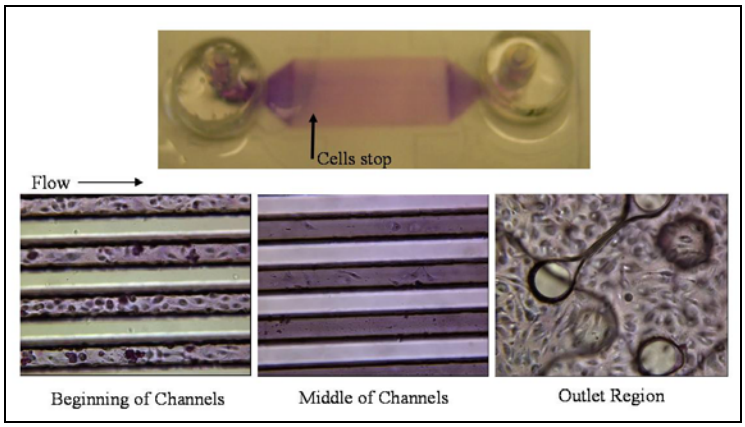


**Figure 5-14: Giemsa staining of ECs using 20% fetal bovine serum and 5 days of culture**

In the next experiment, two modules were seeded with 6.2 million cells, were cultured at 0.002 ml/min for five days, and the level of serum was varied between the modules. The result with 20% serum was similar to the previous experiment. Cell proliferation into the channels was greater with 5% serum and occurred from both the inlet and outlet regions (Figure 5-15). Therefore, five percent serum was used in the remaining experiments.

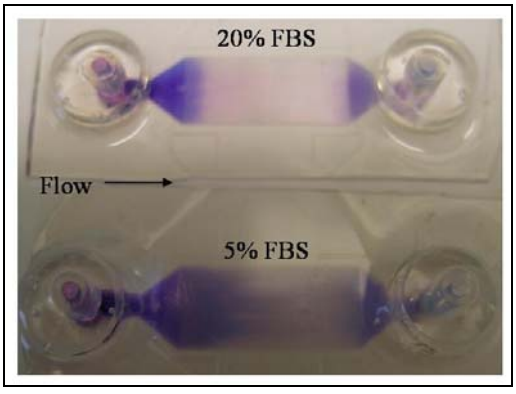


**Figure 5-15: Giemsa staining of ECs using 20% and 5% serum after 5 days of culture**

Seeding the module twice (double seeding) may increase the level of adhesion in the channels. To examine this, two modules were initially seeded with 1.35 million cells and then statically incubated for two hours. The modules were seeded a second time using 4.76 million cells and remained static overnight. The modules were perfused at 0.002 ml/min and were stained after one and five days of culture. Figure 5-16 illustrates that double seeding does not increase cell adhesion or proliferation into the channels after one day of culture. The results from day five are similar to the previous results with 5% FBS.

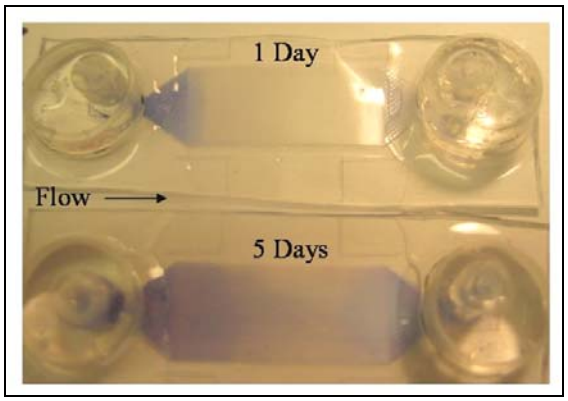


**Figure 5-16: Giemsa staining of double seeding technique after 1 and 5 days of culture**

Next, cell adhesion and proliferation into the channels was evaluated when seeding with a low cell number (2.85 million) versus a high cell number (8.31 million). The cells were cultured at 0.002 ml/min for five days. With low cell numbers, proliferation into the channels occurred from the inlet region. With high cell numbers, more proliferation was seen from the inlet region and also occurred from the outlet region (Figure 5-17). Growth from the outlet was similarly observed in the previous experiments which had a seeding number of 6.2 and 6.11 million cells.

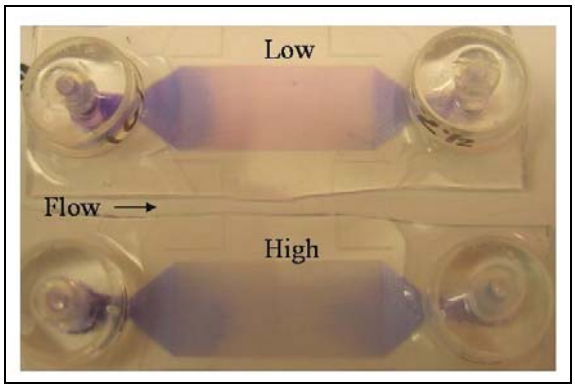


**Figure 5-17: Giemsa staining of low and high cell seeding number after 5 days of culture**

Next, the effect of increasing the seeding flow rate on cell coverage was examined. Normally, the cell suspension was perfused at 0.02 ml/min for only 0.2 ml and the rest of the suspension was seeded at 0.002 ml/min. In this experiment, two modules were seeded with 4.5 million cells using a flow rate of 0.02 ml/min. However, small bubbles started to form in the tubing distal to the module. This could be due to the cells clogging the inlets of the channels and a negative pressure developing in the outlet tubing. To counteract this, the cell suspension was perfused in the opposite direction (infuse mode) to unclog the channels and then perfused back through the module using refill mode and the normal flow rate of 0.002 ml/min. The cells were cultured at that flow rate for five days. The results in Figure 5-18 show that the cell coverage extended further down the length of the channels from both the inlet and outlet regions. However, this was not uniform across the channels and many areas without cells still existed. The high seeding flow rate may also expose the cells to large shear stresses, which could activate or damage the cells.

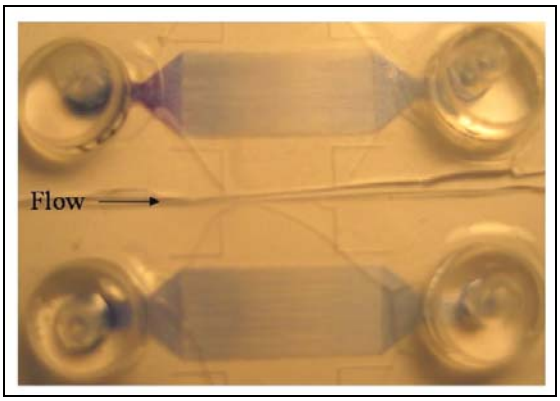


**Figure 5-18: Giemsa staining with high seeding flow rate after 5 days of culture**

Another experiment was performed in which the culture time was extended to seven and fourteen days. Approximately 10 million cells were seeded into the modules using the normal seeding protocol and were cultured at 0.002 ml/min. Cell proliferation into the channels increased from five to seven days. However, areas without cells still existed in the middle of the channels. Very little staining was seen in the module cultured for 14 days. The cells may have died over the culture period. Kiani el al. reported that cells in their microfluidic device reached confluence within nine days but died after ten days of culture [110]. Future work in the biohybrid artificial lung modules will explore cell stability over time.

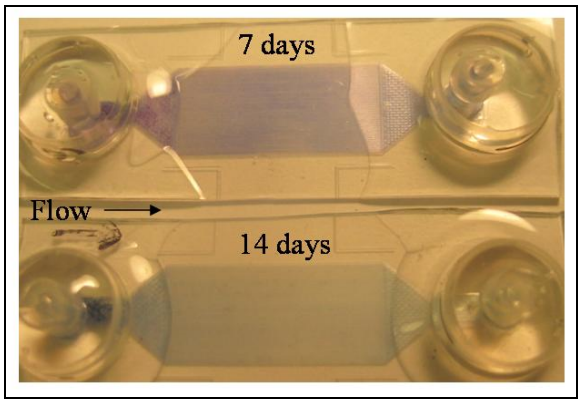


**Figure 5-19: Giemsa staining after 7 and 14 days of culture**

Several conclusions can be made from the experiments described above. Higher cell seeding numbers and 5% serum promoted cell proliferation from the inlet and outlet regions of the modules. Double seeding and higher seeding rates were not useful techniques to improve cell adhesion and coverage. It was difficult to get large numbers of cells into the channels in short periods of time. Obtaining confluence in the module depended mostly on the time of culture. Adding factors to the media to increase cell migration, increasing the culture flow rate or decreasing the length of the channels may decrease the time to reach confluence. Therefore, new modules were fabricated with channel lengths of 1 cm.

Three experiments were performed in modules with shorter channels, and cell coverage and viability was examined with the Live/Dead assay. The modules were seeded with approximately 5 million cells using the normal seeding protocol and remained static overnight. The cells were cultured for ten days at 0.004 ml/min and then evaluated using the Live/Dead assay. The following images are of the inlet regions, middle of channels, and outlet regions of three modules. Cells were confluent and viable (green) in all three modules with very few dead cells (red). The black circles in the inlet and outlet regions are the pillar supports. Several interesting observations were seen using the live/dead assay. First, the cells appeared to pull away from the sides of the channels in all three modules, which can be seen more clearly in the 10x magnification images. As the cells become confluent, they form cell-cell contacts and may pull away from the sharp corners of the semi-circular channels. This phenomenon could be tolerated in the modules as long as the lumens of the channels remained patent. Second, the cells in some areas were not confluent up to the pillars, as seen in Figure 5-21. The large area without cells in the inlet of the third module was most likely due to that area not being de-aired properly.

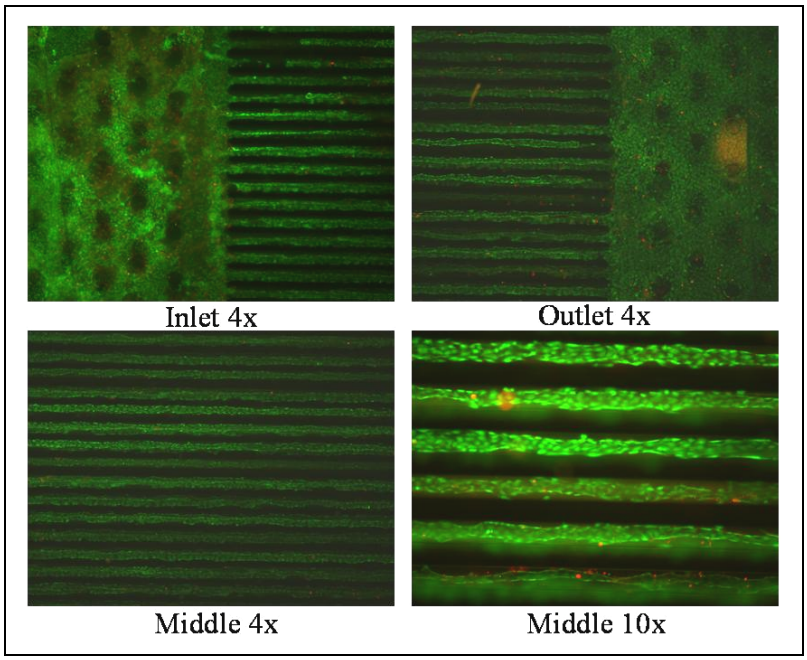


**Figure 5-20: Live/Dead assay of cells in module 1 with shorter channels**

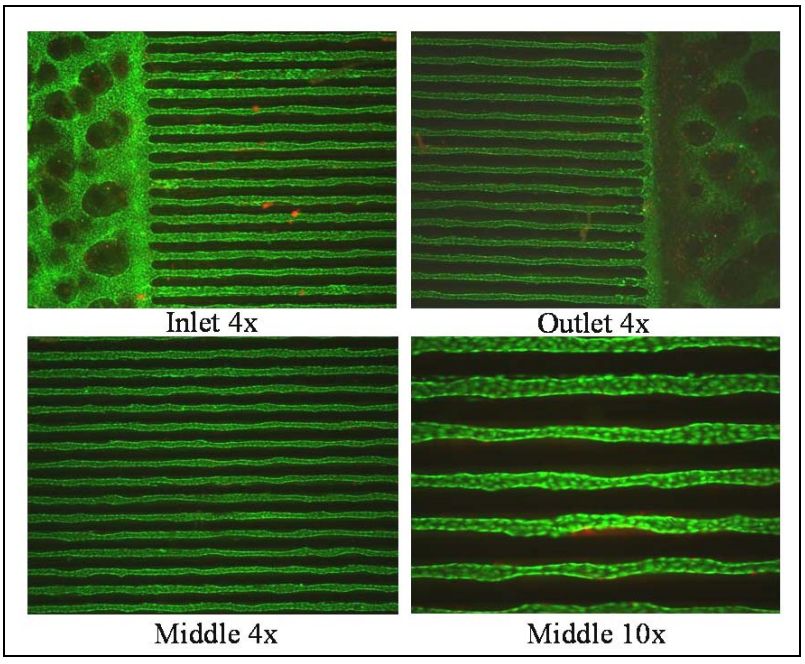


**Figure 5-21: Live/Dead assay of cells in module 2 with shorter channels**

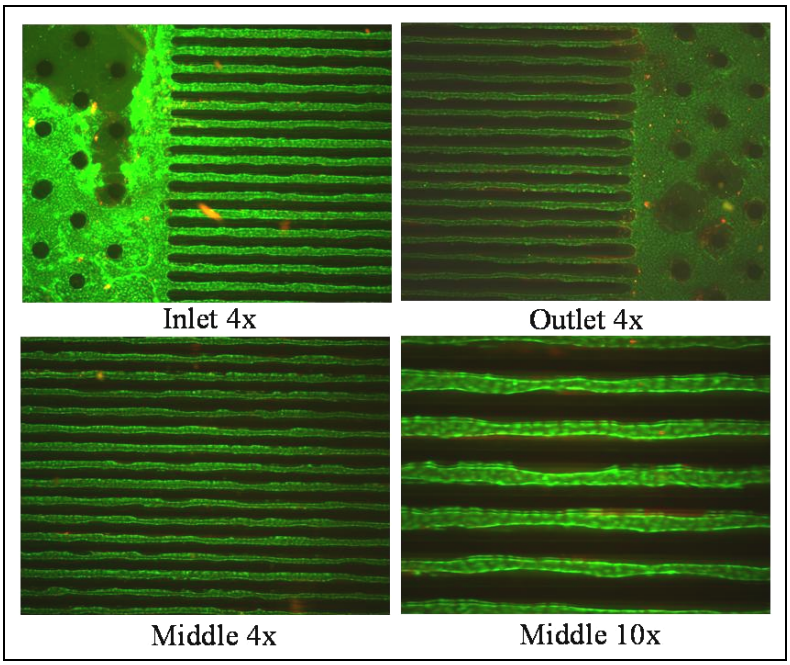


**Figure 5-22: Live/Dead assay of cells in module 3 with shorter channels**

## 5.6 DISCUSSION

The goal of the endothelial cell (EC) research described in this chapter was to demonstrate that ECs can proliferate and reach confluence in 3-D artificial lung modules fabricated in poly(dimethylsiloxane) (PDMS). First, the need for endothelial cells was confirmed by perfusing bovine blood through non-endothelialized modules. Significant thrombosis formation was seen in over half of the channels even with high levels of anticoagulation. Next, EC adhesion and growth was evaluated on 2-D PDMS surfaces that were modified by fibronectin adsorption, the addition of amine groups using radio frequency glow discharge, or a combination of the two. All three surface modifications improved EC growth over seven days of culture compared to unmodified PDMS. However, only fibronectin adsorption resulted in confluent monolayers on flat PDMS and in open PDMS microchannels. Endothelial cell resistance to shear stress was also

evaluated on PDMS treated with the three surface modifications. Cell detachment was less than 15% on fibronectin modified surfaces at a shear rate of 1500 $s^{-1}$. Finally, cell seeding and proliferation was examined in 3-D artificial lung modules that were modified with fibronectin. Early experiments using tungsten wire and first generation microfabricated modules had limited success but led to critical improvements in the cell culture perfusion system. Cell seeding techniques were evaluated in second generation microfabricated modules. Improved cell proliferation was seen when using high cell seeding numbers and 5% serum in the culture medium; however, no seeding technique introduced large numbers of cells into the channels. Instead, cell coverage in the channels was dependent on proliferation from the inlet and outlet regions. After 10 days of culture, confluent and viable monolayers of endothelial cells were observed in modules containing 1 cm long channels.

The work described in this chapter demonstrates that confluent EC monolayers can be achieved in 3-D modules and provides a strong foundation for biohybrid artificial lung technology. However, many aspects of the biohybrid modules need to be evaluated to ensure their success. An artificial lung based on this technology will be required to support a patient from several weeks up to several months. Therefore, experiments need to be performed to evaluate the length of time that ECs can be maintained in the perfused modules. Also, venous cells (human umbilical vein) were used in this work; however, obtaining large numbers of venous cells clinically is difficult. Microvascular cells from adipose tissue are available in larger numbers and could be a more appropriate source of autologous cells for the biohybrid lung. Basic experiments evaluating microvascular EC adhesion and growth in the modules should be evaluated and compared to the results found with venous cells. Next, EC resistance to shear stress must be explored in the 3-D modules. Higher levels of cell detachment may be seen due to

the geometry of the channels. Shear conditioning, slowly increasing the level of shear over the culture time, can be applied to improve cell retention at shear rates that will be seen clinically. Cell phenotype must also be examined to ensure that the cells are maintaining a non-thrombogenic, non-inflammatory phenotype throughout the culture period. If not, the cells could promote thrombosis formation within the channels and cause device failure. Flow cytometry techniques can be utilized to examine the level of inflammatory markers such as tissue factor (TF) and ICAM expression [111]. The biocompatibility of the endothelialized modules must be evaluated by comparing platelet deposition and thrombus formation to heparin-coated modules. Lastly, the effects of hyperoxia on the cells must be examined if a pure oxygen gas source is required for achieving adequate levels of gas exchange. In current modules, hyperoxia will most likely not be an issue due to the thickness of the PDMS (large resistance to transfer). However, the effects of hyperoxia may become important if the PDMS thickness is decreased or if a microporous polymer is used in the modules. If oxidative stress and damage occurs, strategies such as adding nitric oxide to the sweep gas or genetically engineering the cells can be employed to create an oxidative resistant EC phenotype [112-114].

# 6.0 CONCLUSIONS

The goal of this thesis was to develop novel biohybrid artificial lung technology based on microfabrication and tissue engineering techniques. The specific aims included fabricating small prototype modules, evaluating the gas permeance of the modules, and demonstrating the formation of confluent endothelial cell monolayers in the microchannels. Several different fabrication methods were explored, and soft lithography was used to create modules that contained alternating layers of blood microchannels and gas pathways in poly(dimethylsiloxane) (PDMS). The blood microchannels, 56 channels per layer, were designed to have widths of 100 μm, depths of 30 μm, and inter-channel spacing of 50 μm. Each gas layer consisted of one large, open pathway (depth of 30 μm) to increase the interaction between the gas and blood pathways. The gas pathway included pillars with diameters of 100 μm to prevent the pathway from collapsing. Modules were successfully fabricated to contain two blood channels for cell culture modules or 6 layers (4 gas and 2 blood) for gas permeance modules.

The permeance of the modules was found to decrease as the PDMS layer thickness was minimized. The thickness was easily controlled by controlling a processing parameter, the spin speed. The PDMS layer thickness was minimized to 65 μm to achieve oxygen and carbon dioxide permeance of $9.16 \times 10^{-6}$ and $3.55 \times 10^{-5}$ ml/s/cm$^2$/cmHg, respectively. The microvascular scale of the modules leads to a surface area to blood volume ratio of 1000 cm$^{-1}$, which is two orders of magnitude greater than that found in current oxygenators.

Tissue engineering techniques were successfully used to produce confluent monolayers of endothelial cells (ECs) in the blood microchannels. Initial work examining thrombosis in non-endothelialized modules demonstrated the need for endothelial cells. Several different surface modifications were explored to improve EC adhesion and growth on PDMS. The best results for proliferation, confluence, and resistance to shear stress were found on fibronectin modified PDMS. Finally, endothelial cells were seeded and cultured in fibronectin modified modules that contained two layers of rounded microchannels with widths of 100 μm and lengths of 1 cm. Confluent and viable cell monolayers were achieved after ten days of culture. The endothelial cells will provide a more biocompatible surface reducing the need for systemic anticoagulation and the biocompatibility complications associated with current oxygenators and ECMO. The work described in this thesis provides a strong foundation for creating more compact and efficient biohybrid artificial lungs devices in the future.

# APPENDIX A

# ALTERNATIVE FABRICATION TECHNIQUES

## A.1 MOLDING TUNGSTEN WIRE ARRAYS WITH PDMS

### A.1.1 Creating Arrays of Parallel Microchannels

A wire screen (Stainless Steel Type 304, Small Parts, Inc., Miami Lakes, FL) was used to control the spacing between wires [115, 116]. The screen was placed on top of two thin slabs of cured PDMS. The tungsten wires, cut into 2.5cm lengths, were threaded through the screen into both of the PDMS slabs using tweezers and a microscope to aid in visualizing the holes in the screen. After the wires were threaded, the bottom piece of PDMS was removed to expose the wire ends, which were then secured to the remaining PDMS slab with epoxy. Next, the screen was pulled towards and attached to the free ends of the wires creating the array (Figure A-1). The 10 x 10 array shown in Figure A-1 contained 100 μm diameter channels spaced 750 microns apart (using every fifth opening in the screen) and was 2 cm long. The wire screen allowed for spacing down to approximately 70 microns.

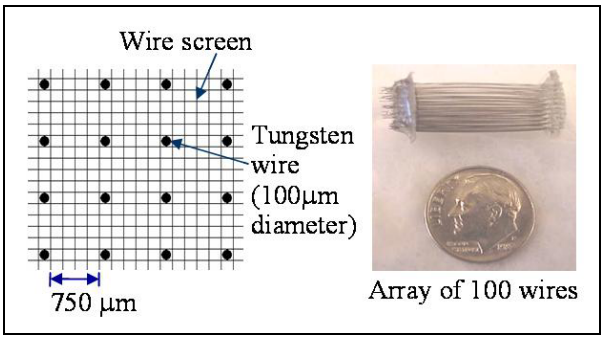


**Figure A-1: Parallel array of 100 tungsten wires**

The 3-D wire array was placed in a 15 ml conical tube, which was filled with PDMS, de-aired, and cured for 48 hours at room temperature. The wires were removed from the mold to create the microchannel array.

### A.1.2 Creating Arrays of Perpendicular Blood and Gas Microchannels

A weaving loom and base was fabricated by our machinist, Brian Frankowski, in order to create 3-dimensional arrays of perpendicular gas and blood channels (Figure A-2). The weaving loom contained 25 small pins (18 ½ gauge needles) on each side to control the inter-channel spacing. The loom could be screwed onto the base, which was fabricated to fit onto the vacuum chuck of the spin-coater. First, a thick layer of PDMS was spin-coated onto the loom and cured at 100°C. The module was then built one layer at a time by wrapping wires of any diameter around the loom in one direction. Next, the loom was placed onto the spin-coater and a layer of PDMS was spun and cured to cover the wires. Changing the spin speed controlled the thickness of the PDMS layer, or in other words, the diffusion distance for gas exchange. The next layer of wires was wrapped perpendicular to the layer below it, spin-coated with PDMS and cured. This process was repeated until the desired number of layers was achieved.

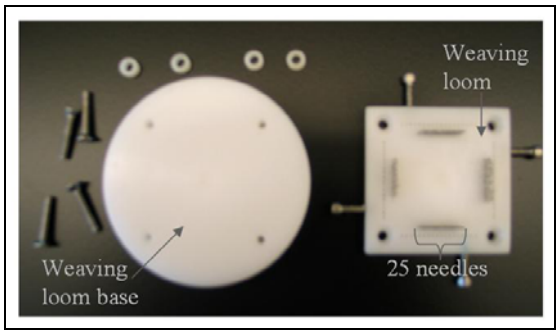


**Figure A-2: Weaving loom used to create perpendicular gas and blood channels from wires**

## A.2 MOLDING SU-8 PILLAR ARRAYS WITH PDMS

The second fabrication technique utilized photolithography processing with a thick, epoxy based negative photoresist, SU-8 (MicroChem Corp., Newton, MA), that could create features several hundred microns thick. Our goal was to produce an array of high aspect ratio pillars, which could be molded with PDMS to form a parallel array of circular microchannels.

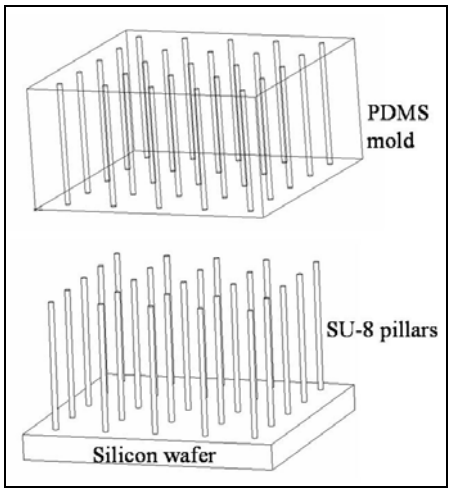


**Figure A-3: Schematic of SU-8 pillar array and corresponding PDMS mold**

SU-8 processing was performed in the MEMS Chemistry Lab at Carnegie Mellon University. We designed a mask using Cadence software that contained 32 different patterns, each 1cm x 1cm. The patterns contained circles with diameters of 21, 28, 35, 42, 49, 56, or 70 μm and spacing of 21, 28, 35, 42, and 49 μm. The mask design was exported to Adobe Acrobat and was printed on a transparency (Magna Graphics, Pittsburgh, PA) as a dark field mask, in which the background was black and the circles were clear. A transparency mask has the advantages of faster and less expensive fabrication over typical soda lime/chrome masks. Silicon wafers were dehydrated at 200°C for five minutes on a hotplate. An adhesion promoter, OmniCoat (MicroChem Corp., Newton, MA), was spun onto the wafer (WS 400A-6NPP/LITE, Laurel Technologies, North Wales, PA) with a spread speed of 500 rpm (acceleration of 100 rpm/s) for five seconds and a spin speed of 3000 rpm (acceleration of 300 rpm/s) for thirty seconds. The wafer was baked for one minute at 200°C. SU-8-100 was spun onto the wafer with a spread speed of 500 rpm (acceleration of 100 rpm/s) for ten seconds and a spin speed of 2000 rpm (acc. 300 rpm/s) for thirty seconds to produce a 150-micron thick layer. The wafer was then soft baked for 20 minutes at 65°C, 10 minutes at 75°C, 10 minutes at 85°C, and 50 minutes at 95°C on a hotplate. The SU-8 was exposed to UV light for 5.75 minutes through the mask. The negative resist was cross-linked where it is exposed, i.e. in the circles. A post exposure bake was performed in two-steps: one minute at 65°C and twelve minutes at 95°C. Finally, the SU-8 was developed in specially formulated SU-8 developer for 20 minutes.

Fabrication of features with aspect ratios as high as twenty can be achieved in SU-8; however, the processing becomes more challenging with thicker resists. We found that many pillars either collapsed or completely delaminated from the wafer as shown in Figure A-4. We improved the processing steps by using Omni Coat (an adhesion promoter), slowly ramping the

soft bake temperature, and increasing the soft bake time. However, we were unable to produce wafers with all of the 32 different patterns intact. The left image in Figure A-4 illustrates 56 μm diameter pillars that remained upright after development, but had non-uniform shape and rough sidewalls. This was attributed to the transparency mask, which did not have as high of resolution as soda lime/chrome masks. We abandoned this technique to create channels due to the difficulty in fabrication.

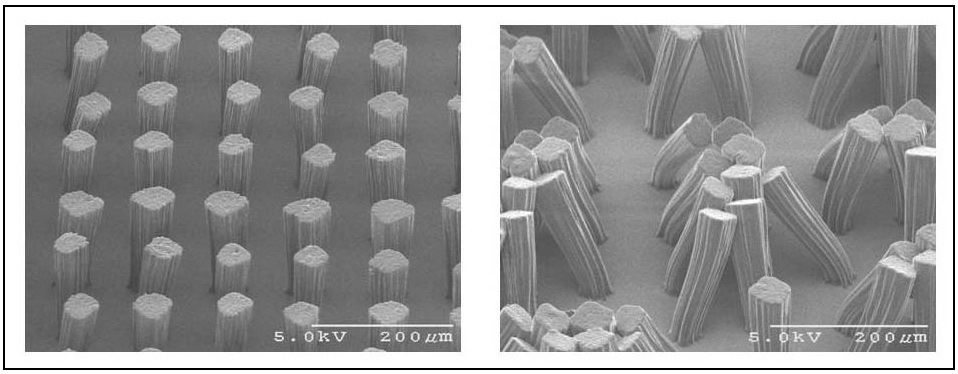


**Figure A-4: Scanning electron micrographs of SU-8 pillars**

## A.3 SACRIFICIAL PHOTORESIST CHANNELS IN PDMS

The next alternative fabrication technique that we explored consisted of creating layers of sacrificial photoresist channels in PDMS [79]. This processing technique, shown in Figure A-5, eliminates the handling and stacking of thin PDMS layers making it easier to minimize the diffusion distance between the gas and blood layers.

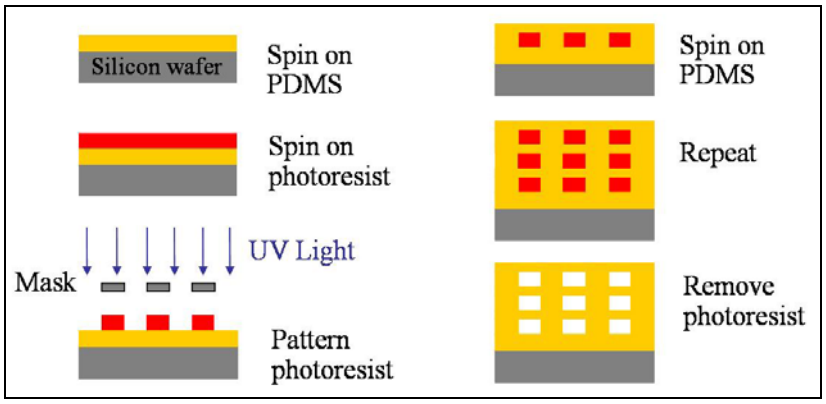


**Figure A-5: Fabrication of sacrificial photoresist channels in PDMS**

The PDMS pre-polymer and curing agent (Sylgard 184) were mixed using a 10:1 ratio (prepolymer:curing agent) and de-aired using a vacuum oven. The PDMS was spin-coated onto a clean, dry silicon wafer at 3000 rpm for 30 seconds to produce a 25-micron layer and cured on a hotplate at 100°C for 45 minutes. All photolithography processing was performed in the Nanofabrication facility at Carnegie Mellon University using the equipment listed in Section 3.2.2. Positive photoresist (AZ4620) was spun onto the wafer at 3000 rpm for thirty seconds to produce a 9-micron layer. The photoresist was soft baked on a hotplate at 110°C for one minute. Initial attempts failed due to resist roughness and the resist retracting from the edges of the wafer (see Figure A-6). This was due to the hydrophobicity of the PDMS, which has a contact angle over 100° [117]. Positive photoresists have contact angles near 75° and approaching this number for PDMS would improve the adhesion between the two layers. The contact angle of PDMS can be reduced by treatment with an oxygen plasma. The PDMS wafers were surface modified using an IPC plasma barrel etcher. The reactor compartment was evacuated to 100 mTorr and exposed to oxygen plasma with a power of 100 W for one minute. After plasma treatment, the photoresist layer was smooth and uniformly covers the wafer (see Figure A-6).

**Figure A-6: Photoresist on unmodified PDMS (top) and on PDMS modified with oxygen plasma (bottom)**

The photoresist was then exposed to UV light for 26 seconds through a mask previously designed by a graduate student at Carnegie Mellon University, which contained 1cm x 1cm die of different photoresist channel widths (250 – 1200 microns) and spacing (10 – 400 microns). The patterned photoresist was developed using AZ400K developer diluted 1:4 with DI water for two minutes to produce the sacrificial channel structures. Another layer of PDMS was spin-coated onto the wafer using the same recipe as above to seal the channels. This process can be repeated until the desired number of layers is achieved. Figure A-7 shows the cross section of a module with two layers of parallel photoresist channels. Next, the sacrificial photoresist channels were removed using photoresist stripper at 40°C for 30 minutes. We were able to successfully create modules with 2 - 3 layers of parallel channels with channel heights of nine microns and channel widths over 250 microns.

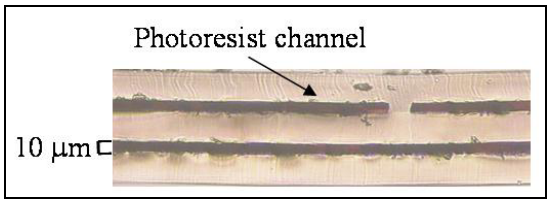


**Figure A-7: Cross section of module with sacrificial photoresist channels**

We needed to modify our processing in order to increase the channel height and minimize the channel width to correspond with our design specifications. The minimum channel dimension, height or width, should be no less than 15 – 20 microns in order to seed endothelial cells, which are approximately fifteen microns in diameter in a cell suspension. To increase the channel height, we incorporated a second photoresist spin in our processing steps. The following processing steps were optimized on a plain silicon wafer using the mask described above. PDMS was mixed, spin-coated onto a silicon wafer, and cured as described above to produce a 25-micron layer. Photoresist (AZ 4620) was spun onto the wafer at 3000 rpm for 30 seconds to produce a 9-micron layer. The photoresist was soft baked on a hotplate at 110°C for one minute. Next, we spun a second layer of resist at 3000rpm and performed a second soft bake for 60 seconds at 110°C. This produced a channel height of 18-20 microns. The wafer was then patterned with UV light for 45 seconds and developed using diluted developer (1:4, AZ400K developer:DI water) to produce the sacrificial channel structures.

To minimize the channel widths, we designed a new mask using Cadence software that consisted of 16 different patterns, which were 1 x 1.5 cm (w x l). Each pattern contained a different channel width (15, 20, 30, 40, 50 and 100 microns) and spacing (20, 50 or 100 microns). The mask also included four alignments marks that could be used to easily create perpendicular channels in subjacent layers. We used the new mask and processing steps to create

18-micron thick channels on PDMS coated wafers. However, many of the features delaminated from the wafer during resist development. The loss of features was due to either the larger thickness of photoresist or the poor adhesion of resist on PDMS. It is known that creating features smaller than 25 microns is quite challenging in larger thicknesses of positive resist. However, aspect ratios (resist thickness: minimum feature size) of approximately three can typically be achieved, which should permit features down to 6 - 7 microns [55]. We used the same processing steps on plain silicon wafers to determine whether the problem was the resist thickness or poor adhesion of resist on PDMS. Some of the smaller feature sizes, including the 15 and 20 μm channels and the 6 μm alignment marks, delaminated from the plain silicon wafer during resist development. However, the processing steps were established using the mask with much larger feature sizes (250 – 1200 μm) and, therefore, needed to be optimized for the new mask. Improved processing is described in Section 3.2.2. This technique was not further pursued due to the problems with photolithography, which would be even more challenging as more layers are fabricated.

## A.4 PHOTOSENSITVE PDMS

The next fabrication technique we explored utilized lithography processing with photopatternable PDMS (WL-5150, Dow Corning, Midland, MI). This silicone acts similarly to a negative photoresist, such as SU-8. It can be spun onto a wafer with thicknesses up to 40 μm and then patterned using UV light to create features with aspect ratios of 1:3 (width:height). The areas that are exposed to UV light are cross-linked and remain on the wafer. The unexposed areas are removed during the development step. The advantage of this processing was the

elimination of handling and stacking thin PDMS layers making it easier to minimize the diffusion distance between the gas and blood layers. This technique is an improvement to the sacrificial photoresist technique described in Appendix A.3 because we have eliminated the challenges of patterning positive resist on PDMS.

Preliminary experiments were performed in the John A. Swanson Micro and Nanosystem (JASMiN) Laboratory at the University of Pittsburgh to establish processing parameters to fabricate a single layer on silicon wafers. A light field mask containing four patterns was designed using Cadence software and fabricated using the direct write lithography machine. This mask was the first design used to overcome some of the limitations of the first generation modules discussed in Section 3.2.4. Each pattern consisted of a 1.5 x 1.5 cm array of seventy-five channels (channel width of 100 μm, channel spacing of 100 μm) and a large inlet and outlet channel to distribute flow to all of the channels while allowing for easier manifolding than previous designs (Figure A-8). The patterns were also oriented on the mask so that parallel gas and blood pathways could be fabricated by rotating the mask 90°.

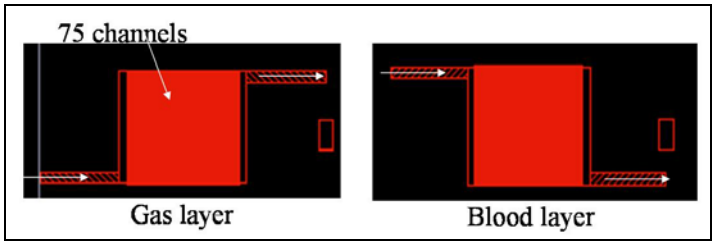


**Figure A- 8: Gas and blood pattern for photopatternable PDMS**

Silicon wafers were dehydrated on a hotplate at 200°C for fifteen minutes. The photopatternable PDMS was spin-coated onto the wafer using a spread step of 500 rpm for ten seconds (acceleration of 100 rpm/s) and a spin step of 1500 rpm for thirty seconds (acceleration

of 300 rpm/s) to create a 22 μm thick layer. The PDMS was then soft baked at 115°C for two minutes. The wafer was exposed through the mask for 150 seconds. A post exposure bake was performed for two minutes at 155°C to promote cross-linking of the areas that were exposed to UV light, which would be all the PDMS around the patterns and the PDMS between channels. Finally, the wafer was developed using silicone film developer (WL-9653, Dow Corning, Midland, MI) to remove the unexposed areas (the channels). To create modules, the wafers would not be developed until the desired number of layers was spin-coated and exposed (see Figure A-9).

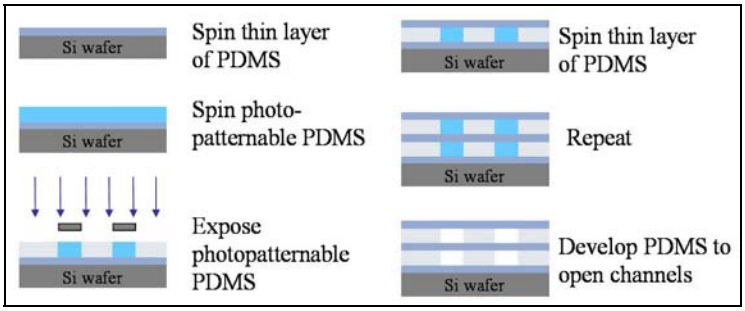


**Figure A-9: Schematic of fabrication process for photopatternable PDMS**

We found that it was difficult to work with the photopatternable PDMS due to tackiness of the material even after soft baking. The material itself is quite expensive in addition to the cost of performing lithography for each layer. The biggest challenge with this technique, however, is performing lithography for multiple layers. The unexposed PDMS of the lower channel could potentially be cross-linked when the upper layer is exposed due to light reflection, thus rendering the lower channels unable to be developed. This problem can be overcome by using a black photoresist, which has been used to create embedded channels in SU-8 [118]. However, this process is still limited to only a few layers. As more layers are added to the module, the bottom

(unexposed) channels are soft baked for longer periods of time, which makes it harder to develop the PDMS. Also, the length of our channels (1.5 cm) will make it difficult to develop the PDMS. Finally, the black photoresist could add resistance to mass transfer or be toxic to the cells and therefore, would need to be removed after developing the unexposed photoresist.

## A.5 DOUBLE MOLDING, STACKING AND BONDING OF POLY(DIMETHYLSILOXANE) LAYERS

The first soft lithography technique that was explored used double molding and stacking of PDMS layers (Figure A-10). Semi-circular channels were etched into a silicon wafer using xenon difluoride plasma. A negative mold of the channels was fabricated by molding the wafer with PDMS. The negative mold was then coated with parylene to provide a non-stick surface. PDMS was then cast on the negative mold to form the layer of microchannels. Finally, the layers could be stacked and bonded to form a module. The advantages of this technique included the ability to create semi-circular channels and to more accurately control channel width and spacing compared to the wire technology.

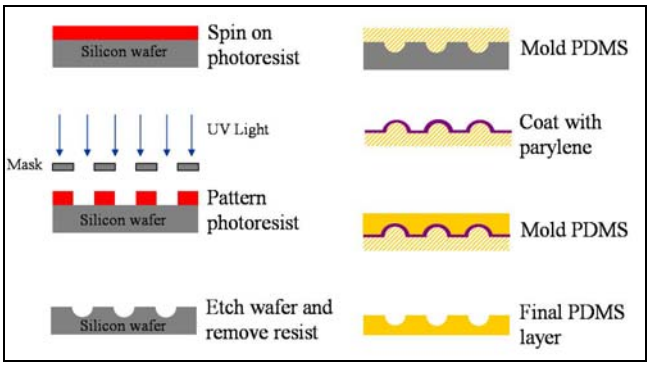


**Figure A-10: Schematic of double molding technique to create PDMS layers**

All photolithography processing was performed in the Nanofabrication facility at Carnegie Mellon University using the equipment listed in Section 3.2.2. Silicon wafers were dehydrated at 200°C for 10 minutes to remove any moisture prior to processing. Hexamethyldisilizane (HMDS) was spun onto the wafer to ensure adequate photoresist adhesion. The positive photoresist, AZ4210 (Clariant Corporation, Somerville, NJ), was spun for 60 seconds at 4000 rpm to produce a 2-micron layer and was soft baked at 120°C for 110 seconds. The photoresist was patterned with UV light using a soda lime/chrome mask that was designed previously by a graduate student at Carnegie Mellon University and contained 1cm x 1cm die of different channels widths (10 – 400 microns) and spacing (250 – 1200 microns). The wafer and mask were placed in contact and exposed to UV light with a power density of 14mW/cm$^2$ for 25 seconds. The photoresist was developed using AZ400K developer diluted 1:3 with DI water for up to 2 minutes. Next, the patterned wafer was etched in a $XeF_2$ etching system (Xactix, Inc., Pittsburgh, PA) to produce semi-circular channels. The plasma etched the wafer laterally (undercutting the patterned photoresist) and vertically and was controlled by the etch time. After etching, the remaining resist was removed with acetone rendering a silicon wafer master ready to be molded with PDMS (Figure A-11).

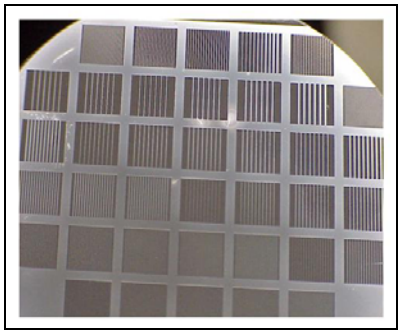

**Figure A-11: Semi-circular channels etched into a silicon wafer**

To create the PDMS layers, the silicon wafer master was first molded with PDMS to produce a negative cast. The PDMS prepolymer and curing agent (Sylgard 184) were mixed in a 10:1 weight ratio. The mixture was either centrifuged at 3300 rpm for 2 minutes or placed in a vacuum oven (25 inHg vacuum) at room temperature for 20 minutes to remove any bubbles introduced during mixing. The PDMS mixture was slowly poured onto the etched silicon wafer, cured for 48 hours at room temperature and then peeled off the master to create a negative mold. The thickness of the negative mold was not critical and therefore not controlled. The PDMS negative mold was then coated with parylene at the Pennsylvania State University Nanofabrication Center to give the mold a "non-stick" surface [103]. The negative mold was cast with PDMS in the second step using a weighted molding technique described by Jo et al. [73] to control the thickness of the final PDMS layer (Figure A-12). Aluminum plates were used to provide a uniform force for molding. The rubber sheets compensated for any non-uniformities in the aluminum plates. The acrylic plates were used to provide a flat surface. After curing, the PDMS positive cast along with the Teflon sheet was peeled off of the negative mold. The PDMS positive casts could easily be peeled off of the Teflon sheet. A total weight of 4.29 lbs produced a thickness of approximately 20 microns. The individual PDMS layers were used in cell culture experiments described in Section 5.3. These layers were not used to fabricate modules since the channel widths and spacing were not designed for this project and were larger than the desired dimensions. The techniques described in Chapter 3 are an improvement to this process by eliminating double molding and the use of weights to control the PDMS thickness.

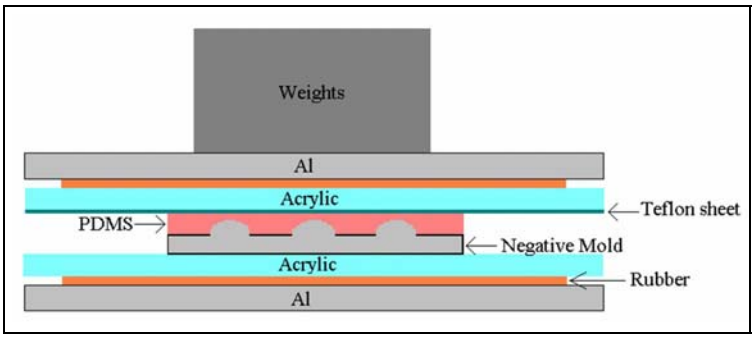


**Figure A-12: Schematic of weighted molding technique to control PDMS thickness**

# APPENDIX B

## UTILIZING MICROPOROUS POLYMER FILMS AS GAS PATHWAYS

We also explored using thin microporous polymers films as the gas pathways as shown in Figure B-1. Sample films were commercially available from several companies, including Advantec MFS, Inc. (Dublin, CA) and Millipore (Billerica, MA). The membrane sheets were several hundred microns thick and were available in polycarbonate, nylon, cellulose acetate, and mixed cellulose ester. The pore size in the films varied from one to ten microns and porosity up to 81% could be achieved. The films were stacked with the PDMS blood layers to form the modules as described below.

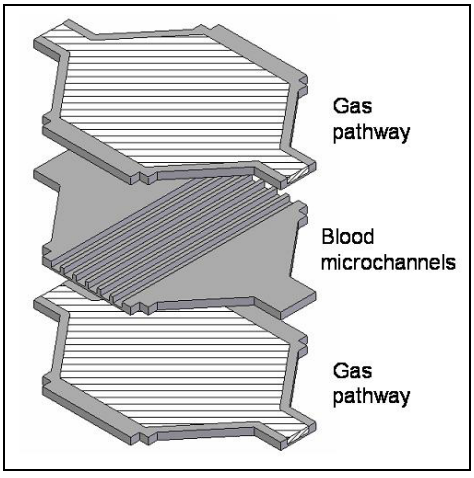


**Figure B-1: Schematic of module using microporous films as gas pathways**

The photolithography processing was performed in the Nanofabrication Facility at Carnegie Mellon University. Each silicon wafer to be processed was cleaned with acetone and propanol and dried with a nitrogen gun. The wafer was then dehydrated in a 200°C oven for 15 minutes. Hexamethyldisilazane (HMDS) was spun onto the wafer using a six-second spread at 500 rpm and a thirty-second spin at 3000 rpm. Next, AZ4620 was spun onto the wafer using a six-second spread at 500 rpm to coat the wafer with resist and then a thirty-second spin at 3000 rpm to create a thickness of 9-10 microns. A five-minute rest period was used to eliminate any non-uniformity in the resist coating. The wafer was then soft baked for 30 minutes in a 90°C oven. A second layer of photoresist was applied using the same spin recipe, rest period, and soft bake as described above to produce a total thickness of approximately 20 microns. Another rest period of one-hour was used to allow rehydration of the photoresist. During this time, the photoresist edge bead was removed in order to promote uniform contact between the mask and the wafer. The wafer and the mask described in Section A.5 were placed into a mask aligner and exposed for 60 seconds using a power density of 14 $mW/cm^2$. The wafer was developed 30 minutes after exposure using AZ400K developer diluted with DI water in a 1:3 ratio. The wafers were diced into four chips and silanated to improve PDMS mold release.

The fabrication process used to create modules with blood microchannels and microporous polymer films is shown in Figure B-2. Poly(dimethylsiloxane) was mixed in a 10:1 ratio (prepolymer:curing agent) and de-aired using a vacuum oven. A plain silicon wafer was spin-coated with PDMS using a twenty-second spread at 500 rpm (acceleration of 86 rpm/s) and a one-minute spin at 500 rpm (acceleration of 258 rpm/s) to create a thick base layer. A five-minute rest period was used to eliminate any non-uniformity in the PDMS layer, and then the PDMS was cured at 100°C for 45 minutes (Step 1). Three silicon chips were spin-coated with

PDMS using the same spread step and a one-minute spin at 3000 rpm (acceleration of 258 rpm/s). The same rest period and curing step were used (Step 2). Next, a very thin PDMS "glue" layer was spun onto one of the PDMS coated chips using a spin speed of 5500 rpm for one minute (acceleration of 258 rpm/s) and was then partially cured at 100°C for two minutes (Step 3). A rectangular piece of membrane (2.5 x 1.6 cm) was carefully placed onto the chip and cured for another two minutes to bond the PDMS to the membrane (Step 4). PDMS was then poured onto the chip to cover the membrane and spin-coated to create a thin "glue" layer, which was cured for two minutes (Step 5). The thick base layer was then placed onto the membrane and cured for 15 minutes for bonding (Step 6). Meanwhile, processing steps 2 – 5 were repeated for the second silicon chip to create the structure shown in Step 7. Next, the structure consisting of the thick base layer, a membrane, and a blood microchannel layer was peeled off of the silicon chip and placed on the structure shown in Step 7 to create a module with two gas layers and two blood layers (Step 8). These steps can be repeated until the desired number of layers is achieved.

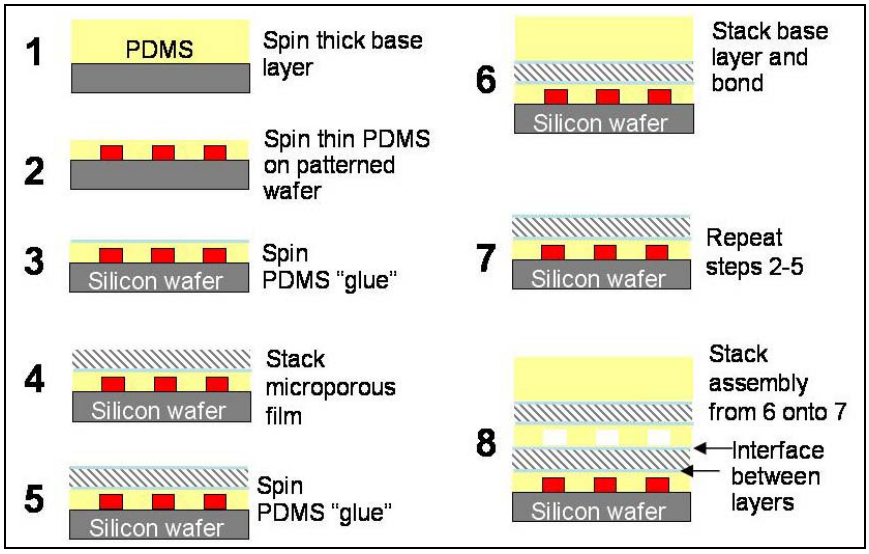


**Figure B-2: Module fabrication process using microporous polymer films as gas pathways**

Modules with two or three layers of both gas and blood pathways were fabricated using polycarbonate, nylon, cellulose acetate, and mixed cellulose ester films. Both nylon and mixed cellulose ester membranes were difficult to handle and were easily damaged. A two-layer module with polycarbonate membranes is shown in Figure B-3. The membrane pore size was ten microns and the porosity was 60%. The layer of PDMS "glue" was less than 20 microns thick demonstrating the ability to minimize the diffusion distance for gas exchange. Partially curing the PDMS glue adequately bonded the membranes to the blood layers. A partial cure time of two minutes was needed to prevent the PDMS "glue" from filling in the blood microchannels; however, partial cure times in excess of two minutes created inconsistencies in the bonding. The thick base layer aided in handling and peeling the structures from the silicon chips.

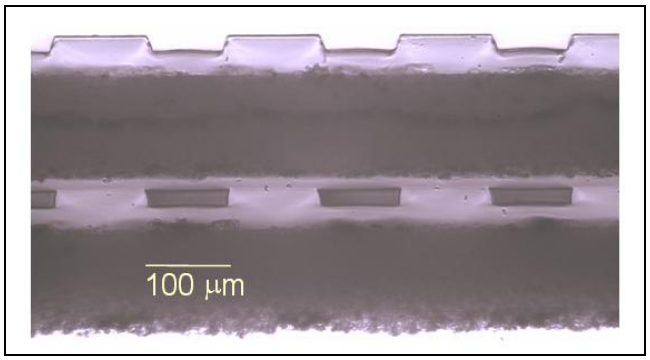


**Figure B-3: Cross section of module with polycarbonate microporous films**

The cross-sectional image of the module created with this technique appears promising, but several issues still need to be explored to evaluate the feasibility of this process. Higher magnification images of the cross-section need to be examined to determine if the PDMS glue penetrated into the microporous film, which would increase the diffusion distance and reduce the size of the gas pathway. The edges of the films need to be inspected to ensure that the films are

sealed to prevent leaks. Peeling and stacking the module becomes more difficult as more layers are stacked. Finally, the modules need to be manifolded and perfused with gas to determine the pressure drop versus flow characteristics of the gas pathways and to determine if the bonding can withstand the required pressures.

## APPENDIX C

```
% %--Circle
% x=-3:0.01:3;
% y=(sqrt(9-x.^2));
% plot(x,y)
%
% length_act=pi*6/2
%
% f=gradient(y,x);
% integrand=sqrt(1+f.^2);
% arc_length=trapz(x,integrand)
%
% area_act=pi/2*3^2
% area_calc=trapz(x,y)

clear all
data = load('trial1.txt');
x=data(:,1);            %CHANNEL X dim
y=data(:,3);            %CHANNEL Height
subplot(1,3,1)
plot(x,y)

%-------CHANNEL 1
x1=x(200:445);
y1=y(200:445);
grad1=gradient(y1,x1);

channel1_x=x(217:426);
channel1_y=y(217:426);
subplot(1,3,2)
plot(channel1_x,channel1_y)

f=gradient(channel1_y,channel1_x);      %gradient
integrand1=sqrt(1+f.^2);
arc_length_1=trapz(channel1_x,integrand1)

channel1_area=trapz(channel1_x,channel1_y)
```

```
%---------------Channel 2
channel2_x=x(512:723);
channel2_y=y(512:723);
subplot(1,3,3)
plot(channel2_x,channel2_y)

f2=gradient(channel2_y,channel2_x);        %gradient
integrand2=sqrt(1+f2.^2);
arc_length_2=trapz(channel2_x,integrand2)

channel2_area=trapz(channel2_x,channel2_y)
```

# APPENDIX D

## ERROR PROPAGATION CALCULATIONS FOR PERMEANCE

The oxygen and carbon dioxide permeance (K) of the modules was calculated based on Equation 13. The flow rate (Q) and transmembrane pressure (P) were measured for *n* samples. The surface area (SA) was found by measuring the arc length and width of the channels, as described in Chapter 4.

$$K = \frac{Q}{P \cdot SA} \qquad \textbf{Equation 13}$$

All of the measurements used to calculate the permeance have error associated with them; for example, the flow rate (Q) is really Q + ΔQ. Therefore, the calculated permeance will have an error due to the contributions of the individual errors. The total error can be found by calculating the error propagation.

A few rules exist for calculating the error propagation. For adding or subtracting two variables, the error is found by adding the squares of the variance and taking the square root of the summation. For example, if z = x + y, then $\Delta z = \sqrt{(\Delta x)^2 + (\Delta y)^2}$ . For multiplying or dividing two variables, the relative error is found using the following equation.

$$\frac{\Delta z}{z} = \sqrt{\left(\frac{\Delta x}{x}\right)^2 + \left(\frac{\Delta y}{y}\right)^2} \qquad \textbf{Equation 14}$$

The rules described above were used in a stepwise manner to calculate the permeance error. First the error of the surface area was found. The average channel width (w) and arc length (a) were measured to be 104.25 ± 1.26 μm and 129.85 ± 1.56 μm, respectively. The wetted perimeter (wp) was calculated by adding the width and the arc length. The error associated with the wetted perimeter was then:

$$\Delta wp = \sqrt{(\Delta a)^2 + (\Delta w)^2} = 2.0\,x10^{-4}\,cm$$

The surface area was calculated by multiplying the wetted perimeter by the length of the module, L =1.8 ± 0.0001 cm, and was found to be 0.042 cm. The error associated with the surface area was then:

$$\Delta SA = SA \cdot \sqrt{\left(\frac{\Delta L}{L}\right)^2 + \left(\frac{\Delta wp}{wp}\right)^2} = 3.6\,x10^{-4}\,cm$$

Next, the error of the denominator (P * SA) of Equation 13 was calculated using a pressure of 25.3 ± 0.5 cm.

$$\Delta(P * SA) = (P * SA) \cdot \sqrt{\left(\frac{\Delta SA}{SA}\right)^2 + \left(\frac{\Delta P}{P}\right)^2} = 2.3\,x10^{-2}\,cm$$

Finally the error associated with the oxygen and carbon dioxide permeance was calculated for all four modules using the following equation.

$$\Delta K = K \cdot \sqrt{\left(\frac{\Delta Q}{Q}\right)^2 + \left(\frac{\Delta P * SA}{P * SA}\right)^2} \qquad \textbf{Equation 15}$$

The following tables includes the values for the average $O_2$ and $CO_2$ flow rates that were measured, the average calculated $O_2$ and $CO_2$ permeance, and the errors associated with the calculation. The calculated error propagation values are similar or greater than the standard deviations reported in Chapter 4, which is expected since error propagation is a more conservative way to find the error.

| | **OXYGEN** | | |
|---|---|---|---|
| **Module** | **Flow (Q)** ml/s | **Average Permeance (K)** ml/s · cm$^2$ · cmHg | **Error (ΔK)** ml/s · cm$^2$ · cmHg |
| M1 (500rpm) | $6.21 \times 10^{-4} \pm 3.50 \times 10^{-5}$ | $5.18 \times 10^{-6}$ | $2.91 \times 10^{-7}$ |
| M2 (500rpm) | $6.66 \times 10^{-4} \pm 3.86 \times 10^{-5}$ | $5.61 \times 10^{-6}$ | $3.25 \times 10^{-7}$ |
| M3 (1000rpm) | $1.11 \times 10^{-3} \pm 3.03 \times 10^{-5}$ | $9.16 \times 10^{-6}$ | $2.51 \times 10^{-7}$ |
| M4 (1000rpm) | $1.07 \times 10^{-3} \pm 4.22 \times 10^{-5}$ | $8.74 \times 10^{-6}$ | $3.46 \times 10^{-7}$ |

| | **CARBON DIOXIDE** | | |
|---|---|---|---|
| **Module** | **Flow (Q)** ml/s | **Average Permeance (K)** ml/s · cm$^2$ · cmHg | **Error (ΔK)** ml/s · cm$^2$ · cmHg |
| M1 (500rpm) | $2.12 \times 10^{-3} \pm 1.24 \times 10^{-4}$ | $1.77 \times 10^{-5}$ | $1.04 \times 10^{-6}$ |
| M2 (500rpm) | $1.97 \times 10^{-3} \pm 2.77 \times 10^{-4}$ | $1.65 \times 10^{-5}$ | $2.32 \times 10^{-6}$ |
| M3 (1000rpm) | $4.19 \times 10^{-3} \pm 6.84 \times 10^{-4}$ | $3.50 \times 10^{-5}$ | $5.71 \times 10^{-6}$ |
| M4 (1000rpm) | $4.23 \times 10^{-3} \pm 6.04 \times 10^{-4}$ | $3.55 \times 10^{-5}$ | $5.06 \times 10^{-6}$ |

## BIBLIOGRAPHY


1. Seeley, R.R.S., T.D.; Tate, P., *Respiratory System*, in *Anatomy & Physiology*. 1998, WCB McGraw-Hill: New York, NY. p. 732-775.

2. Galletti, P.M. and C.K. Colton, *Artificial lungs and blood-gas exchange devices*, in *The Biomedical Engineering Handbook*, J.D. Bronzino, Editor. 2000, CRC Press LLC: Boca Raton. p. 1-19.

3. Newhouse, M.T., *Tennis anyone? The lungs as a new court for systemic therapy.* CMAJ., 1999. 161(10): p. 1287-1288.

4. ER, W., *The Pathway for Oxygen: Structure and Function in the Mammalian Respiratory System*. 1984: Harvard University Press. 272-300.

5. Forster, R.E., *Diffusion of gases across the alveolar membrane*, in *Handbook of Physiology Section 3: The Resiratory System Volume IV*, A.P. Fishman, Editor. 1987, American Physiological Society. p. 71-88.

6. Federspiel, W.J., P.J. Sawzik, H.S. Borovetz, G.D. Reeder, and B.G. Hattler, *Temporary Support of the Lungs - the Artificial Lung*, in *The Transplantation and Replacement of Thoracic Organs*, D.K.C. Cooper, L.W. Miller, and G.A. Patterson, Editors. 1996, Kluwer Academic Publishers: Boston. p. 717-728.

7. *Lung Disease Data: 2006*, in *www.lungusa.org*. 2006.

8. *Adult (Acute) Respiratory Distress Syndrome (ARDS) Fact Sheet*, in *www.lungusa.org*. 2006.

9. Weinacker, A.B. and L.T. Vaszar, *Acute respiratory distress syndrome: physiology and new management strategies.* Annu.Rev.Med., 2001. 52: p. 221-237.

10. Asimakopoulos, G., P.L. Smith, C.P. Ratnatunga, and K.M. Taylor, *Lung injury and acute respiratory distress syndrome after cardiopulmonary bypass.* Ann Thorac Surg, 1999. 68(3): p. 1107-15.

11. *Chronic Obstructive Pulmonary Disease (COPD) Fact Sheet (Chronic Bronchitis and Emphysema)*, in *www.lungusa.org*. 2006.

12. Ramnath, V.R., D.R. Hess, and B.T. Thompson, *Conventional mechanical ventilation in acute lung injury and acute respiratory distress syndrome.* Clin Chest Med, 2006. 27(4): p. 601-13; abstract viii.

13. Slutsky, A.S., *Lung Injury Caused by Mechanical Ventilation.* Chest, 1999. 116(90001): p. 9S-a-15.

14. Ichiba, S. and R.H. Bartlett, *Current status of extracorporeal membrane oxygenation for severe respiratory failure.* Artif.Organs, 1996. 20(2): p. 120-123.

15. Zwischenberger, J.B. and R.H. Bartlett, *An introduction to extracorporeal life support*, in *ECMO Extracorporeal Cardiopulmonary Support in Critical Care*, J.B. Zwischenberger and R.H. Bartlett, Editors. 1995, Extracorporeal Life Support Organization: Ann Arbor, MI. p. 11-14.

16. Dark, J.H., *Extracorporeal Respiratory Support*, in *Techniques in Extracorporeal Circulation*, P.H. Kay, Editor. 1992, Butterworth-Heinemann Ltd: Boston. p. 309-320.

17. Wendel, H.P. and G. Ziemer, *Coating-techniques to improve the hemocompatibility of artificial devices used for extracorporeal circulation.* Eur.J.Cardiothorac.Surg., 1999. 16(3): p. 342-350.

18. Larsson, R., *Heparin-Binding to Improve Biocompatibility*, in *Encyclopedia of Biomaterials and Biomedical Engineering*, G.E. Wnek, Bowlin, G.L., Editor. 2004, Marcel Dekker, Inc.: New York, NY. p. 753-761.

19. Mols, G., T. Loop, K. Geiger, E. Farthmann, and A. Benzing, *Extracorporeal membrane oxygenation: a ten-year experience.* Am.J.Surg, 2000. 180(2): p. 144-154.

20. Federspiel, W.J., Henchir, K.A., *Lung, Artificial: Basic Principles and Current Applications*, in *Encyclopedia of Biomaterials and Biomedical Engineering*. 2004, Marcel Dekker, Inc.: New York, NY. p. 910-921.

21. Hattler, B.G. and W.J. Federspiel, *Gas Exchange in the Venous System: Support for the Failing Lung*, in *The Artificial Lung*, S.N. Vaslef and R.W. Anderson, Editors. 2002, Landes Bioscience. p. 133-174.

22. PW, D., D.W. DS, D.S. F, V.N. G, and V. PR, *Mass Transfer Characteristics of Artificial Lungs.* ASAIO J., 2001. 47: p. 628-633.

23. Vaslef, S.N., *Implantable artificial lungs: Fantasy or feasibility?* New Surgery, 2002. 1(2).

24. Federspiel, W.J., Svitek, R.G., *Lung, Artificial: Current Research and Future Directions*, in *Encyclopedia of Biomaterials and Biomedical Engineering*. 2004, Marcel Dekker, Inc.: New York, NY. p. 922-931.

25. Mortensen, J.D., *Intravascular oxygenator: a new alternative method for augmenting blood gas transfer in patients with acute respiratory failure.* Artif.Organs, 1992. 16(1): p. 75-82.

26. Mortensen, J.D. and G. Berry, *Conceptual and design features of a practical, clinically effective intravenous mechanical blood oxygen/carbon dioxide exchange device (IVOX).* Int.J.Artif.Organs, 1989. 12(6): p. 384-389.

27. Conrad, S.A., A. Bagley, B. Bagley, and R.N. Schaap, *Major findings from the clinical trials of the intravascular oxygenator.* Artif.Organs, 1994. 18(11): p. 846-863.

28. Conrad, S.A., J.M. Eggerstedt, V.F. Morris, and M.D. Romero, *Prolonged intracorporeal support of gas exchange with an intravenacaval oxygenator.* Chest, 1993. 103(1): p. 158-161.

29. Conrad, S.A., J.B. Zwischenberger, J.M. Eggerstedt, and A. Bidani, *In vivo gas transfer performance of the intravascular oxygenator in acute respiratory failure.* Artif.Organs, 1994. 18(11): p. 840-845.

30. Eash, H.J., B.J. Frankowski, K. Litwak, W.R. Wagner, B.G. Hattler, and W.J. Federspiel, *Acute in vivo testing of a respiratory assist catheter: implants in calves versus sheep.* ASAIO Journal, 2003. 49(4): p. 370-377.

31. Eash, H.J., H.M. Jones, B.G. Hattler, and W.J. Federspiel, *Evaluation of plasma resistant hollow fiber membranes for artificial lungs*, in *ASAIO Journal*. 2004.

32. Federspiel, W.J., J.F. Golob, T.L. Merrill, L.W. Lund, J.A. Bultman, B.J. Frankowski, M. Watach, K. Litwak, and B.G. Hattler, *Ex vivo testing of the intravenous membrane oxygenator.* ASAIO J., 2000. 46(3): p. 261-267.

33. Federspiel, W.J., T. Hewitt, M.S. Hout, F.R. Walters, L.W. Lund, P.J. Sawzik, G. Reeder, H.S. Borovetz, and B.G. Hattler, *Recent progress in engineering the Pittsburgh intravenous membrane oxygenator.* ASAIO J., 1996. 42(5): p. M435-M442.

34. Federspiel, W.J., T.J. Hewitt, and B.G. Hattler, *Experimental evaluation of a model for oxygen exchange in a pulsating intravascular artificial lung.* Ann.Biomed.Eng, 2000. 28(2): p. 160-167.

35. Federspiel, W.J., M.S. Hout, T.J. Hewitt, L.W. Lund, S.A. Heinrich, P. Litwak, F.R. Walters, G.D. Reeder, H.S. Borovetz, and B.G. Hattler, *Development of a low flow resistance intravenous oxygenator.* ASAIO J., 1997. 43(5): p. M725-M730.

36. Golob, J.F., W.J. Federspiel, T.L. Merrill, B.J. Frankowski, K. Litwak, R. H., and B.G. Hattler, *Acute in-vivo testing of an intravascular respiratory support catheter.* ASAIO J., 2001. 47(5): p. 432-7.

37. Hattler, B.G. and W.J. Federspiel, *Progress with the development of the intravenous membrane oxygenator.* Perfusion, 1999. 14(4): p. 311-315.

38. Hattler, B.G., L.W. Lund, J. Golob, H. Russian, M.F. Lann, T.L. Merrill, B. Frankowski, and W.J. Federspiel, *A respiratory gas exchange catheter: in vitro and in vivo tests in large animals.* Journal of Thoracic and Cardiovascular Surgery, 2002. 124(3): p. 520-530.

39. Eash, H.J.M., K.M; Frankowski, B.J.; Hattler, B.G.; Federspiel, W.j., *Evaluation of Fiber Bundle Rotation for Enhancing Gas Exchange in a Respiratory Assist Catheter.* ASAIO J, 2007. 53: p. in press.

40. Cattaneo, G., A. Strauss, and H. Reul, *Compact intra- and extracorporeal oxygenator developments.* Perfusion, 2004. 19(4): p. 251-5.

41. Cattaneo, G.F., H. Reul, T. Schmitz-Rode, and U. Steinseifer, *Intravascular blood oxygenation using hollow fibers in a disk-shaped configuration: experimental evaluation of the relationship between porosity and performance.* Asaio J, 2006. 52(2): p. 180-5.

42. Cattaneo, G.F.R., H., *New Fiber Configuration for Intravenous Gas Exchange.* The International Journal of Artificial Organs, 2005. 28(3): p. 244-250.

43. Svitek, R.G., B.J. Frankowski, and W.J. Federspiel, *Evaluation of a pumping assist lung that uses a rotating fiber bundle.* Asaio J, 2005. 51(6): p. 773-80.

44. Svitek, R.G., *Development of a Paracorporeal Respiratory Assist Lung*, in *Chemical Engineering*. 2006, University of Pittsburgh: Pittsburgh, PA. p. 171.

45. Wu, Z.J.G., M.; Litwak, K.N.; Griffith, B.P., *Progress Toward an Ambulatory Pump-Lung.* The Journal of Thoracic and Cardiovascular Surgery, 2005. 130(4): p. 973-978.

46. Kung, H.H.M., L.F.,; Kung, M., in *http://www.chem-biol-eng.northwestern.edu/people/faculty/projects/Kung_Artificial_Organs.pdf*. 2006.

47. Lee, J.K.K., M.C.;Kung, H.H.; Mockros, L.F., *Microchannel Technologies for Artificial Lungs.* ASAIO J, 2006. 52(2): p. 66A.

48. *The UMMOX: Design of an artificial lung for humans, based on the "microlung" concept*, in *www.umecc.nl*, U.M.E.C. Centre, Editor. 2004.

49. Sillen, R.M.J.S., E.; KleinSoetebier, F.; Oostveen, M.; Huinck, J.; Bouwes, H.; Bargman, N.; Kuik, L.; Bons, P.; Houston, R.; Kalkman, C.J.; Christiani, J.; Saumer, M., *The Micro-Lung for Artificial Respiration "From Micro-Oxygenator to UMMOX"*, in *www.umecc.nl*. 2004.

50. Sillen, R.M.J.S., E.; KleinSoetebier, F.; Oostveen, M.; Huinck, J.; Bouwes, H.; Bargman, N.; Kuik, L.; Bons, P.; Houston, R.; Kalkman, C.J.; Christiani, J.; Saumer, M. *The Micro-Lung for Artificial Respiration From Micro-Oxygenator to UMMOX*. in *Microsystems in Practice, 5th Symposium*. 2004. Utrecht, The Netherlands.

51. Dasse, K.A., B.F. Monzyk, and R.J. Gilbert, *Development of a photolytic artificial lung (PAL).* ASAIO J., 2002. 48(2): p. 139.

52. Vollmer, A.P., R.F. Probstein, R. Gilbert, and T. Thorsen, *Development of an integrated microfluidic platform for dynamic oxygen sensing and delivery in a flowing medium.* Lab Chip, 2005. 5: p. 1059-1066.

53. Dasse, K.A., B.F. Monzyk, E.C. Burckle, J.R. Busch, and R.J. Gilbert, *Development of a photolytic artificial lung: preliminary concept validation.* Asaio J, 2003. 49(5): p. 556-63.

54. Monzyk, B.F., E.C. Burckle, L.M. Carleton, J. Busch, K.A. Dasse, P.M. Martin, and R.J. Gilbert, *Photolytically driven generation of dissolved oxygen and increased oxyhemoglobin in whole blood.* Asaio J, 2006. 52(4): p. 456-66.

55. Maluf, N., *An Introduction to Microelectromechanical Systems Engineering*. 2000, Norwood: Artech House, Inc.

56. Chen, C.S., M. Mrksich, S. Huang, G.M. Whitesides, and D.E. Ingber, *Micropatterned surfaces for control of cell shape, position, and function.* Biotechnol.Prog., 1998. 14(3): p. 356-363.

57. Folch, A. and M. Toner, *Cellular micropatterns on biocompatible materials.* Biotechnol.Prog., 1998. 14(3): p. 388-392.

58. Kane, R.S., S. Takayama, E. Ostuni, D.E. Ingber, and G.M. Whitesides, *Patterning proteins and cells using soft lithography.* Biomaterials, 1999. 20(23-24): p. 2363-2376.

59. Tan, J., H. Shen, K.L. Carter, and W.M. Saltzman, *Controlling human polymorphonuclear leukocytes motility using microfabrication technology.* J.Biomed.Mater.Res., 2000. 51(4): p. 694-702.

60. Bhatia, S.N., M.L. Yarmush, and M. Toner, *Controlling cell interactions by micropatterning in co-cultures: hepatocytes and 3T3 fibroblasts.* J.Biomed.Mater.Res., 1997. 34(2): p. 189-199.

61. den Braber, E.T., J.E. de Ruijter, H.T. Smits, L.A. Ginsel, A.F. von Recum, and J.A. Jansen, *Effect of parallel surface microgrooves and surface energy on cell growth.* J.Biomed.Mater.Res., 1995. 29(4): p. 511-518.

62. Turner, A.M., N. Dowell, S.W. Turner, L. Kam, M. Isaacson, J.N. Turner, H.G. Craighead, and W. Shain, *Attachment of astroglial cells to microfabricated pillar arrays of different geometries.* J.Biomed.Mater.Res., 2000. 51(3): p. 430-441.

63. Takayama, S., E. Ostuni, X. Qian, J.C. McDonald, X. Jiang, M.-H. Wu, P. Leduc, D.E. Ingber, and G.M. Whitesides, *Patterning the Topographical Environment for Mammalian Cell Culture Using Laminar Flows in Capillaries.* Microtechnologies in Medicine and Biology, 1st Annual International, Conference On, 2000: p. 322-325.

64. Li, M., J.D. Glawe, H. Green, D.K. Mills, M.J. McShane, and B.K. Gale, *Effect of high-aspect-ratio microstructures on cell growth and attachment.* Microtechnologies in Medicine and Biology, 1st Annual International, Conference On, 2000: p. 531-536.

65. Kikuchi, Y., K. Sato, H. Ohki, and T. Kaneko, *Optically Accessible Microchannels Formed in a Single-Crystal Silicon Substrate for Studies of Blood Rheology.* Microvasc.Res., 1992. 44: p. 226-240.

66. Kikuchi, Y., *Effect of Leukocytes and Platelets on Blood Flow through a Parallel Array of Microchannels: Micro- and Macroflow Relation and Rheological Measures of Leukocyte and Platelet Activities.* Microvasc.Res., 1995. 50: p. 288-300.

67. Sutton, N., M.C. Tracey, I.D. Johnston, R.S. Greenaway, and M.W. Rampling, *A Novel Instrument for Studying the Flow Behaviour of Erythrocytes through Microchannels Simulating Human Blood Capillaries.* Microvasc.Res., 1997. 53: p. 272-281.

68. Cokelet, G.R., R. Soave, G. Pugh, and L. Rathbun, *Fabrication of in vitro microvascular blood flow systems by photolithography.* Microvasc.Res., 1993. 46(3): p. 394-400.

69. Tracey, M.C., R.S. Greenaway, A. Das, P.H. Kaye, and A.J. Barnes, *A Silicon Micromachined Device for Use in Blood Cell Deformability Studies.* IEEE Transactions on Biomedical Engineering, 1995. 42(8): p. 751-761.

70. Wilding, P., J. Pfahler, H.H. Bau, J.N. Zemel, and L.J. Kricka, *Manipulation and flow of biological fluids in straight channels micromachined in silicon.* Clin.Chem., 1994. 40(1): p. 43-47.

71. Brody, J.P., Y. Han, R.H. Austin, and M. Bitensky, *Deformation and flow of red blood cells in a synthetic lattice: evidence for an active cytoskeleton.* Biophys.J., 1995. 68(6): p. 2224-2232.

72. Frame, M.D., G.B. Chapman, Y. Makino, and I.H. Sarelius, *Shear stress gradient over endothelial cells in a curved microchannel system.* Biorheology, 1998. 35(4-5): p. 245-261.

73. Jo, B., L.M. Van Lerberghe, K.M. Motsegood, and D.J. Beebe, *Three-Dimensional Micro-Channel Fabrication in Polydimethylsiloxane (PDMS) Elastomer.* Journal of Microelectromechanical Systems, 2000. 9(1): p. 76-81.

74. McDonald, J.C., D.C. Duffy, J.R. Anderson, D.T. Chiu, H. Wu, O.J. Schueller, and G.M. Whitesides, *Fabrication of microfluidic systems in poly(dimethylsiloxane).* Electrophoresis, 2000. 21(1): p. 27-40.

75. Anderson, J.R., D.T. Chiu, R.J. Jackman, O. Cherniavskaya, J.C. McDonald, H. Wu, S.H. Whitesides, and G.M. Whitesides, *Fabrication of topologically complex three-dimensional microfluidic systems in PDMS by rapid prototyping.* Anal.Chem., 2000. 72(14): p. 3158-3164.

76. Unger, M.A., H.P. Chou, T. Thorsen, A. Scherer, and S.R. Quake, *Monolithic microfabricated valves and pumps by multilayer soft lithography.* Science, 2000. 288(5463): p. 113-116.

77. Satyanarayana, S., R.N. Karnik, and A. Majumdar, *Stamp-and-stick room-temperature bonding technique for microdevices.* Microelectromechanical Systems, Journal of, 2005. 14(2): p. 392-399.

78. Wu, H., Huang, B., Zare, R.N., *Construction of microfluidic chips using polydimethylsiloxane for adhesive bonding.* Lab Chip, 2005. 5: p. 1393-1398.

79. Bucaro, M.A., J.M. Calvert, A.S. Rudolph, B. Spargo, and R. Kapur, *Photolithography As A Tool To Fabricate Polymeric Flow Chambers For In-Vitro Cellular Applications.* IEEE, 1997: p. 217-219.

80. BouÃ¯s, D., G.A.P. Hospers, C. Meijer, G. Molema, and N.H. Mulder, *Endothelium in vitro: A review of human vascular endothelial cell lines for blood vessel-related research.* Angiogenesis, 2001. 4(2): p. 91-102.

81. Pearson, J.D., *Normal endothelial cell function.* Lupus, 2000. 9(3): p. 183-8.

82. Heyligers, J.M.M.A., C.H.P.; Verhagen, H.J.M.; de Groot, PH.G.; Moll, F.L., *Improving Small-Diameter Vascular Grafts: From the Application of an Endothelial Cell Lining to the Construction of a Tissue-Engineered Blood Vessel.* Annals of Vascular Surgery, 2005. 19(3): p. 1-9.

83. Hoenig, M.R., G.R. Campbell, and J.H. Campbell, *Vascular grafts and the endothelium.* Endothelium, 2006. 13(6): p. 385-401.

84. Schmidt, S.P.B., G.L., *Endothelial Cell Seeding: A Review,* in *Tissue Engineering of Vascular Prosthetic Grafts,* P. Zilla, Greisler, H.P., Editor. 1999, R.G. Landes Company: Austin, TX. p. 61-68.

85. Arts, C.H.P., J.D. Blankensteijn, G.J. Heijnen-Snyder, H.J.M. Verhagen, P.P.A. Hedeman Joosten, J.J. Sixma, B.C. Eikelboom, and P.G. de Groot, *Reduction of Non-endothelial Cell Contamination of Microvascular Endothelial Cell Seeded Grafts Decreases Thrombogenicity and Intimal Hyperplasia.* European Journal of Vascular and Endovascular Surgery, 2002. 23(5): p. 404-412.

86. Laredo, J., Xue, L., Greisler, H.P., *Vascular Grafts: Development Strategies,* in *Encyclopedia of Biomaterials and Biomedical Engineering,* G.E. Wnek, Bowlin, G.L., Editor. 2004, Marcel Dekker, Inc.: New York. p. 1726-1734.

87. Borenstein, J.C., W.; Hartman, L.; Kaazempur-Mofrad, M.; King, K.; Sevy, A.; Shin, M.; Weinberg, E.; Vacanti, J., *Living 3-Dimensional Microfabricated Constructs for the Replacement of Vital Organ Function.* 2003, Draper Labs. p. 22-27.

88. Borenstein, J.T., Weinberg, E.J., Kaazempur-Mofrad, M.R., Vacanti, J.P., *Tissue Engineering of Microvascular Networks*, in *Encyclopedia of Biomaterials and Biomedical Engineering*. 2004, Marcel Dekker, Inc. p. 1594-1603.

89. Borenstein, J.T., H. Terai, K.R. King, E.J. Weinberg, M.R. Kaazempur-Mofrad, and J.P. Vacanti, *Microfabrication Technology for Vascularized Tissue Engineering.* Biomedical Microdevices, 2002. 4(3): p. 167-175.

90. Fidkowski, C., M.R. Kaazempur-Mofrad, J. Borenstein, J.P. Vacanti, R. Langer, and Y. Wang, *Endothelialized microvasculature based on a biodegradable elastomer.* Tissue Eng, 2005. 11(1/2): p. 302-9.

91. Shin, M.M., K.; Ishii, O.; Terai, H.; Kaazempur-Mofrad, M.; Borenstein, J.; Detmar, M.; Vacanti, J.P., *Endothelialized Networks with a Vascular Geometry in Microfabricated Poly(dimethyl siloxane).* Biomedical Microdevices, 2004. 6(4): p. 269-278.

92. Wang, G.J.C., C.L.; Hsu, S.H.;Chiang, Y.L., *Bio-MEMS fabricated artificial capillaries for tissue engineering.* Microsyst. Technol., 2005. 12: p. 120-127.

93. Wang, G.J.H., Y.F.; Hsu, S.H.;Horng, R.H., *JSR photolithography based microvessel scaffold fabrication and cell seeding.* Biomedical Microdevices, 2006. 8: p. 17-23.

94. Wang, G.J.H., Y.F., *Structure optimization of microvascular scaffolds.* Biomedical Microdevices, 2005. 10: p. 51-58.

95. Ostrovidov, S., J. Jiang, Y. Sakai, and T. Fujii, *Membrane-based PDMS microbioreactor for perfused 3D primary rat hepatocyte cultures.* Biomed Microdevices, 2004. 6(4): p. 279-87.

96. Tourovskaia, A., Figueroa-Masot, X., Folch, A., *Differentiation-on-a-chip: A microfluidic platform for long-term cell culture studies.* Lab Chip, 2005. 5: p. 14-19.

97. Boland, T., V. Mironov, A. Gutowska, E.A. Roth, and R.R. Markwald, *Cell and Organ Printing 2: Fusion of Cell Aggregates in Three-Dimensional Gels.* The Anatomical Record Part A, 2003. 272A: p. 497-502.

98. Mironov, V., T. Boland, T. Trusk, G. Forgacs, and R.R. Markwald, *Organ Printing: computer-aided jet-based 3D tissue engineering.* Trends Biotechnol., 2003. 21(4): p. 157-161.

99. Wilson, W.C. and T. Boland, *Cell and organ printing 1: protein and cell printers.* The Anatomical Record Part A, 2003. 272A(2): p. 491-496.

100. de Jong, J., B. Ankone, R.G. Lammertink, and M. Wessling, *New replication technique for the fabrication of thin polymeric microfluidic devices with tunable porosity.* Lab Chip, 2005. 5: p. 1240-1247.

101. Anderson, J.M., N.P. Ziats, A. Azeez, M.R. Brunstedt, S. Stack, and T.L. Bonfield, *Protein adsorption and macrophage activation on polydimethylsiloxane and silicone rubber.* J.Biomater.Sci.Polym.Ed, 1995. 7(2): p. 159-169.

102. Bordenave, L., R. Bareille, F. Lefebvre, J. Caix, and C. Baquey, *Cytocompatibility study of NHLBI primary reference materials using human endothelial cells.* J.Biomater.Sci.Polym.Ed, 1992. 3(6): p. 509-516.

103. Desai, T.A., J. Deutsch, D. Motlagh, W. Tan, and B. Russell, *Microtextured Cell Culture Platforms: Biomimetic Substrates for the Growth of Cardiac Myocytes and Fibroblasts.* Biomedical Microdevices, 1999. 2(2): p. 123-129.

104. Ott, M.J. and B.J. Ballermann, *Shear stress-conditioned, endothelial cell-seeded vascular grafts: improved cell adherence in response to in vitro shear stress.* Surgery, 1995. 117(3): p. 334-339.

105. Feugier, P., R.A. Black, J.A. Hunt, and T.V. How, *Attachment, morphology and adherence of human endothelial cells to vascular prosthesis materials under the action of shear stress.* Biomaterials, 2005. 26(13): p. 1457-1466.

106. Ng, K.W.L., D.T.W.; Hutmacher, D.W., *The Challenge to Measure Cell Proliferation in Two and Three Dimensions.* Tissue Eng, 2005. 11(1/2): p. 182-191.

107. Leclerc, E., Y. Sakai, and T. Fujii, *Cell Culture in 3-Dimensional Microfluidic Structure of PDMS (polydimethylsiloxane).* Biomedical Microdevices, 2003. 5(2): p. 109-114.

108. Zengerle, R.L., M.; Kluge, S.; Richter, A. *Carbon Dioxide Priming of Micro Liquid Systems*. in *Proceedings of Microelectromechanical Systems, IEEE*. 1995.

109. Cartwright, T.S., G.P., *Culture Media*, in *Basic Cell Culture Second Edition*, J.M. Davis, Editor. 2002, Oxford University Press: New York, NY. p. 69-106.

110. Scott, R.C.P., C.B.; Rosano, J.M.; Pandian, P.; Pant, K.; Sundaram, S.; Kiani, M.F. *Particle/Endothelial Cell Adhesion in a Microvascular Network on a PDMS Chip*. in *BMES*. 2006. Chicago, IL.

111. Jankowski, R.J., D.A. Severyn, D.A. Vorp, and W.R. Wagner, *Effect of retroviral transduction on human endothelial cell phenotype and adhesion to Dacron vascular grafts.* J.Vascular Surgery, 1997. 26: p. 676-684.

112. Pitt, B.R., M. Schwarz, E.S. Woo, E. Yee, K. Wasserloos, S. Tran, W. Weng, R.J. Mannix, S.A. Watkins, Y.Y. Tyurina, V.A. Tyurin, V.E. Kagan, and J.S. Lazo, *Overexpression of metallothionein decreases sensitivity of pulmonary endothelial cells to oxidant injury.* Am J Physiol Lung Cell Mol Physiol, 1997. 273(4): p. L856-865.

113. McElroy, M.C., J.P. Wiener-Kronish, H. Miyazaki, T. Sawa, K. Modelska, L.G. Dobbs, and J.F. Pittet, *Nitric oxide attenuates lung endothelial injury caused by sublethal hyperoxia in rats.* Am J Physiol Lung Cell Mol Physiol, 1997. 272(4): p. L631-638.

114. Ceneviva, G.D., E. Tzeng, D.G. Hoyt, E. Yee, A. Gallagher, J.F. Engelhardt, Y.-M. Kim, T.R. Billiar, S.A. Watkins, and B.R. Pitt, *Nitric oxide inhibits lipopolysaccharide-induced apoptosis in pulmonary artery endothelial cells.* Am J Physiol Lung Cell Mol Physiol, 1998. 275(4): p. L717-728.

115. Sundback, C., T. Hadlock, M. Cheney, and J. Vacanti, *Manufacture of porous polymer nerve conduits by a novel low-pressure injection molding process.* Biomaterials, 2003. 24(5): p. 819-830.

116. Hadlock, T., C. Sundback, D. Hunter, M. Cheney, and J.P. Vacanti, *A polymer foam conduit seeded with Schwann cells promotes guided peripheral nerve regeneration.* Tissue Eng, 2000. 6(2): p. 119-127.

117. Hillborg, H., J.F. Ankner, U.W. Gedde, G.D. Smith, H.K. Yasuda, and K. Wikstrom, *Crosslinked polydimethylsiloxane exposed to oxygen plasma studied by neutron reflectometry and other surface specific techniques.* Polymer, 2000. 41: p. 6851-6863.

118. Chuang, Y.J.T., F.G.; Cheng, J.H.; Lin, W.K., *A novel fabrication method of embedded micro-channels by using SU-8 thick-film photoresists.* Sensors and Actuators A, 2003. 103: p. 64-69.